UNIVERSIDADE FEDERAL DO CEARÁ

CENTRO DE TECNOLOGIA

DEPARTAMENTO DE ENGENHARIA AMBIENTAL E HIDRÁULICA

PROGRAMA DE PÓS-GRADUAÇÃO EM ENGENHARIA CIVIL

DANIEL GURGEL DO AMARAL MOTA

PREDICTION OF SOIL SHEAR STRENGTH PARAMETERS USING ARTIFICIAL NEURAL NETWORKS

FORTALEZA

2019

DANIEL GURGEL DO AMARAL MOTA

PREDICTION OF SOIL SHEAR STRENGTH PARAMETERS USING ARTIFICIAL NEURAL NETWORKS

Dissertação apresentada ao Programa de Pós-Graduação em Engenharia Civil do Centro de Tecnologia da Universidade Federal do Ceará, como requisito parcial à obtenção do título de Mestre em Engenharia Civil. Área de concentração: Geotecnia

Orientador: Prof. Dr. Silvrano Adonias Dantas Neto

FORTALEZA

2019

Dados Internacionais de Catalogação na Publicação
Universidade Federal do Ceará
Biblioteca Universitária
Gerada automaticamente pelo módulo Catalog, mediante os dados fornecidos pelo(a) autor(a)

M871p Mota, Daniel Gurgel do Amaral.
Prediction of soil shear strength parameters using artificial neural networks / Daniel Gurgel do Amaral Mota. – 2019.
158 f. : il. color.

Dissertação (mestrado) – Universidade Federal do Ceará, Centro de Tecnologia, Programa de Pós-Graduação em Engenharia Civil: Geotecnia, Fortaleza, 2019.
Orientação: Prof. Dr. Silvrano Adonias Dantas Neto.

1. Redes Neurais Artificiais. 2. Resistência ao cisalhamento de solo. 3. Coesão. 4. Ângulo de atrito. I. Título.

CDD 624.15

DANIEL GURGEL DO AMARAL MOTA

PREDICTION OF SOIL PARAMETERS USING ARTIFICIAL NEURAL NETWORKS

Dissertação apresentada ao Programa de Pós-Graduação em Engenharia Civil do Centro de Tecnologia da Universidade Federal do Ceará, como requisito parcial à obtenção do título de Mestre em Engenharia Civil. Área de concentração: Geotecnia

Aprovada em: 08/08/2019.

BANCA EXAMINADORA

Prof. Dr. Silvrano Adonias Dantas Neto (Orientador)

Universidade Federal do Ceará (UFC)

Prof. Dr. Alfran Sampaio Moura

Universidade Federal do Ceará (UFC)

Prof. Dr. Lucas Feitosa de Albuquerque Lima Babadopulos

Universidade Federal do Ceará (UFC)

Prof. Dr. Manoel Porfírio Cordão Neto

Universidade de Brasília (UnB)

To God.

To all of my family and friends who gave me the strength to do my best.

ACKNOWLEDGEMENTS

This study was financed in part by the Coordenação de Aperfeiçoamento de Pessoal de Nível Superior (CAPES) – Finance Code 001.

This study was financed in part by the Fundação Cearense de Apoio ao Desenvolvimento Científico e Tecnológico.

To all of the employees of the Departamento de Engenharia Hidráulica e Ambiental (DEHA), specially to my tutor Silvrano, because all of them were part of my development in the academic and professional fields.

To my friends, which motivated me and gave me the strength to keep moving forward at every moment I thought I was not going to succeed. To the group ADH, for all of the great discussions, which certainly made this journey more pleasant.

To my family, for all of the help that has always been given to me and for the love received, which have made me become a better person.

To my grandfather Olimar, who was always a person to unite the family, making us gather not only for celebrations, but also for moments that brought all of us together, made us better persons and, most of all, that made us a family. Thank you for being part of these memories I will never forget.

“The more I read, the more I acquire, the more certain I am that I know nothing.”

Voltaire

RESUMO

A previsão da resistência ao cisalhamento do solo é extremamente importante para a concepção de projetos em Geotecnia, os quais muitas vezes utilizam teorias de equilíbrio limite ou análise tensão-deformação com modelo elastoplástico de Morh-Coulomb. No entanto, a obtenção dos parâmetros de resistência através de ensaios diretos de laboratório ou campo pode ser inviável, o que culminou na ampla utilização de correlações baseadas em testes de campo como CPT (Cone Penetration Test) e SPT (Standard Penetration Test). Na previsão do ângulo de atrito efetivo (ϕ'), tem-se uma ampla utilização do valor de N_{SPT} como variável de entrada, muito embora alguns autores apontam para a incapacidade de utilização desse parâmetro só e, por conseguinte, apresentam correções a partir da tensão confinante (σ'_{v0}) (Kulhawy e Mayne, 1990; Hatanaka e Uchida, 1996). Por sua vez, na previsão da coesão não-drenada (c_u), as correlações apontam para resultados expressivos obtidos a partir da utilização da resistência à penetração do CPT como parâmetro de entrada no modelo (Rémai, 2013; Zein, 2017; Otoko et al., 2019). Entretanto, a utilização dessas correlações apresenta capacidade limitada, uma vez que não foram calibradas para a obtenção de c' e ϕ' simultaneamente em solos com ambas as parcelas de resistência ou mesmo para estimativa da coesão efetiva (c'). Dessa forma, tendo em vista a capacidade de generalização das redes neurais artificiais na modelagem de problemas complexos, alguns estudos foram propostos com o intuito de estimar c' e ϕ' a partir de variáveis de entrada obtidas em laboratório (Das e Basudhar, 2008; Göktepe, 2008; Shooshpasha, Amiri & MolaAbasi, 2014; Braga 2014). O objetivo do presente estudo é propor redes neurais artificiais para prever c' e ϕ' a partir de parâmetros coletados em campo N_{SPT}, σv_0' e tipo de solo, de forma a facilitar a concepção de projetos em casos em que a coleta de amostras indeformadas se mostre inviável. Para tal, um banco de dados de 168 amostras foi coletado e usado para treinamento, teste e validação de redes neurais. A comparação dos modelos mostrou que a previsão de c' e ϕ' simultaneamente teve a melhor eficiência entre os modelos que utilizaram RNA, superando também os resultados obtidos através das correlações lineares e não-lineares. A utilização de RNA superou também a eficiência das correlações existentes propostas por Dunham (1954), Godoy (1983) e Hatanaka & Uchida (1996) para a previsão de ϕ', assim como de Decourt (1989) e Terzaghi & Peck (1996) para a previsão de c_u.

Palavras-chave: Redes neurais artificiais, resistência ao cisalhamento de solo, coesão, ângulo de atrito

ABSTRACT

Predicting soil shear strength is extremely important for designing in Geotechnical Engineering since project conception is often based on limit equilibrium theory or stress-strain analysis with the Morh-Coulomb elastic-plastic model. However, obtaining the resistance parameters through direct laboratory or field tests may be unfeasible, which resulted in the wide use of correlations based on field tests such as CPT (Cone Penetration Test) and SPT (Standard Penetration Test). In effective friction angle (ϕ') prediction, N_{SPT} value is vastly used as the input variable, although some authors point to the inability of using this parameter alone and, therefore, add the overburden stress (σ_{v0}') as a correction factor (Kulhawy and Mayne, 1990; Hatanaka and Uchida, 1996). In the prediction of undrained cohesion (c_u), the correlations present expressive results from the use of CPT penetration resistance as an input parameter in the model (Rémai, 2013; Zein, 2017; Otoko *et al* ., 2019). However, the use of these correlations has limited capacity as they have not been calibrated to obtain c 'and ϕ' simultaneously for soils that presented both shear resistance parts or to estimate effective cohesion (c'). Thus, considering the generalization capacity of artificial neural networks in the modeling of complex problems, some studies have been proposed to estimate c 'and ϕ' from input variables obtained in from laboratory tests (Das and Basudhar, 2008; Göktepe, 2008; Shooshpasha, Amiri & MolaAbasi, 2014; Braga 2014). The aim of the present study is to propose artificial neural networks to predict c 'and ϕ' from field collected parameters N_{SPT}, σ_{v0}' and soil type, in order to facilitate the design of projects in cases in which the collection of undisturbed samples proves to be impracticable. To this end, a database of 168 samples was gathered and used for training, testing and validation of neural networks. Comparison of the models showed that the prediction of c 'and ϕ' simultaneously had the best efficiency between the models that used ANN, also surpassing the results obtained by linear and nonlinear correlations. Furthermore, the utilization of ANN presented a superior efficiency when compared to existing correlations proposed by Dunham (1954), Godoy (1983) and Hatanaka & Uchida (1996) for the prediction of ϕ', as well as those of Decourt (1989) and Terzaghi & Peck (1996) for the estimation of c_u.

Keywords: Artificial neural network, soil shear strength, cohesion, friction angle.

FIGURE LIST

TABLE LIST

LIST OF SYMBOLS, ABBREVIATIONS AND INITIALS

ANN	Artificial Neural Network / Networks
B	Skempton pore water pressure parameter for saturation
c	Cohesion of soil
c'	Effective cohesion of soil
C	Bentonite content
CEC	Constant Error Carousel
CF	Correction Factor
c_u	Undrained resistance of cohesive soils
Conf (e±)	Confidence for a given error
D_{10}	Effective particle diameter
D_{50}	Approximate average particle diameter
Dr	Relative density
d_k	Desired output of neuron
e_0	Initial void ratio
e	Void ratio
e	Euler's number
Fc	Fine content
FM	Fitness modulus
Gc	Gravel content
Gs	Specific gravity
GMDH	Group Method Data Handling
H	Output of pulse in a biological neuron
LL	Liquid limit
MDD	Maximum dry density
MLP	Multilayer perceptron
MPCNN	Max-Pooling Convolutional Neural Network
NANN	Nested Artificial Neural Network
NI ( )	Input Node Interrogator result for a given variable
N_{SPT}	Standard penetration test blow count
$N_{SPT,1}$	Normalized standard penetration test blow count
N_{60}	Corrected standard penetration test blow count at 60% energy efficiency

OMC	Optimal moisture content
PL	Plastic limit
R^2	Coefficient of determination
Sc	Sand content
SPT	Standard Penetration Test
u	Pore pressure
U	Uniformity coefficient
UU	Undrained and unconsolidated
V-C	Vapnik-Chervonenkis
v_k	Induced local field or activation potential
u_k	Linear combiner
w_{kj}	Synaptic weight of neuron K
$w_{kj}(t+1)$	Synaptic weight of neuron K in time t+1
x	Random variable
$\bar{x}$	Sample mean
x_0	Entry signal applied to the bias
x_m	Input data
y_k	Output signal of neuron K
α	Alpha parameter defined by Nagaraj
α	Momentum
β	Beta parameter defined by Nagaraj
Δw_{kj}	Correction of weight
ε	Error
ε_1	Major principal strain
ε_2	Minor principal strain
$\varphi(\cdot)$	Activation function
ϕ	Friction angle of soil
ϕ’	Effective friction angle of soil
ϕ_r	Residual friction angle
γ_d	Dry unit weight
γ_n	Natural Unit weight
η	Learning ratio

ρ_d	Dry specific mass of soil
ρ_s	Specific mass of grain
σ_1	Major principal stress
σ_2	Minor principal stress
σ'_1	Major effective principal stress
σ'_2	Minor effective principal stress
σ_h	Horizontal normal stress
σ_{h0}	Initial horizontal normal stress
σ_v	Vertical normal stress
σ'_{v0}	Effective initial vertical stress
σ_{v0}	Initial vertical normal stress
ω	Natural moisture content

SUMMARY

1 INTRODUCTION

The first chapter of this work will address the research motivation as well as the main questions to be answered throughout the research. Also, the main research goals are listed, the methodology is described briefly, and the structure is shown to provide a better understanding of the work.

1.1 Research motivation

The understanding of shear strength of soils is of much relevance when it comes to project designing using either limit equilibrium or stress-strain analysis. Many authors have then studied soil shear strength behavior, relating it to other characteristics and in-situ test results. These authors proposed correlations on friction angle (ϕ) and cohesion (c) prediction so difficulties and costs for undisturbed sampling could be diminished or even avoided for simple projects. Most correlations were then proposed as an alternative to laboratory tests and were developed based either on N_{SPT} values or CPT penetration resistance, presenting good results on friction angle and cohesion prediction (Dunham, 1954; Meyerhof, 1956; Kishida, 1967; Peck *et al*., 1974; Muromachi *et al*., 1974; Shioi e Fukui, 1982; Godoy, 1983 apud Cintra *et al*., 2003; Teixeira, 1996 apud Cintra, *et al*., 2003; Hatanaka e Uchida, 1996; Terzaghi e Peck, 1967; Sanglerat, 1972; Nixon, 1982; Decourt, 1989).

Although the results obtained from existing correlations were proven to be consistent, these models were unable to predict both cohesion and friction angle simultaneously for soil mixtures in which it presents both shear resistance parts. In addition, the cohesion prediction models were modeled for undrained conditions, giving undrained resistance (c_u) as an output. For that matter, artificial neural networks (ANN) were proposed on shear resistance parameters prediction because of the generalization and capacity on modelling complex problems (Göktepe *et al*., 2008; Das & Basudhar, 2008; Shooshpasha, Amiri & MolaAbasi, 2014; Braga, 2014). However, the ANN proposed by Göktepe *et al*. (2008), Das & Basudhar (2008) and Braga (2014) only relied on laboratory test results, still making it necessary to collect undisturbed soil samples and for that matter being unpractical since direct shear or triaxial compression tests could be carried on the specimen for a more precise study. Shooshpasha, Amiri & MolaAbasi (2014), on the other hand, developed a model base on normalized energy number of SPT blow counts (N_{60}), overburden stress (σ_{v0}') and fines content (FC) for soils from Taiwan and Turkey after two major earthquakes. This simplification showed to be benefic on

effective cohesion (c') and effective friction angle (ϕ') prediction but, since it was calibrated for soils after seism and so lateral confining stress might be increased, it might bring to errors in prediction for non-seismic regions such as Brazil.

In view of this, ANN models on c' and ϕ' prediction are proposed in the present work, based on easy-to-collect input, N_{SPT}, σ_{v0}' and soil type, in order to give simple and accurate response for various soil type and site conditions in situations in which obtaining undisturbed soil samples is unfeasible.

1.2 Objectives

This study's main purpose is to propose artificial neural networks of perceptron type that can be used to predict soil shear strength parameters (c', ϕ') from SPT results.

In order to guide the research, the specific objectives were established as follows:

- To define input parameters of the models;
- To gather a vast database of samples containing shear strength test results, σ'_{v0}, N_{SPT} and soil classification, in order to build models that can be used to predict soil parameters for various soil types;
- To evaluate the correlations among soil shear strength parameters and SPT test results.
- To propose linear and non-linear regression-based models on prediction of soil shear strength parameters;
- To verify the importance of each input variable in c' and ϕ' prediction;
- To propose ANN that can be used to obtain the desired output;
- To verify the influence of number of iterations for ANN modelling;
- To analyze the influence of different activation functions in ANN modelling;
- To test the influence of complete soil classification as input in ANN modelling in comparison with soil group classification;
- To compare the results obtained by means of the proposed ANN with those obtained using existing methods.

1.3 Methodology

The first step of this work consisted in a literature review of soil shear strength, existing correlations for prediction of soil shear strength parameters, artificial neural networks

and applications of ANN in geotechnical Engineering. Simultaneously, results of SPT and shear strength tests performed on undisturbed samples were gathered from the existing literature so data could be used during training, testing and validation of ANN and regression models.

A total of 168 samples were collected containing results for various soil types which were then randomly divided into three groups: training, testing and validation. The models generated were ANN with different architectures and regression-based models. In turn, ANN models were trained and tested by software QNET 2000, which performed adjustments in the networks by using an error correction algorithm. Later, the results of ANN and regression-based models generated in this work were compared to that obtained from applying existing correlations on shear strength parameters prediction. The best model was chosen as being the one that obtained the greatest correlation between predicted and real values of c' and ϕ'.

1.4 Work structure

This dissertation is divided into five chapters, which will be described briefly in this section. The first chapter addresses the motivations of the study along with its objectives and a concise description of the methodology. The second chapter focuses on the literature review on soil shear strength, shear strength correlations, artificial neural networks and applications of ANN, in order to give a better understanding of the studied phenomena, and an overview of the artificial neural networks. In the third chapter, the methodology of this study is presented together with all its limitations and boundary conditions, which define the applicability of the proposed models. The presentation and analysis of the results are presented in the fourth chapter herein along with a discussion of the objectives and results. Finally, the fifth chapter shows the conclusions obtained from this research together with the suggestions for other studies that can fill in gaps left when predicting soil parameters.

2 LITERATURE REVIEW

The purpose of this section is to explain the main concepts addressed herein. Firstly, the shear strength of the soils will be explained as a result of the particle interaction and the field stress, since it is important to know this behavior in order to understand which soil properties could have the most influence on its shear strength parameters.

Thus, the models for prediction of shear strength parameters will be exposed and explained, while focusing on their pros and cons as a tool to achieve design parameters. Moreover, this will explain the working of these models so they can be compared to the results obtained by the ANN.

Lastly, the Artificial Neural Networks will be explained in order to give an understanding of its concept, how its process of calculation and prediction works, and the network training and validation.

2.1 Soil shear strength

In Geotechnical Engineering as in general Mechanics, the understanding of mechanical behavior of soils is of utmost importance in project design since it governs how the structures will respond to loads applied in the mass. For that matter, some constitutive models were proposed, being the Morh-Coulomb criterion the most used in Geotechnics due to its precise and practical modelling, in which soil mechanical behavior is defined by a cohesive, given by cohesion (c'), and a frictional part, given by (ϕ') as shown in Equation 1. The cohesive part is a result of electrical forces among particles, being much relevant in fine-grained soils due to the size and polarity of grains. On the other hand, coarse-grained soils have the mechanical behavior governed mostly by particle-to-particle contact, which means that the frictional part of shear strength is more noticeable. However, true cohesion might also be found in coarse-grained soils when particles stay in contact for long periods, resulting in cementing of contacts, which can be observed in the genesis of sandstone from sand. Figure 1 shows the nature of the mechanisms between particles for fine and coarse-grained soils. Authors have also studied the characteristics that affect it, such as soil composition, structure, particle size and presence of wate, (Lambe & Whitman, 1969).

$$\tau_s = c' + \sigma' \tan(\phi') \quad (1)$$

Figure 1 – Nature of particle contacts for coarse and fine-grained soils

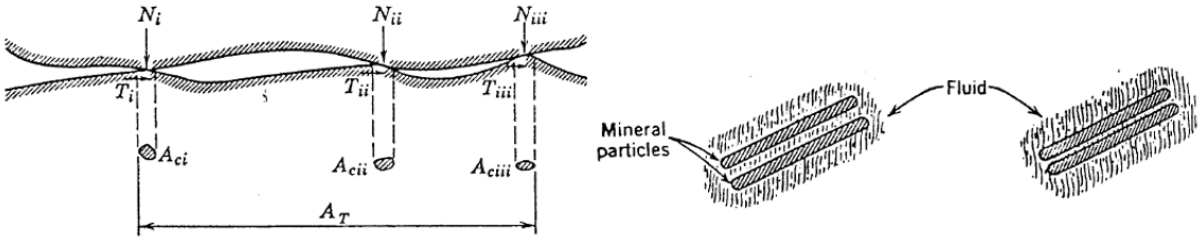

Source: Adapted from Lambe and Whitman (1969)

Lambe and Whitman (1969) also quote that, once the shear strength is frictional, it may be correlated to the field stress according to the basic laws of friction. Figure 2 shows some stress-strain results of laboratory tests for many load conditions, in which it may be found that the failure occurs at higher stresses for greater confining stresses, as can be attested by test numbers 1 and 2, with σ_v at failure varying from 470.4 kPa, for σ_{v0} = 98 kPa, to 1362.2 kPa, for σ_{v0} = 294 kPa.

Figure 2 – Stress-strain behavior of soils under different load conditions

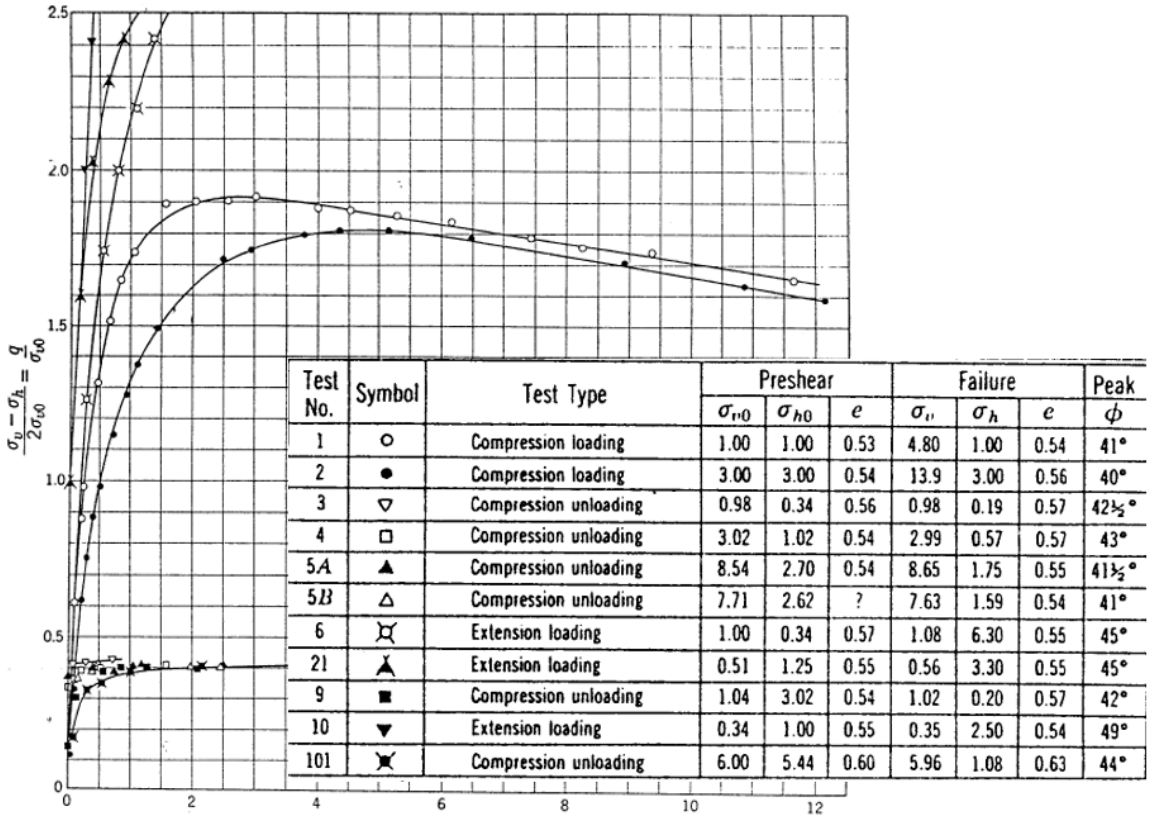

Test No.	Symbol	Test Type	Preshear			Failure			Peak
			σ_{v0}	σ_{h0}	e	σ_v	σ_h	e	ϕ
1	○	Compression loading	1.00	1.00	0.53	4.80	1.00	0.54	41°
2	●	Compression loading	3.00	3.00	0.54	13.9	3.00	0.56	40°
3	▽	Compression unloading	0.98	0.34	0.56	0.98	0.19	0.57	42½°
4	□	Compression unloading	3.02	1.02	0.54	2.99	0.57	0.57	43°
5A	▲	Compression unloading	8.54	2.70	0.54	8.65	1.75	0.55	41½°
5B	△	Compression unloading	7.71	2.62	?	7.63	1.59	0.54	41°
6	⧖	Extension loading	1.00	0.34	0.57	1.08	6.30	0.55	45°
21	⧗	Extension loading	0.51	1.25	0.55	0.56	3.30	0.55	45°
9	■	Compression unloading	1.04	3.02	0.54	1.02	0.20	0.57	42°
10	▼	Extension loading	0.34	1.00	0.55	0.35	2.50	0.54	49°
101	⧓	Compression unloading	6.00	5.44	0.60	5.96	1.08	0.63	44°

Source: Adapted from Lamb and Whitman (1969)

A recent study by Wei *et al.* (2019) showed some experimental results on the influence of field stress and moisture content to granitic sands and clays. The authors performed direct shear tests on undisturbed samples of granitic soils at various depths (A: 0-45 cm; B: 45-170 cm; BC: 170-430 cm; C: > 430 cm) and with different moisture contents, which varied from 7% to 28%, and under the saturated condition. They set the rate of shear stress application to 2.4 mm/min so the moisture content variation was neglected and applied normal stresses of 50, 100, 150 and 200 kPa.

The results in Figure 3 show the increase in shear strength with the decrease of moisture content, which can be explained as a result of the increase in matric suction (Lu & Likos, 2004). Wei *et al.* (2019) also concluded that the shear strength would decrease with the increase in depth for granitic soils, which could be a result of soil structure and compaction, as shown in Figure 4. Lastly, they conclude that cohesion and friction angle have high variation with the change in moisture content, normal stress and particle texture for granitic soils.

Figure 3 – Shear stress at failure *vs* net normal stress with variation in moisture content

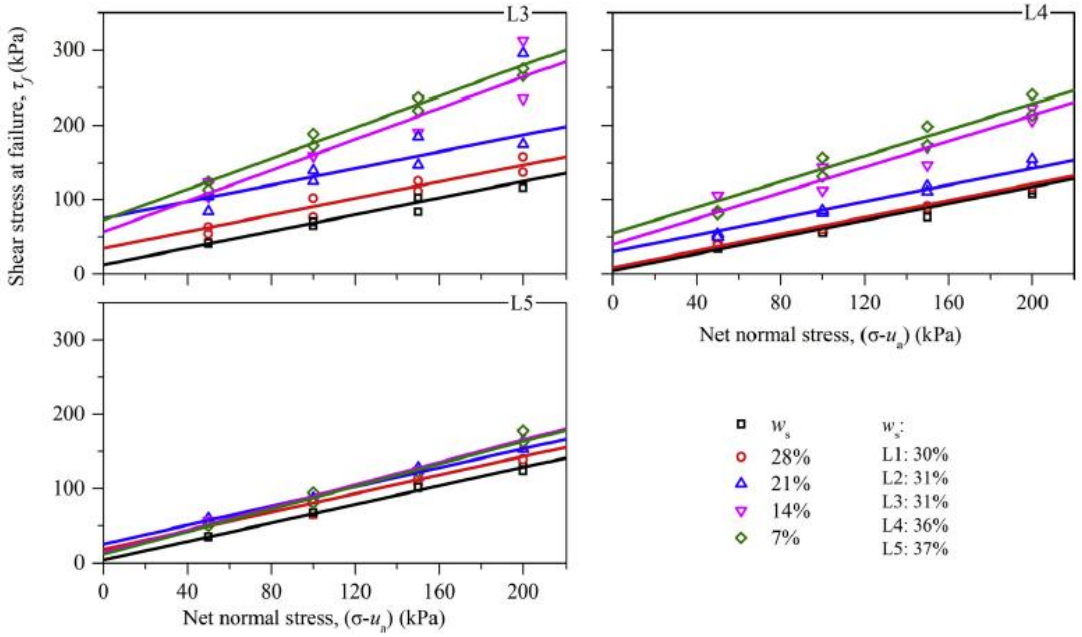

Source: Wei *et al.* (2019)

Figure 4 – Shear stress *vs* shear displacement at different depths and moisture content

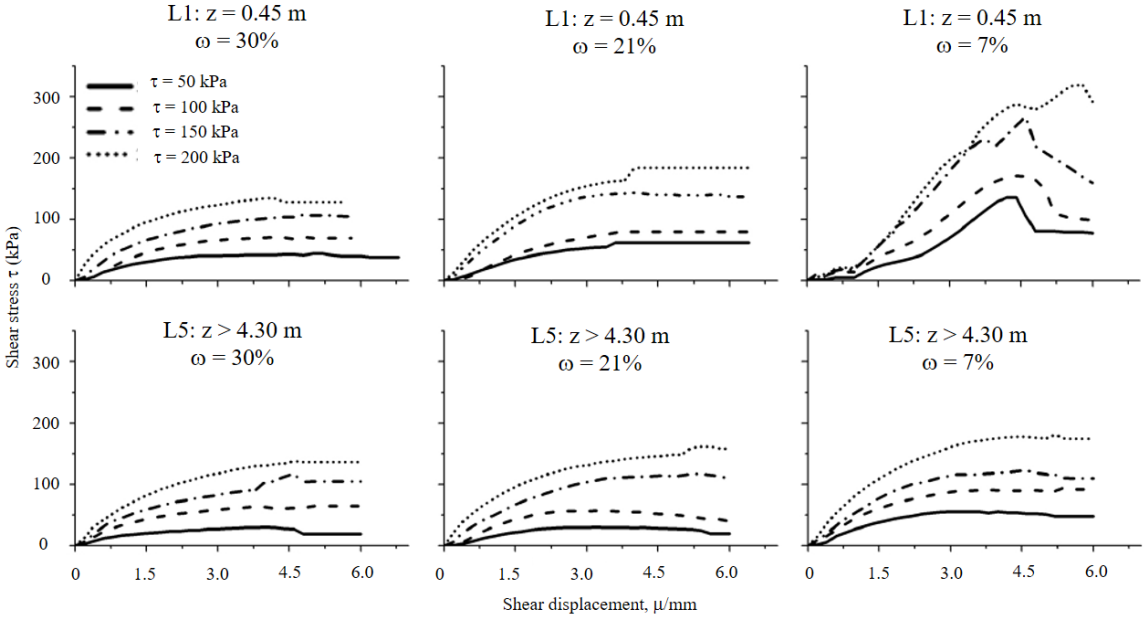

Source: Adapted from Wei *et al.* (2019)

2.2 Existing models for prediction of soil shear strength parameters

Soil shear strength parameters measurement is carried by performing triaxial compression or direct shear tests in laboratory on undisturbed samples. However, even though this process is precise, there are major difficulties that may be encountered during sampling, for instance, collection of specimen from great depths or long distance transportation of samples. Correlations were then proposed in order to give information about soil mechanical behavior in cases in which undisturbed sampling is unfeasible, although their accuracy was reduced when compared to measurement in laboratory. Moreover, the proposed equations were calibrated for purely cohesive or frictional soils and thus lack on predicting both c' and ϕ' simultaneously for soil mixtures.

2.2.1 Prediction of friction angle

Over the years, many methods have been proposed on prediction of friction angle mostly for sandy soil, considering only the frictional part of its mechanical behavior, since analytical models were unable to give precise results on both cohesion and friction angle simultaneously. These methods have focused on estimating this parameter based on much simpler data, such as SPT and CPT test results, in order to making the Engineering practice much more precise and simpler. Some well-known empirical N_{SPT}-based methods developed

over the years and applied in geotechnical practice, which were proposed by Dunham (1954), Godoy (1983) and Hatanaka & Uchida (1996) are shown in Equations 2, 3 and 4.

$$\phi' = \sqrt{12 \cdot N_{SPT}} + 25° \quad (2)$$

$$\phi' = 0.4 \cdot N_{SPT} + 28° \quad (3)$$

$$\phi' = \sqrt{20 \cdot N_{SPT}} + 20° \quad (4)$$

The models presented in Table 1 not only show the equations proposed by each author, but also expose similarities in the functions proposed among the models, which consists mainly of the direct correlation between the increase of N_{SPT} and the following increase in the friction angle. This generalization, however, fails to note the differences in mechanical behavior for different grain size distribution, and often underestimates or overestimates shear strength parameters.

With this in mind, in the early stages of ϕ' modeling, Dunham (1954) *apud* Shooshpasha, Amiri and MolaAbasi (2015) proposed models in which the friction angle was calculated from N_{SPT}-based equations, which depended on the particle shape and grain size distribution. The study was carried out on sandy soils and, as shown in Figure 5, the more angular and well-grained is the soil, the higher the friction angle calculated.

Figure 5 – Dunham (1954) results for predicted values based on N_{SPT}

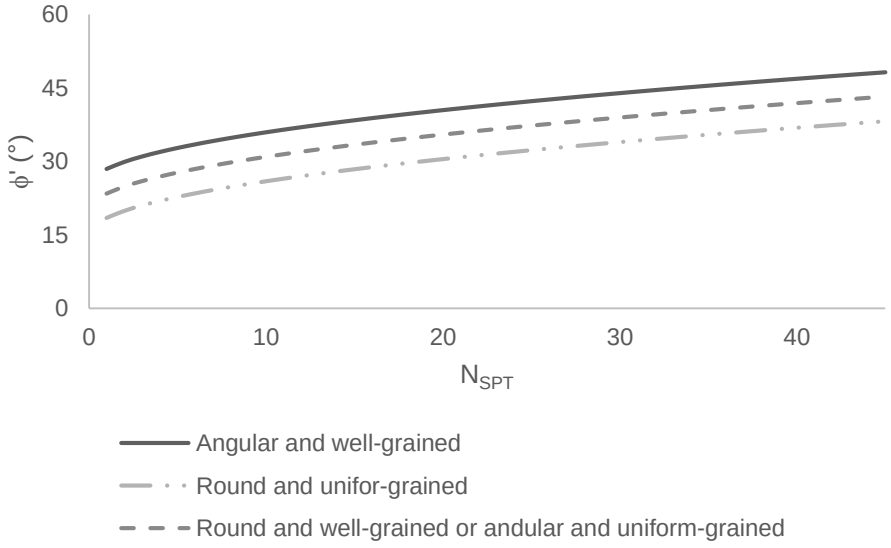

Source: Author adaptation

Some other authors such as Meyerhof (1956) and Peck *et al.* (1974) proposed different correlations based on friction angle results for saturated sands, which were widely used in Geotechnical Engineering practice. Years later, Godoy (1983) *apud* Cintra (2003) also

proposed an equation for prediction of the friction angle based on saturated results for pure sand that was similar to that obtained by Meyerhof (1956). Provided that this more recent equation was based on data from Brazilian soils, the results obtained by Godoy (1983) had a significant relevance in Engineering practice in Brazil and are widely used.

Likewise, more recently Hatanaka and Uchida (1996) studied the correlation between the standard penetration value and shear strength of volcanic sandy and gravelly soils (*Shirasu*). In order to do so, the authors recalled the influence of soil density and confining stress to correct the N_{SPT}, since Meyerhof (1956) *apud* Hatanaka and Uchida (1996) presented results that attested σ_v' influences on friction angle prediction.

The study was carried out by extracting twelve samples from six sites by means of the in-situ freezing technique, so high-quality subjects were collected and used SPT to verify soil penetration resistance along its profile. All samples were collected under the water level and then submitted to laboratory tests in order to find the physical properties together with the saturated ($B \geq 0.95$) drained triaxial test results, shown in Table 1.

Table 1 – Hatanaka and Uchida (1996) soil characterization

Sample	γ_s (kN/m³)	D_{50} (mm)	γ_d (kN/m³)	e	Dr (%)	N_{SPT}	σ_v' (kPa)	$N_{SPT,1}$	ϕ'
IK1	26.75	0.29	13.33	1.00-1.01	34	9	68.6	11	36
IK2	26.17	0.38-0.40	12.94	0.99-1.06	57	17	98	17	38.2
NA	25.87	0.16-0.21	13.03	0.89-0.97	81	10	127.4	8.8	32.7
NG1	26.17	0.33-0.45	14.41	0.74-0.90	74	18	39.2	28	43.4
NG2	25.87	0.43-0.49	13.62	0.86-0.93	81	15	68.6	18	37.8
NG5	26.66	0.43-0.51	14.31	0.86-0.89	79	10	137.2	8.5	35.1
KY1	24.21	0.34-0.48	11.07	0.89-0.99	72	5.7	58.8	7.4	39
KY2	25.97	0.41-0.45	13.43	0.79-0.85	59	5.4	68.6	6.5	31
KY3	25.38	0.37-0.47	13.23	1.12-1.37	59	6.4	78.4	7.2	35
KG	23.81	0.19-0.24	9.02	1.57-1.78	70	11	49	16	40.4
KA1	24.30	0.45-0.75	8.13	1.12-1.8	81	4.5	78.4	5	28
KA2	23.72	0.15-0.45	8.72	1.55-1.69	78	4	88.2	4.2	30

Source: Adapted from Hatanaka and Uchida (1996)

Triaxial tests were carried at strain rate fixed within 0.1% to 0.2% per minute until a maximum of 15% and $N_{SPT,1}$ is the normalized standard penetration value given by Equation 5, in which σ_v' is in kPa. This equation proposes a normalization of the N_{SPT} value, considering the effect of confining stress in shear strength behavior.

$$N_{SPT,1} = \frac{N_{SPT}}{\sqrt{\frac{\sigma_v'}{98}}} \quad (5)$$

The proposal of Equation 5 for correction of the standard penetration test value was very relevant since the previous models showed in Table 1 ignored the influence of field stress. Moreover, the results from triaxial tests in Table 1 displayed the variation in friction angle for similar N_{SPT} presented a better adjustment to the normalized values. Nevertheless, the authors point that even though *Shirasu* soils present high variation in void ratio, this property does not affect its shear strength.

Afterwards, in order to obtain a new equation for friction angle estimation based on $N_{SPT,1}$, the authors plotted a scatter graph $N_{SPT,1}$ *versus* ϕ' in which the most commonly used in Japan empirical equations were applied to the data. These equations can be seen in Figure 6, which displays the underestimation resulted from their use since the real values were all placed above a line given by Equation 6.

Figure 6 – Hatanaka and Uchida (1996) data scatterplot for N_{SPT} versus friction angle for most commonly used models in Japan

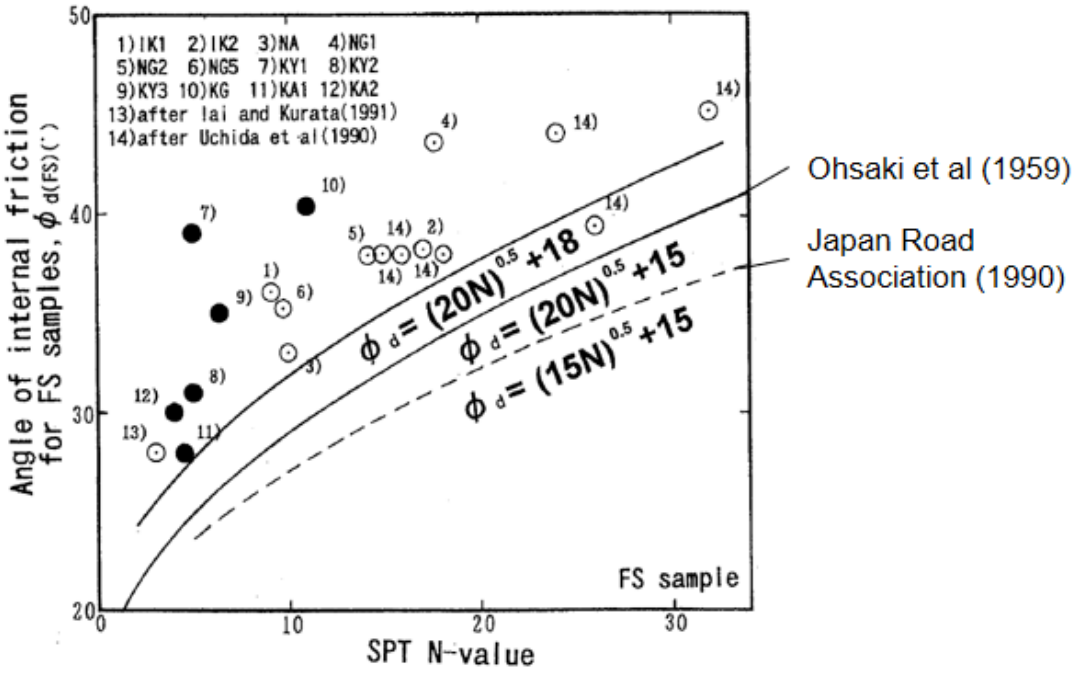

Source: Adapted from Hatanaka and Uchida (1996)

$$\phi' = \sqrt{20 \cdot N_{SPT}} + 18° \quad (6)$$

Furthermore, the authors applied Equation 5 to normalize the input data, realizing data had a similar trend that could be defined by Equation 7 within the range of ± 3°. Later, the model was applied to gravelly soils tested by LPT (Large Scale Penetration Test) using the

same normalization equation, which also resulted in good consistence. Figure 7 displays the application of the proposed model, showing that it fitted the data better. Nevertheless, Hatanaka and Uchida (1996) highlight that the model reliability is valid for $N_{SPT,1}$ within the database range, which was $3.5 \leq N_{SPT,1} \leq 30$.

Figure 7 – Hatanaka and Uchida (1996) proposed model application and adjustment

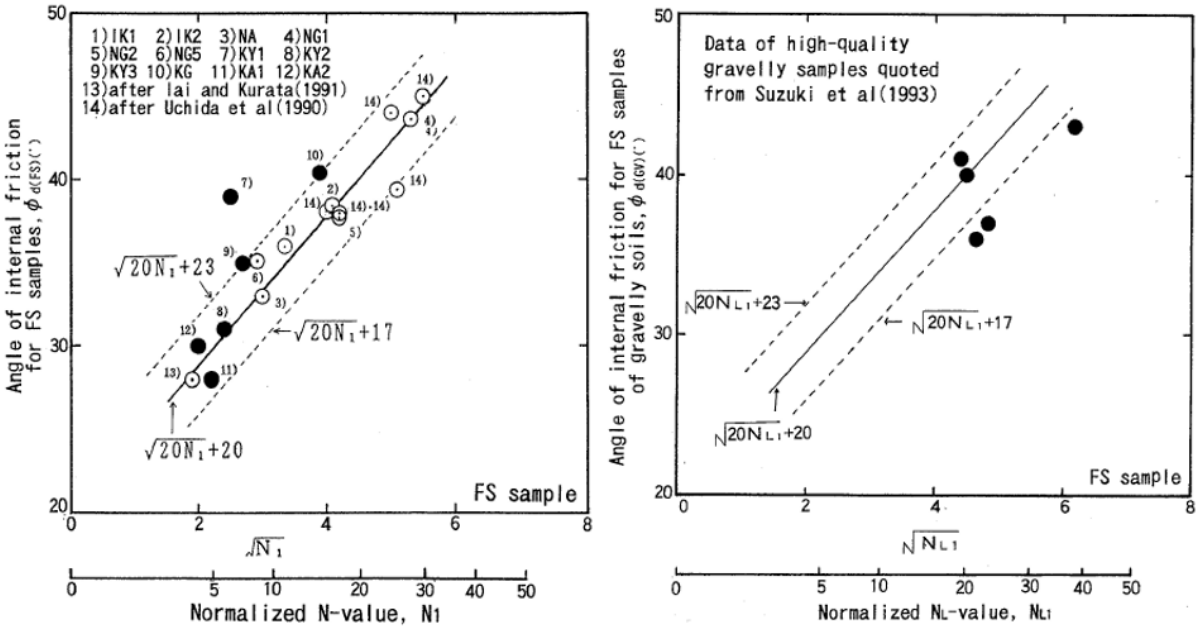

Source: Adapted from Hatanaka and Uchida (1996)

$$\phi' = \sqrt{20 \cdot N_{SPT,1}} + 20° \quad (7)$$

2.2.2 Prediction of cohesion

Cohesion estimation models are similar to that proposed for friction angle, being based on N_{SPT} or pressure values obtained by CPT. However, since cohesive soils are mostly fine-grained, they are often subjected to undrained conditions, which is their most adverse condition, which is why the models proposed in the literature have the undrained resistance (c_u) as output. Equations 8 and 9 present some of the empirical equations proposed for estimating c_u (kPa) proposed by Decourt (1989) and Terzaghi & Peck (1996), respectively. From Equations 8 and 9, it is noticeable that the proposed models have severe disparities among the predicted outputs, reaching differences of up to approximately three times for the same N_{SPT}.

$$c_u = 12.5\ N_{SPT} \quad (8)$$

$$c_u = 4.4\ N_{SPT} \quad (9)$$

The equations presented shown that although the data collection was easy and the models simple, their use in the Engineering practice escalated, resulting in several different correlations. For instance, Decourt (1989) pointed out that this is due to the difference in energy applied during the tests, which are affected by equipment characteristics, soil conditions and human influence. From the soil conditions, the author listed a series of factors that influenced in the SPT energy efficiency, as follows: void ratio, average particle size, coefficient of uniformity, pore water pressure, particle angularity, cementation, current stress level, prestressing and aging. For example, for a change in current level of stress level the penetration resistance is not much influenced for clayey soils, meanwhile the opposite is true for sandy soils.

Furthermore, Denisov *et al.* (1963) *apud* Decourt (1989) are quoted in the work for their contribution to the study of aging. In their experiment, aged soils had a drop in deformations when compared to non-aged soils, even though the variation of friction angle was very slight.

Decourt (1989) then presented a correlation for c_u estimation for clayey soils for São Paulo insensitive clays. Equation 8 provides the proposed correlation, which was formulated from hundreds of triaxial tests on unconsolidated and undrained samples with natural saturation and N_{60}, which consists of corrected standard penetration test blow counts for 60% energy efficiency. The author also points to the option of setting the confining stress equal to, or greater than, the in-situ octahedral stress in order to assure the subjects were over-consolidated.

More recently, Terzaghi and Peck (1996) studied the undrained shear strength of clays, also taking into consideration some of the factors that influence this mechanical property. In order to do so, the authors performed in-situ plate loading tests at varying depths, along with undrained and unconsolidated triaxial tests (UU triaxial tests) over undisturbed specimens of 38 mm and 98 mm in diameter, which were collected at each level by thin-walled tube samplers. The in-situ experiment was performed at the depths of 6.1 m; 12.2 m; 18.3 m and 24.4 m by excavating 900 mm boreholes and using an 865 mm diameter plate, together with a hydraulic jack to apply a load at a constant rate of 2.5 mm/min on the soil, resulting in approximately 30 minutes elapsed until failure. A similar elapsed time until failure was obtained by the triaxial results, being consistent among the experiments.

Results of the tests in Figure 8 display a difference in the measured shear strength for the various diameters of the specimen, which Terzaghi and Peck (1996) explained was a result of the fissure spacing scale when compared to the subject dimensions. The authors then

stated that these fissures were found to have an increase both in spacing and in depth, which would result in significant differences in resistance gain from the expected triaxial values compared to in-situ results. Also, the slip planes in the UU triaxial tests are free to occur in any direction and stress relief is caused by releasing the confining pressure, which results in a gain in shear strength. With this in mind, the reduction in the dimensions of the tested specimen was presumed to result in higher undrained shear strength, as can be seen in Figure 8, where results from using 38 mm diameter subjects were up to 50% more than from an in-situ loading test.

However, the results of the experiments indicated a much more significant correlation between the undrained shear strength mobilized by the soil mass and penetration test results than the triaxial tests. Stroud (1974) *apud* Terzaghi and Peck (1996) suggested a correlation based on SPT results, since it showed good adjustment to the measured data, having had less interference from changes in depth. This was probably due to the greater soil mass that is mobilized when carrying in-situ tests, which reduces the effects of the fissures on c_u.

Figure 8 – Terzaghi and Peck (1996) in-situ and laboratory test results for different sample size collected at various depths

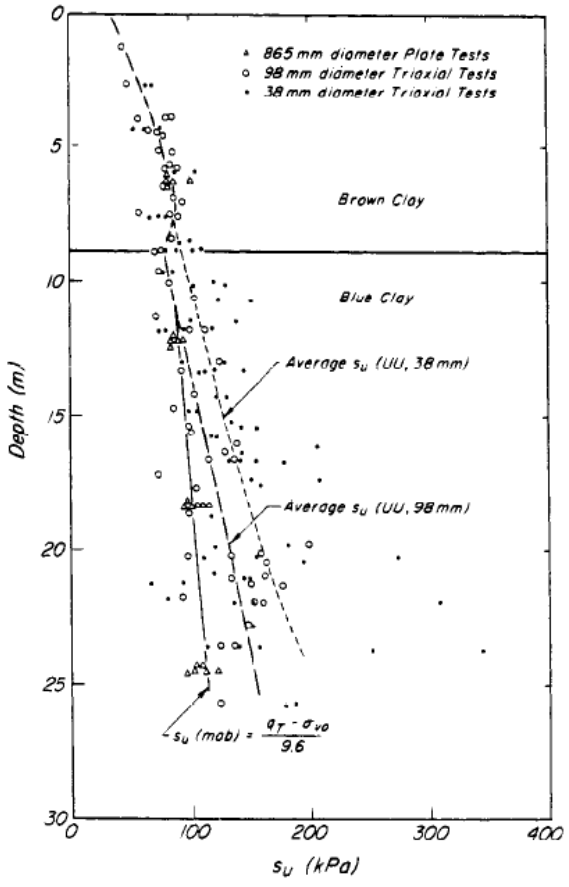

Source: Terzaghi and Peck (1996)

Terzaghi and Peck (1996) then used a scatterplot for the mobilized in-situ shear strength versus the plasticity index (PI) of the tested soils, resulting in the graph shown in Figure 9. Results from the various sites presented indicated an inverse correlation between these two variables, since increases in PI were followed by a decrease in c_u. Nevertheless, the authors also stated that the scatter of data in Figure 9 was increased by the influence of the fissures over the CPT results, this effect thus intensifying for stiff clays. For that reason, it may be inferred that the presence of plasticity in clays reduces the effects caused by the fissures.

Figure 9 – Terzaghi and Peck (1996) penetration test results *versus* plasticity index

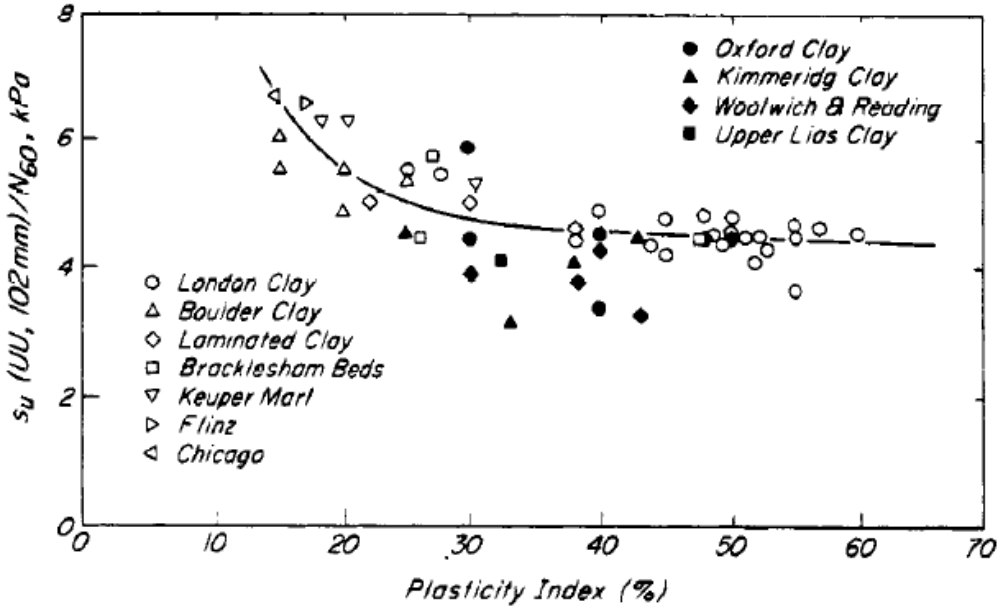

Source: Terzaghi and Peck (1996)

Lastly, Terzaghi and Peck (1996) concluded that the N_{SPT} was the best input variable for a simple model that would estimate the undrained shear strength of clays, since it was not influenced by the soil plasticity and results of their experiments showed a good match with the predicted values. This can be seen in Figure 10, which presents the correlation between SPT blow counts and c_u throughout the depth, with a noticeable simple linear correlation. Furthermore, a significant adjustment to undrained shear strength may be seen as it follows increases in N_{SPT} and depth, although for a specific number of SPT blow counts the variation of c_u at distinct depths was low. All things considered, Terzaghi and Peck (1996) proposed a correlation shown in Equation 9 based on N_{SPT} for London clays with PI = 50%. Nevertheless, for Chicago glacial clays tested, as for other location clayey soils, the resulting correlation could be different, taking into consideration other soil characteristics that affect the shear strength.

Figure 10 – Variation of c_u throughout depth and N_{60}

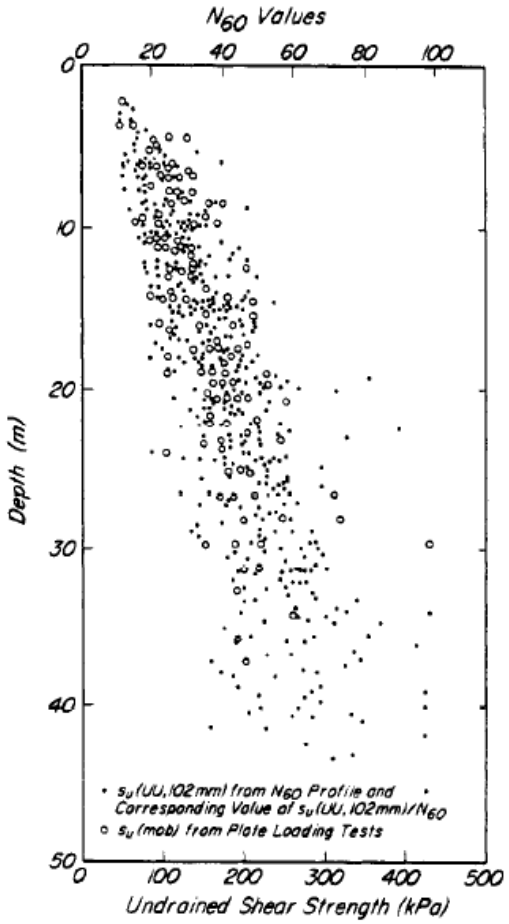

Source: Terzaghi and Peck (1996)

2.3 Artificial Neural Networks

This section will explain the functioning of Artificial Neural Networks (ANN) based on multilayer perceptron, starting from the biological neuron. Then, the functioning of the ANN will be explained, addressing the main concepts such as network architecture, training and validation.

2.3.1 Biological neurons

The Artificial Neural Network (ANN) concept was first thought from the biological neurons (Kovács, 2002). Hence, it is important to have an understanding of how these cellules function

The neurons are widely known to be the main working parts of the biological nervous system and are capable of receiving and transmitting electric pulses (spikes) through

their cell body. The anatomy of these cells can be seen in Figure 11 along with the spike propagation through them. It is also important to note that the pulse may have an excitatory or inhibitory nature, depending on the acting neurotransmitter.

Figure 11 – Anatomy of biological neuron and pulse transmission between adjacent cells

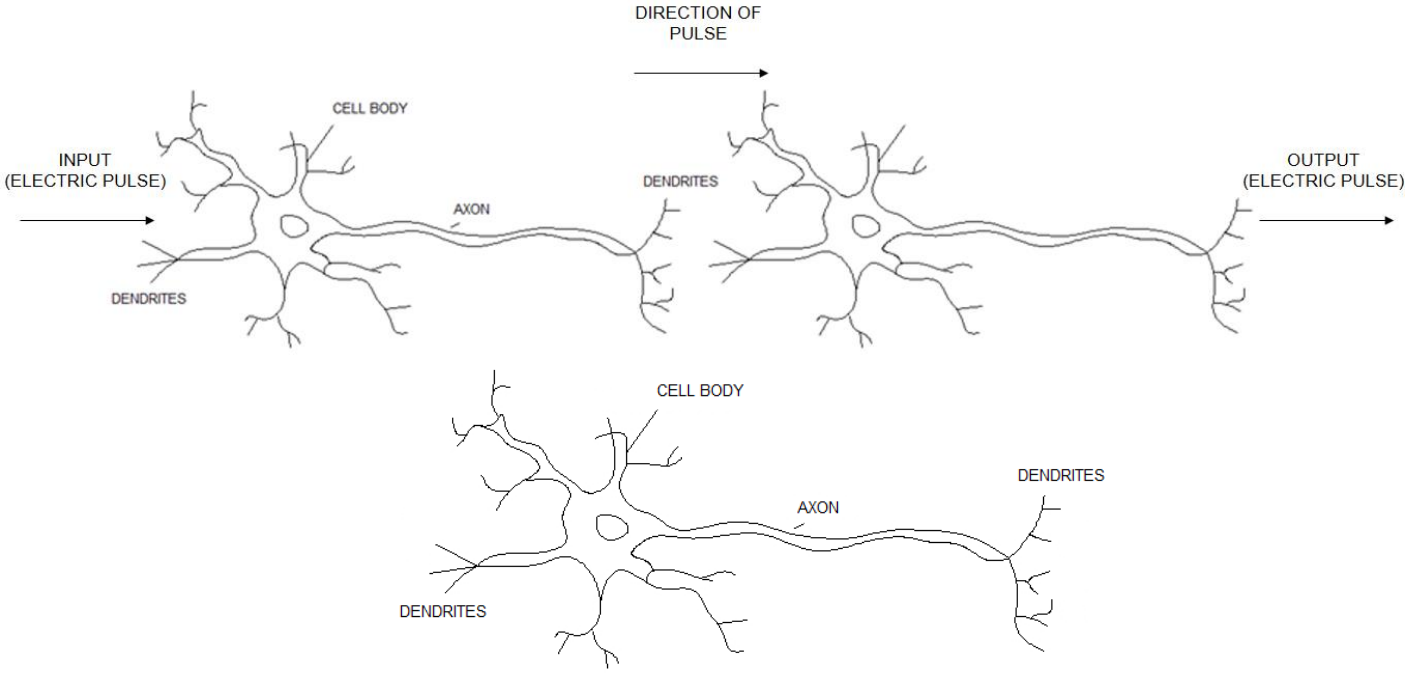

Source: Adapted from Araujo, 2013

In addition, these spikes may come from external sources, but mostly move from one cellule to another in a vast network, in which a neuron is connected to many others, as seen in Figure 11. Each cellule has a single output, which results from the combination of all pulses received from the others in a way that each spike is only transmitted ahead, if a minimum energy, known as action potential, is reached. Figure 12 shows the behavior of the electric energy, until reaching the minimum energy for the pulse. After the pulse is propagated, the energy rapidly declines and then the process restarts, until the action potential is reached again.

Figure 12 also shows the energy of the spikes are totaled until the action potential is reached and the output (H) is propagated.

Figure 12 – Electric energy behavior of pulse

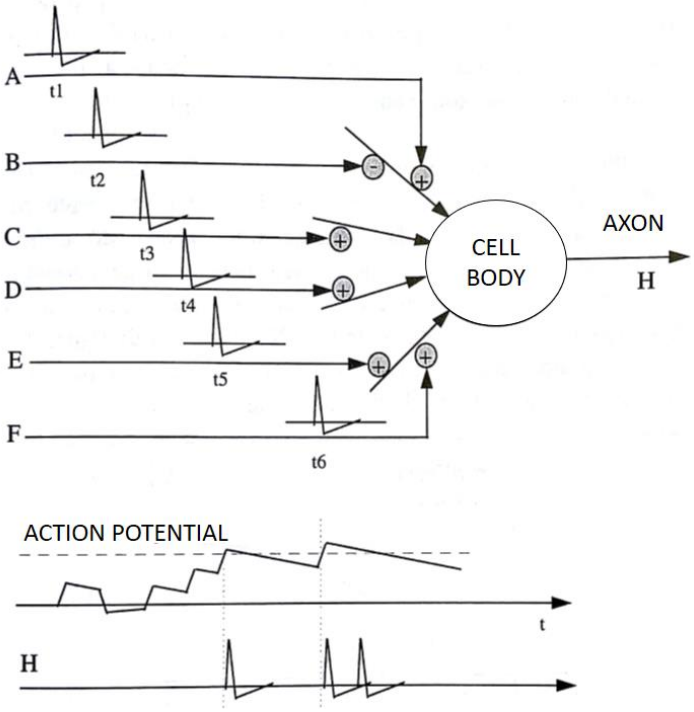

Source: Adapted from Kovács, 2002

2.3.2 The Artificial Neuron

Based on the biological neurons, a processing unit known as Artificial Neuron was then proposed by McCulloch and Pitts (1943), which would later result in the creation of Artificial Neural Networks (ANN) (Haykin, 2001). Kovács (2002) adds that the proposal of this element was inspired by some studies that considered the Boolean nature of intelligence, enabling scientists to mimic its functioning.

The basic model of the Artificial Neuron proposed by McCulloch and Pits (1943) (Figure 13) was conceived as a Boolean element with two types of entry: excitatory or inhibitory, like the biological cells. By doing so, there were only two possible outputs: 0 and 1 or 1 and -1. This would make it possible to separate the data into two classes, which could be useful for simple data discrimination, while more complex discrimination could not be achieved by this configuration.

Figure 13 – McCulloch and Pitts Boolean neuron

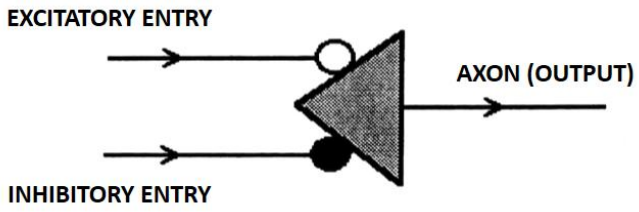

Source: Adapted from Kovács, 2002

In order to use the artificial neuron in more complex applications, it was then defined as a linear discriminator. Haykin (2001) explains that this discriminator (Figure 14) is divided into three parts:

1) Entry synapses: all the entry signals (x_m), their respective weights (w_{km}) and a bias (b_k) are gathered into this first part of the neuron. The index "m" represents the entry and the "k" refers to the neuron "k".
2) Summation: this part represents the sum of the entries weighted by each respective weight, which defines the linear combiner.
3) Activation function: this function limits the amplitude of the output data in order to normalize it.

Figure 14 – Non-linear artificial neuron scheme and parts

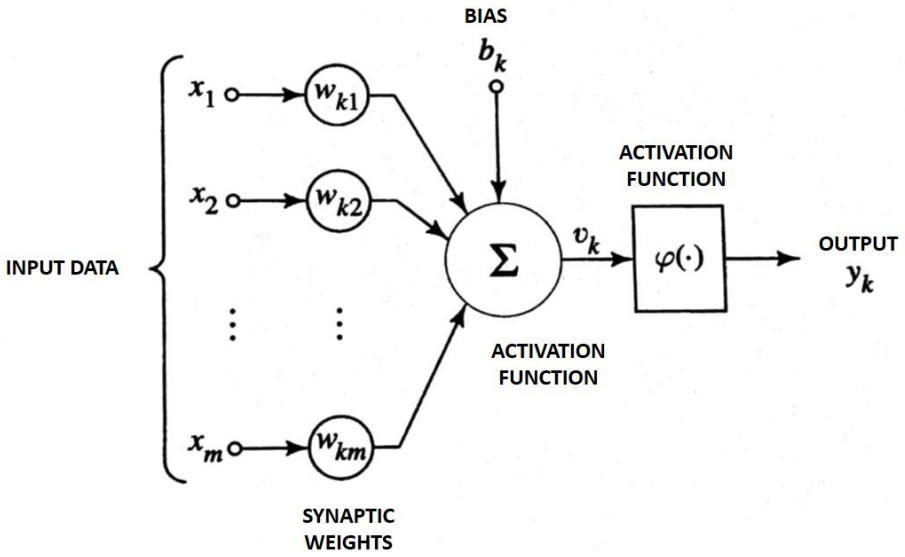

Source: Adapted from Haykin, 2001

where: x_m = entry signal; w_{km} = synaptic weight; b_k = bias or threshold; v_k = induced local field, or activation potential; $\varphi(\cdot)$ = activation function; y_k = output signal.

In mathematical terms, the artificial neuron can be expressed by equations 10, 11 and 12.

$$u_k = \sum w_{kj} x_j = \{w\}^T \{x\} \quad (10)$$

$$v_k = u_k + b_k = \sum w_{kj} x_j + b_k = \{w\}^T \{x\} + b_k \quad (11)$$

$$y_k = \varphi(v_k) = \varphi(\sum w_{kj} x_j + b_k) = \varphi(\{w\}^T \{x\} + b_k) \quad (12)$$

The input signals are organized in the input data vector $\{x\} = [x_1, x_2, \ldots x_m]$ which has the information to explain the phenomena behavior and depend on every application of ANN. The required order, *m*, is also variable from one application to another and can also be used to define the V-C dimension (Vapnik-Chervonenkis dimension).

The V-C dimension is used for measuring the capacity of the classification functions used in the learning process. This means that the greater *m* is, the more powerful is the ANN on separating distinct data in distinct classes. However, having a great *m* also makes it necessary to have a big quantity of training examples (Haykin, 2001). The training processes will be further explained in this document.

In the functioning of the artificial neuron, the input data are then summed in a linear combiner (u_k) being weighted by the synaptic weights, as shown in Equation 10. Just like the $\{x\}$, a synaptic weight vector is defined $\{w\} = [w_{k1}, w_{k2}, \ldots w_{km}]$ having the same order of $\{x\}$. Moreover, unlike the first concept made by McCulloch and Pitts (1943) the vector $\{w\}$ nature is not only excitatory or inhibitory, it also functions as an operator that will emphasize this behavior for each input signal.

After obtaining u_k, the bias is then introduced, being summed to the linear combiner and resulting in the induced local field, or activation potential, v_k. This element of the neuron is an external parameter and is similar to the activation potential of the biological neuron. It is also important to note that it is responsible for an affine transformation of the function.

Lastly, the induced local field is used as input for a function so the output signal, y_k, is obtained. As for this function, Haykin (2009) indicates two types, while in his other work Haykin (2001) points out that it can assume one of the three types:

- Threshold function:

Also referred as *Heaviside Function*, it is expressed as a function that has only two different output values, as seen in Equation 13. An example of this type of function is shown in Figure 15 and it is referred to as “step function”.

$$y_k = \varphi(v_k) = 1, if\ v_k \geq 0, \text{ or}$$
$$y_k = \varphi(v_k) = 0, if\ v_k < 0 \quad (13)$$

- Partially linear function;

Similar to the Threshold Function, this type of function has a greater and a minimum value beyond which the values on the y-axis are constant. However, in between this interval this function has a linear behavior. Haykin (2001) explains that this behavior can be used to approximate a non-linear amplifier.

- Sigmoid function:

Finally, the sigmoid function is presented as a function that has both the linear and non-linear behavior, being the most commonly used in ANN applications. This comes from the fact that this kind of function has a balance on linear and non-linear behavior. Also, it is differentiable throughout its whole domain, which is very important during the training of the ANN process.

Figure 15 – Representation of common activation functions

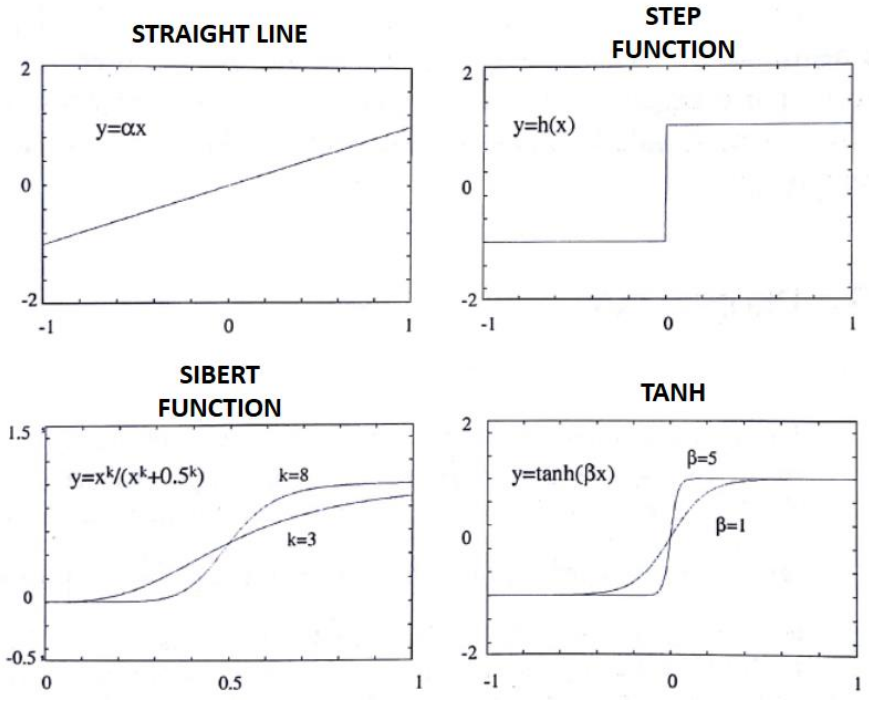

Source: Adapted from Kovács, 2002

Haykin (2001) also shows that the most commonly used sigmoid functions in ANN applications are: hyperbolic tangent, logistic function.

Furthermore, Kovács (2002) mentions that the most commonly used functions in ANN applications (Figure 15) are: straight line, step type function, Siebert function and hyperbolic tangent.

Nevertheless, some authors such as Araujo (2015), Dantas Neto *et al.* (2017) and Dantas Neto *et al.* (2014) have used the sigmoid function showed in Equation 14 in their works in order to explain soil strength behavior.

$$\varphi(x) = \frac{1}{1+e^{v_k}} \tag{14}$$

2.3.3 Neuron representations and network architecture

The artificial neuron can also be represented in a much simpler way known as a signal flux graph. In this representation, the operators in the neuron are hidden since they are already known, as shown in Figure 16.

Figure 16 – Artificial Neuron as a signal flux graph

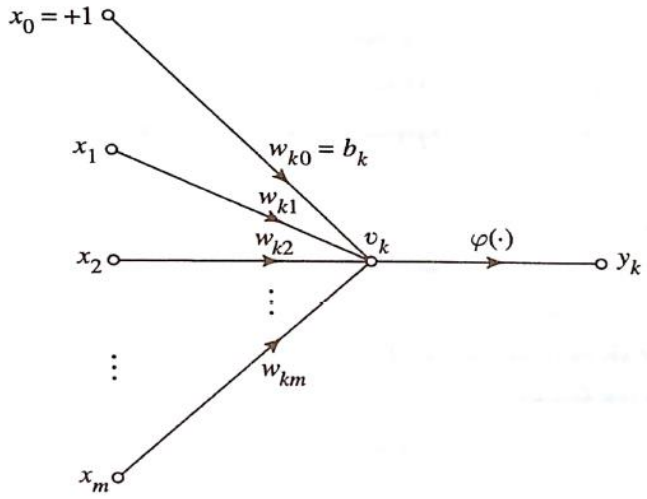

Source: Haykin, 2001

One of the important characteristics of the graph is that it represents the bias as a part of the weight vector applied to an entry signal $x_0 = +1$. By doing so, the calculi further made in the training and validation processes are simplified. So the weight vector can be defined as $\{w\} = [w_0 = +1, w_{k1}, w_{k2}, \ldots w_{km}]$.

Concerning the representation of the ANN architecture, it would be very complicated to use the signal flow graph, since information would be repeated or unnecessary for that analysis. For that matter, in this situation the neuron is usually represented as a single dot along with its entry and output signals (Figure 17).

Figure 17 – Artificial Neuron as an architectural graph

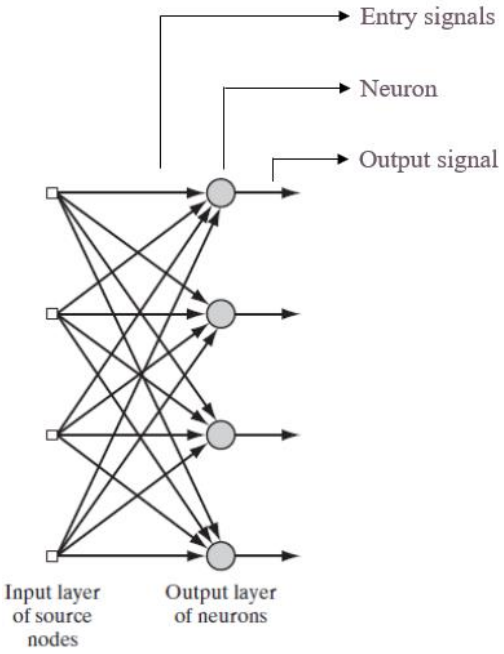

Source: Adapted from Haykin, 2009

With the knowledge of the parts that form each single artificial neuron, how they work and how they can be represented, it is important now to understand how they interact with one another.

Usually, these processing units are set out in one or more layers, depending on the problem to be solved. Figure 17 has shown a network with only one layer, while Figure 18 shows an architecture with two layers (one hidden layer and one output layer). The decision for the number of layers and neurons per each one depends on the complexity of the problem to be solved.

Another point worthy of note is the connection between neurons of different layers, which can occur when they are connected to every neuron of the adjacent layer or to only part of them. Frequently, ANN applications use a completely connected architecture.

As seen in Figures 17 and 18, the layers can either be hidden, their neurons being called hidden neurons, or output, with output neurons. It is important to notice that the more complex the architecture, the higher the number has to be of training and validation samples.

Figure 18 – Artificial Neural Network with two layers

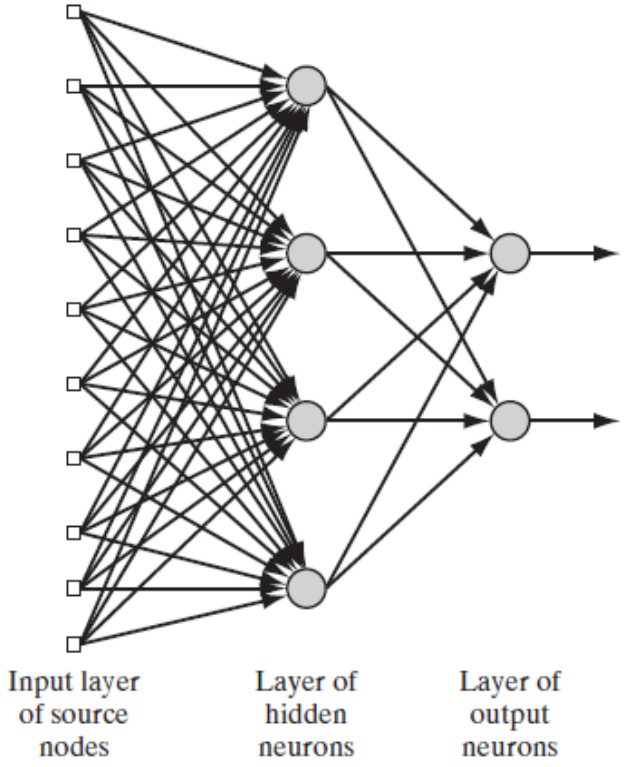

Source: Haykin, 2009

2.3.4 Training process

After proposing the architecture, it is necessary to train and validate the model. The training process consists of adjusting the weight vector by comparing the results obtained (y_k) in a previous configuration with the desired result (d_k) of already known sample data. This comparison generates an error (e_k) for each neuron and can be mathematically expressed as the result of Equation 15, in which coefficient "n" stands for the time "n" while the operation is done.

$$e_k(n) = d_k(n) - y_k(n) \tag{15}$$

Error e_k is then used to adjust the weights by a quantity measured by Equation 16, in which the parameter η is the learning ratio and Δw_{kj} represents how much the weight is corrected. Finally, Equation 17 shows the expression for obtaining the corrected error in time (n+1).

$$\Delta w_{kj}(n) = \eta e_k(n) x_j(n) \tag{16}$$

$$w_k(n+1) = w_{kj}(n) + \Delta w_{kj}(n) \tag{17}$$

Moreover, the training process goes as long as the error is minimized for all the neurons, which happens when a global minimum is reached in the cost function, E(n). Equation 18 may provide this function.

$$E(n) = \frac{1}{2} {e_k}^2 \tag{18}$$

Haykin (2001) also shows that another parameter, momentum constant (α), is required to stabilize the search for the minimum of the cost function.

Once the correction of the weights is completed and the cost function minimized, the network is then validated by means of another group of known samples that has not yet been used. This process is called validation and aims to verify the generalization capacity of the ANN from data not used in the training process.

2.3.5 Applications of Artificial Neural Network in Geotechnics

Applications of artificial intelligence in order to develop more efficient machines have been the object of study for some time. Schmidhuber (2014) shows that the first uses of neural networks, in the way they are used today, date from at least the 1960s with the use of nonlinear layers of neurons. However, deep learning was only reached in 1991 when pre-processing data with the help of unsupervised learning networks, and the term "deep learning" was first used in 2006.

In the meantime, the studies focused on building programs and machines capable of replicating human behavior, such as visual, writing and audio recognition. Although, in order to do so, various techniques were used in the training of ANN such as: GMDH (Group Method Data Handling), backpropagation and Max-pooling. All those techniques were then combined in different ways so that a neural network could be made that would overcome the main barrier of deep learning: backpropagation training.

Schmidhuber (2014) quotes several works of little and great relevance on the development of these neural networks. One of these works, published by Hochreiter (1991), deserves considerable focus, since it explained the main reason why training ANN by backpropagation was hard and sensitive: gradient descent. It was found that the gradient during backpropagation for deep learning would either explode or vanish, making the training unstable. Many later studies have attempted to solve this problem, which became known as "the long time lag problem", by pre-training; increasing the computer processing capacity; Hessian-free

optimization or avoiding the error gradients for the weight matrices by guessing the weights; use of linear methods; optimal weight reaching and use of Evolino (a technique which consists of evolving the weights), Schmidhuber (2014).

Another problem encountered in the development of neural networks was the loss of data memorization through time of training. Typical ANN would forget the data learnt after 10 steps, what also made deep learning as difficult as generalization. This could be solved by using CEC (Constant Error Carousels), which helps keep and evaluate information, while it also overcomes the long time lag problem by means of a self-fixed weight equal to one, and an identity function. This also keeps the explosion and vanishing of the back-propagated error and creates a LSTM (Long Short Term Memory) network. This type of ANN is still used for speech recognition, protein and other molecule identification and prediction of properties, robot localization and control, online driver distraction detection, and also for meta-learning, when a machine had learned to run its own weight correction code, (Schmidhuber, 2014).

Then in 2006, the ANN began to prove their efficiency in official competitions when a Neoconitron-inspired, Creceptron-like, MPCNN (Max-Pooling Convolutional Neural Network) was the winner of an international handwriting recognition contest in the languages French, Arabic and Farsi. Later in the decade, other ANN won official competitions in various areas, achieving efficiency that was human-like and even greater than human-like. In 2010, Cireşan *et al.* (2010) broke a world record for handwriting recognition, achieving an overall error of 0.35% with the use of a multilayer perceptron with simple backpropagation training on a GPU (Graphic Processing Unit). The authors overcame very complex neural networks and showed that the deformations generated resulted in an insensitive in-class variation program. This was extremely important during training, since this technique created an infinity set of samples that were rarely repeated during the processing by scaling, rotating and applying horizontal shearing on the original data. From these results they concluded that the advances in processing capacity of computers and other machines are more relevant than the advances in the training algorithm.

In conclusion, Schmidhuber (2014) points out that most of the ANN used in the winning contests are either LSTM trained by CTC or feed-forward GPU-MPCNNs. Also, the author demonstrates that the coding in competing linear units is more important than the activation function.

In Geotechnical Engineering, the use of artificial intelligence (AI) has been used for many purposes, since there is much uncertainty and complexity in the prediction of soil behavior. Shahin, Jaksa and Maier (2001), Das (2013) and, more recently, Juwaied (2018) have

presented the state of art and the uses of ANN that have been applied in Geotechnical Engineering.

According to those authors, the use of ANN in this field has had a success in the prediction of soil parameters and understanding of phenomena. Some of the uses have been listed below in Table 2.

Table 2 – Applications of ANN in Geotechnical Engineering

Use	**Researchers**
Pile driving	Goh (1996); Abu-Kiefa (1998); Harnedi & Kassim (2013); Momeni *et al.* (2015); Maizir *et al.* (2015)
Prediction of pile bearing capacity	Lee & Lee (1996); The *et al.* (1997); Shahin (2010); Park & Cho (2010); Wardani *et al.* (2013)
Subsurface contamination	Rizzo & Dougherty (1996)
Aquifer characterization	Gangopadhya *et al.* (1999)
Designing of deep foundations	Nawari *et al.* (1999)
Analysis of side resistance of drilled shafts	Goh *et al.* (2005)
Lateral load capacity of piles	Das & Basudhar (2006)
Prediction of friction capacity of piles	Samui (2008)
Prediction of pile settlement	Nejad & Jaksa (2010)
Prediction of soil parameters	Tizpa *et al.* (2014), Goh (1995a; 1995c)

Source: Adapted from Juwaied (2018)

Table 2 shows that, although they have a wide range of applications, most of the relevant studies have focused on predictions and behavior of piles. For example, Goh (1995) applied an ANN to estimate load capacity of pile driving compared with the semi-empirical formulae proposed by the Engineering News (EN), Hiley and Janbu, presented in Equations 19, 20 and 21. The results have then suggested that neural network proposed for Q_u predictions had achieved a higher coefficient of correlation in comparison to the conventional methods (Table 3).

$$Q_u = \frac{WH}{s+c} \tag{19}$$

$$Q_u = \frac{e_f WH}{s+0{,}5(c_1+c_2+c_3)} \cdot \frac{W+n^2 W_p}{W+W_p} \tag{20}$$

$$Q_u = \frac{WH}{k_u \times s} \quad (21)$$

Table 3 – Regression analysis for estimation of load capacity of pile driving load capacity

Method	**Coefficient of correlation**	
	Training data	Testing data
Neural Network	0.96	0.97
Engineering News (EN)	0.69	0.61
Hiley	0.48	0.76
Janbu	0.82	0.89

Source: Adapted from Goh (1995)

Also, Goh (1995) showed that ANN could be used when predicting soil parameters. To do so, Goh (1995a; 1995c) performed tests in a chamber filled with sand with known properties and different stress and boundary conditions in order to determine the Dr (relative density) from Cone Penetration Tests (CPT). Further tests were carried out to determine hydraulic conductivity of clay liners, both studies resulting in good non-linear correlations with coefficient of correlation above 0.94 in the testing data. These results showed better efficiency than the empirical formulae tested on the same data.

Another use of ANN was proposed by Najjar, Basheer and Naouss (1996) to predict optimum moisture content (OMC) and maximum dry density (MDD) of compacted soils. In their paper, they mention that the existing models for prediction of these parameters have limitations, since they can only predict one at a time and depend on various variables such as compaction effort, type of compaction, grain size and distribution, among other soil characteristics. The various equations previously proposed for standard compaction effort and their independent variables are shown in Table 4, which also shows the coefficient of correlations obtained in each study.

Table 4 shows the proposed models based on analytical analysis are not practical and rather tedious, although coefficients of determination up to 0.951 were achieved.

To model an artificial neural network for prediction of OMC and MDD, Najjar, Basheer and Naouss (1996) had synthetic soils analyzed during a standard Proctor test. A total of 39 blends (33 for training and 6 for testing) containing bentonite, silt, sand and gravel were then used to develop the ANN in order to have a vast scale of soil types, including non-plastic types. The results in Figure 19 showed high coefficients of determination: OMC $R^2 = 0.884$ and MDD $R^2 = 0.890$. However, the disadvantage of this proposed ANN is that it requires other

laboratory tests (LL, PL and G_s), which could be unnecessary, since standard Proctor tests could be conducted on the soil, exempting the need for them. Hence, the study proposed by these authors had more relevance on validating the use of artificial neural networks.

Figure 19 – Regression analysis for ANN applied for OCM and MDD prediction

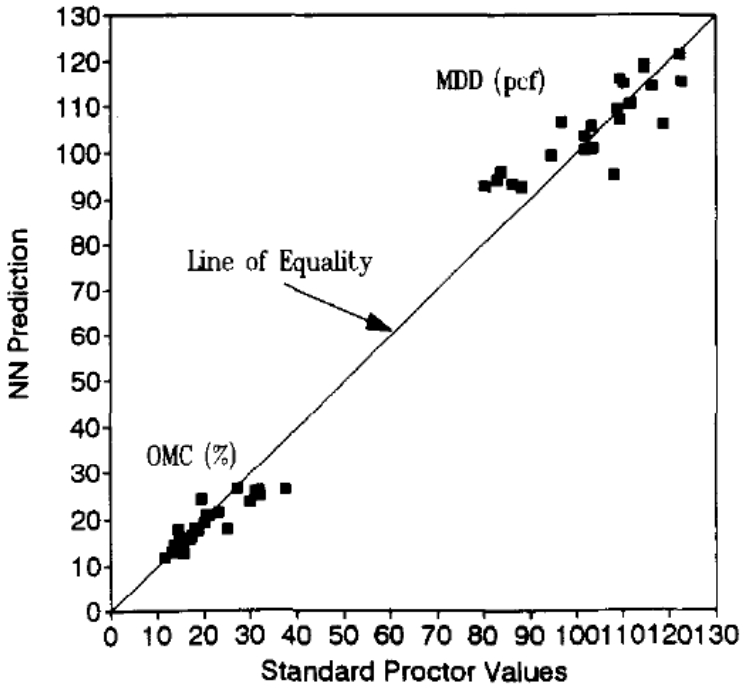

Source: Najjar, Basheer and Naouss (1996)

Table 4 – Prediction models for compaction parameters of soils

Authors	**Dependent variables**	**Independent variables**	**R^2**	**Equation**
Wang and Huang model A	MDD (pcf)	G_S, PL, FM, D_{10}	0.951	$MMD = ({}^{G_S}/_{100}) \cdot (45.6 - 1.28 \cdot FM \cdot \log D_{10} - 6.64 \cdot 10^2 \cdot FM \cdot PL + 1.43 \cdot FM)$
Wang and Huang model B	MDD (pcf)	Gs, FM, U, C	0.912	$MMD = ({}^{G_S}/_{100}) \cdot (45.9 - 7.5 \cdot FM - 0.45 \cdot \log U - 7.54 \cdot 10^{-2} \cdot C \cdot FM$
Wang and Huang model A	OMC (%)	PL, FM, U	0.880	$OMC = 0.01 \cdot [2614 + 12.7 \cdot PL - 95 \cdot FM^2 - 88.1 \cdot (\log U)^2]$
Wang and Huang model B	OMC (%)	D_{50}, C, FM	0.791	$OMC = 0.01 \cdot (1035 - 905 \cdot \log D_{50} + 0.22 \cdot C^2 + 106 \cdot FM \cdot \log D_{50})$
Jeng and Strohm	MDD (pcf)	LL, PL, G_S	0.840	$MDD = 0.89\,(LL - LP) - 1.26 \cdot LL + 89.8 \cdot G_S - 102.7$
Jeng and Strohm	OMC (%)	LL, PL	0.820	$OMC = 0.61 \cdot LL - 0.42 \cdot (LL - LP) + 2.14$
Nagaraj	OMC (%)	LL	-	$OMC = (\alpha \cdot \beta)^{0,5}$
Nagaraj	MDD (pcf)	LL	-	$MDD = {}^{62.4}/_{[\left({}^{1}/_{G_S}\right) + \left({}^{\alpha^2}/_{OMC}\right)]}$

Source: Adapted from Najjar, Basheer and Naouss (1996)

G_s = Specific gravity; FM = fitness modulus; U = uniformity coefficient; D_{50} = approximate average particle diameter (mm); α = 9.46 + 0.2575*LL; R^2 = coefficient of determination; PL = plastic limit; D_{10} = effective particle diameter (mm); C = bentonite content (%); LL = liquid limit; β = 8.829 + 0.228*LL.

Bearing that in mind, Ghaboussi and Sidarta (1998) took advantage of these characteristics of the data by modeling a NANN that automatically determined its own architecture by adding modules with information about the soil history of loading to increase its learning and prediction capacity. In the experiment, a set of data was used consisting of 30 test samples of triaxial test (15 under drained condition and 15 under undrained condition) that had as input data in the model the following:

- σ_1: major principal stress;
- σ_3: minor principal stress;
- u: porepressure
- σ'_1: major effective principal stress
- σ'_2: minor effective principal stress;
- ε_1: major principal strain
- ε_3: minor principal strain
- e_0: initial void ratio

The output of the network was the stress variation which was plotted in two types of graphs: q x ε_1 and q x u (Figure 20). The results from their study made it clear that the use of NANN has several benefits in prediction of behavior of path dependent materials, such as soil, and showed a good adhesion to the experimental data.

Figure 20 – ε versus q plots of results obtained from Ghaboussi and Sidarta NANN model compared with experimental results

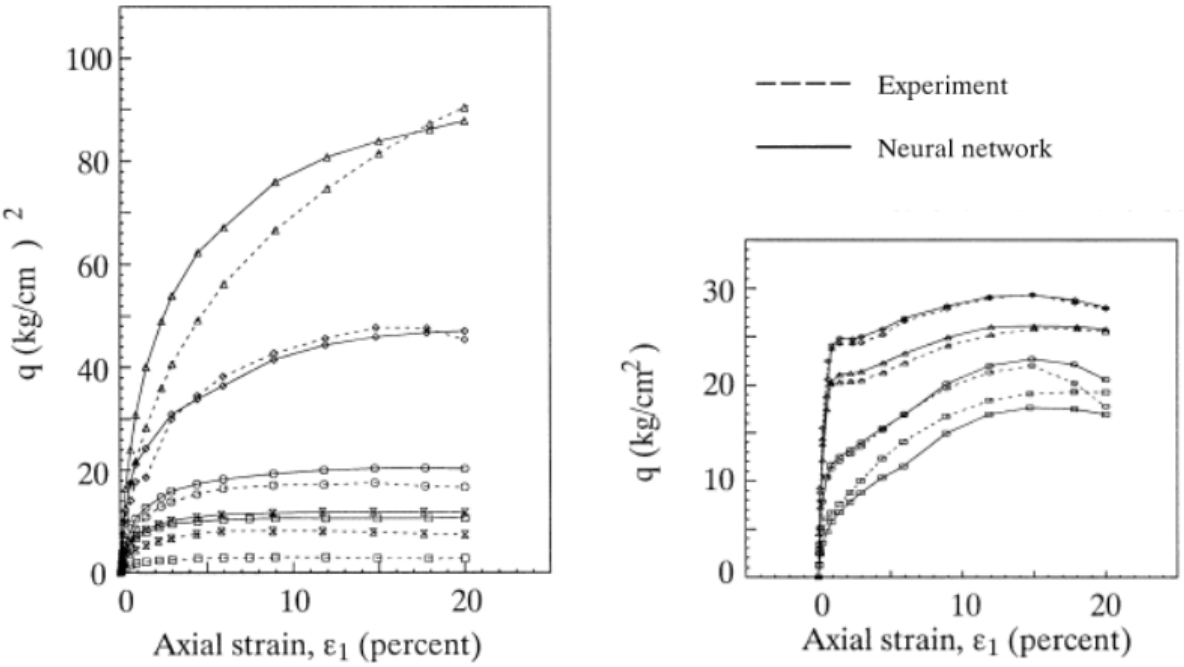

Source: Adapted from Ghaboussi and Sidarta (1998)

Similar to the use of NANN proposed by Ghaboussi and Sidarta (1998), another study on cohesionless soils was conducted by Penumado and Zhao (1999), in which they generated an artificial neural network based on a published literature database. In their paper, they sought to predict sand and gravel shear strength behavior under drained conditions. In order to do so, they chose the soil parameters and characteristics shown in literature to govern the behavior of cohesionless soils as input data: mineralogy, particle shape, uniformity coefficient, coefficient of curvature, effective particle size, void ratio and effective confining pressure. Their proposed ANN output was a model that could represent the deviator stress-axial strain and volumetric strain-axial strain.

The experiment was conducted with a total of 251 samples of triaxial compression tests from which 126 were for sand and 125 gravel, the confining pressure having varied over a wide range from 35 to 69,000 kPa. However, since sand grains are crushable, two models were proposed to diminish this effect, dividing the samples submitted to low pressures, defined arbitrarily as less than 700 kPa, and high pressures, above 700kPa. In turn, only one model was developed for gravel to predict the behavior. The authors chose the architecture of 11 x 15 x 2, which is shown in Figure 21.

Figure 21 – ANN architecture proposed by Penumado and Zhao (1999)

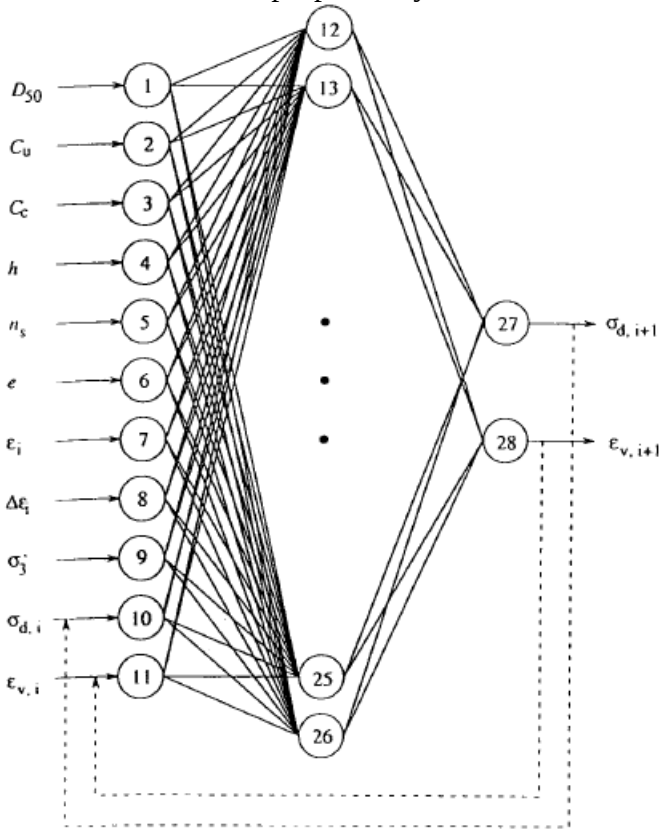

Source: Penumado and Zhao (1999)

Figure 22 shows the typical results obtained by the sand-low model, in which the behavior of deviator stress-axial strain and volumetric strain-axial strain are well represented. The results obtained by Penumado and Zhao (1999) have shown a good prediction for all three models proposed (sand-low, sand-high and gravel), having a high accuracy on the effects in both dilatation and compression for a wide range of confining pressures.

Figure 22 – Results of ANN proposed by Penumado and Zhao (1999) compared to experimental data

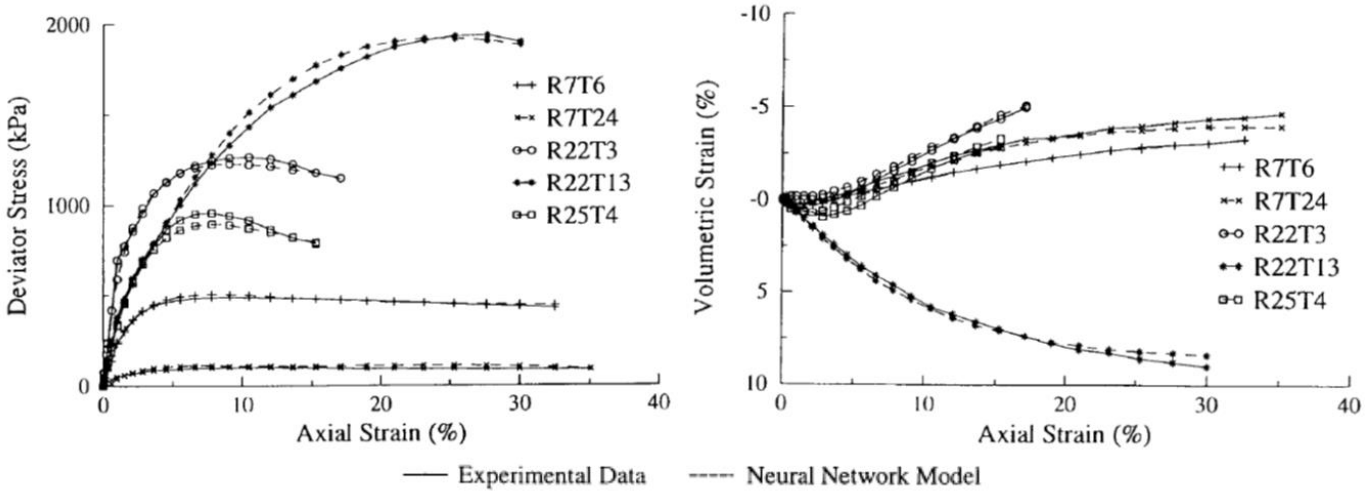

Source:Adapted from Penumado and Zhao (1999)

More recently Tizpa *et al.* (2014) published a more complete paper that used Artificial Neural Networks to predict compaction characteristics, permeability parameters and soil shear strength. By doing so, their model could be used to simplify the design of landfills, since the design parameters could be predicted from much simpler laboratory tests.

Tizpa *et al.* (2014) used a database of 580 samples with different types of soils that were divided into modeling of permeability (155), optimal moisture content and maximum dry density (320) and shear strength parameters (105). In order to choose the more relevant input data for each model, the authors ran a sensitivity analysis using a multi-layer perceptron (MLP), in which each variable was excluded from the model one at a time. For example, in the first MLP analysis, the parameter G_c weight was set to zero in order to verify the variation on prediction when removing this variable, as shown in Figure 23. For both MDD and OMC, the results of excluding G_c showed a dependency, since its exclusion resulted in scatter of data when plotted in a measured values/predicted values graph, making it a relevant variable for the input. A summary of the results of that analysis for both MDD and OMC is shown in Table 5 and, as can be noted, for both models the plastic limit (PL) is the most relevant input variable.

After completing the sensitivity analysis, the authors decided the input variables for both models were gravel content (G_c), representing the percentage of mass of soil with grain size greater than 4.75 mm; sand content (S_c), representing percentage of mass of grains with size in the range 0.075 mm to 4.75 mm; fine content (F_c), which states for the percentage of grain size smaller than 0.075 mm; grain relative density (G_S); liquid limit (LL); and plasticity limit (PL).

The permeability coefficient prediction had a similar procedure. At first, a sensitivity analysis was carried out and then the variables were chosen in order to get the best-matched model. A consequence of that is Tizpa *et al.* (2014) then concluded that for permeability prediction the compaction degree had a strong influence. The input data chosen was: G_c, S_c, F_c, G_S, LL and Cd.

Table 5 – Coefficient of determination of ANN for each excluded weight

Output	Statistic	Total	Ex. G_c	Ex. S_c	Ex. F_c	Ex. G_s	Ex. LL	Ex. PL
MDD	COD	0.92	0.57	0.57	0.67	0.64	0.74	0.42
OMC		0.92	0.84	0.83	0.83	0.85	0.81	0.65

Source: Adapted from Tizpa *et al.* (2014)

Figure 23 – Scatterplot showing sensitivity analysis for ANN input data after excluding G_c from the model proposed by Tizpa *et al.* (2014)

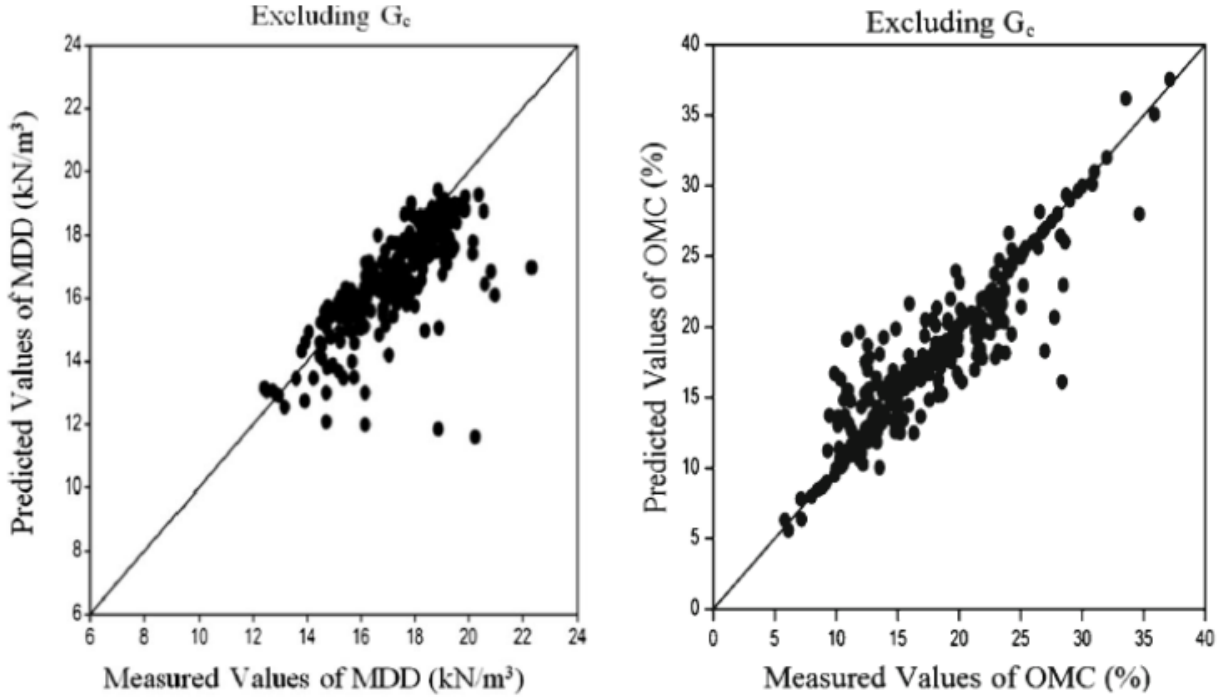

Source:Adapted from Tizpa *et al.* (2014)

A more recent study on ANN in Geotechnical Engineering was then conducted by Sharma *et al.* (2016). In their paper, they proposed a network in which it was possible to predict the elastic modulus of soils from simpler data: particle size fraction, plastic limit, liquid limit, unit weight and specific gravity. In order to do this, 90 samples were chosen from three different regions of India (Mahabaleshwar, Malshej Ghat and Lucknow) in order to have a heterogeneous set of input data, as shown in Table 6, which was then collected in the laboratory tests. In the same way as the input, the elastic modulus of the soils was also obtained in laboratory tests, by unconfined compression tests.

Once in possession of that data, the authors proposed a multiple regression analysis which had its results compared with the ones obtained from an ANN. Equation 20 shows the equation obtained from the multiple regression analysis, which had an outstanding adhesion ($R^2 = 0.95$), and had the same input variables as those used in the ANN (Figure 24).

Table 6 – Statistics of input data for Sharma *et al.* (2016) models

Parameters	**Minimum**	**Maximum**	**Mean**	**Median**	**Standard Deviation**
Gravel (%)	0.00	70.00	5.76	0.00	14.86
Sand (%)	1.00	69.00	19.90	11.00	19.26
Fines (%)	13.00	99.00	74.45	89.00	26.76
Plastic Limit (%)	13.00	43.00	25.28	25.00	7.24
Liquid Limit (%)	26.00	89.00	51.80	51.00	15.07
Unit Weight (kN/m³)	13.18	18.04	15.85	15.85	1.39
Specific Gravity	2.78	2.81	2.67	2.66	0.05
Modulus of Elasticit (MPa)	0.20	118.00	40.74	26.00	39.92

Source: Adapted from Sharma *et al.* (2016)

$$E = 291.759 - 0.723\,G - 0.815\,S - 1.673\,F + 0.115\,PL - 0.104\,LL + 8.687\,\gamma - 90.256\,SG \quad (20)$$

Where E is the elastic modulus; G is the percentage of gravel-sized particles; S is the percentage of sand-sized particles; F is the percentage of fines; PL is the plastic limit of the soil; LL is the liquid limit; γ is the unit weight of the soil (kN/m³), and SG is the specific gravity of the soil.

Compared to the multiple regression, an ANN with the architecture shown in Figure 24 was conceived using 72 samples for training and 18 for testing. The results showed an even better adhesion of the output to the real data, having obtained $R^2 = 0.99$ for training and $R^2 = 0.98$ for testing after 1,000,000 epochs (Figure 25).

Sharma *et al.* (2016) then concluded that both models have a good prediction of the elastic modulus and, although the multiple regression is simpler and more easily used, these results validate the use of ANN in the prediction of soil parameters.

Figure 24 – Architecture of ANN model proposed by Sharma *et al.* (2016)

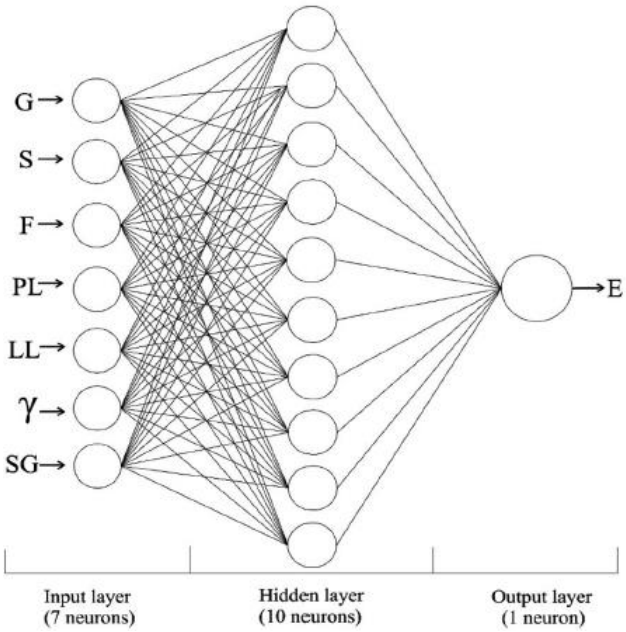

Source: Sharma *et al.* (2016)

Figure 25 – Epochs *versus* mean squared error for Sharma *et al.* (2016) model

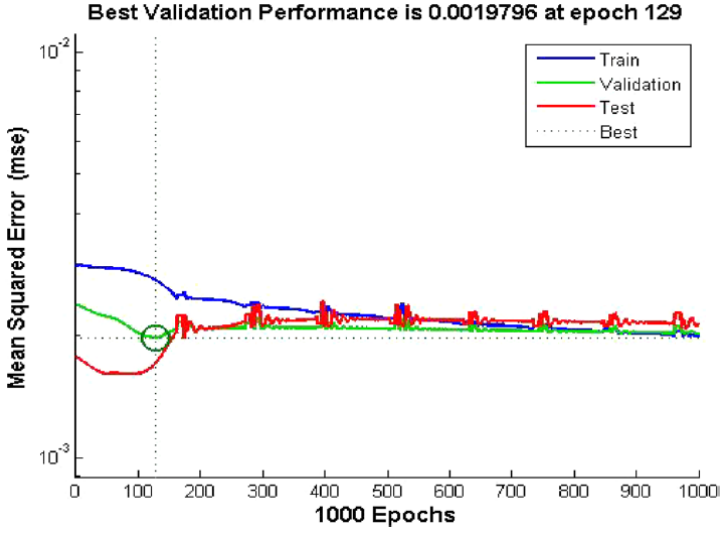

Source: Sharma *et al.* (2016)

2.3.6 Shear strength parameters prediction with the use of neural networks

In the last two decades, studies on shear strength parameter prediction with the use of neural networks were issued, all of them designed to reach better correlations between in-situ shear strength and soil properties than that from existing empirical models. By doing so, these authors intended to improve the reliability of project design. Some of these ANN models will be addressed in this subsection.

Shear strength parameters prediction of clays by means of artificial neural networks was proposed by Goktepe *et al.* (2008). In their study, the authors conducted 79 CU triaxial tests on normally consolidated plastic clays from the Antalya region in Turkey. The database, whose characteristics are shown in Table 7, presents low friction angle values and great cohesion values, which is typical for clayey soils. However, the study excluded the overburden stress, which is believed to interfere on soil resistance.

Table 7 – Goktepe *et al.* (2008) - Database characteristics

Soil	**Minimum-Maximum**
Natural moisture content, w (%)	15.80–42.90
Natural unit weight, γ_n (kN/m³)	15.20–19.42
Dry unit weights, γ_d (kN/m³)	12.94–16.08
Liquid limits, LL (%)	33.10–42.70
Plasticity limits, PL (%)	22.80–29.10
ϕ‘ (°)	2.14-21.99
c' (kPa)	31.38-127.49

Source: Adapted from Goktepe *et al.* (2008)

From the database, Goktepe *et al.* (2008) proposed linear, non-linear regression and then ANN models to estimate c’ and ϕ’ from w and PI. Equations 21 and 22 show the results of the linear regression analysis, in which ε represents the errors. The equations obtained for prediction of c’ and ϕ’ presented reasonable coefficients of correlation of 0.72 and 0.87, respectively, even though the proposed models were simple.

$$\phi' = -6.38 + 0.58 \cdot w + 0.05 \cdot PI + \varepsilon \quad (21)$$

$$c' = 1.61 - 0.03 \cdot w - 0.01 \cdot PI + \varepsilon \quad (22)$$

Non-linear multiple regression correlations were also proposed, showing slightly better results than those from equations 21 and 22. Equations 23 and 24 for cohesion and friction angle presented R^2 equal to 0.73 and 0.90, respectively, which are already satisfactory. Notwithstanding, the authors indicate the relevance of ω on the results for all models proposed from linear and non-linear regression analysis.

$$\phi' = 0.0077w^2 + 0.1305w - 0.0125PI^2 + 0.4242PI - 0.0012\ w\ PI + \varepsilon \quad (23)$$

$$c' = 0.0006w^2 - 0.0737w - 0.0002PI^2 - 0.0282PI + 0.001\ w\ PI + \varepsilon \quad (24)$$

However, Goktepe *et al.* (2008) produced further results on estimating these parameters with the use of feed-forward multilayer perceptrons (MLP). To this end, the authors proposed models using the hyperbolic tangent as an activation function for two types of learning algorithms: gradient descent with momentum term algorithm and Lavenberg-Marquardt method. First, the training was carried out using the gradient descending method for MLP with one or two hidden layers until an ANN with the architecture 2 x 70 x 2 was achieved, resulting in a better performance than the regression models. Nevertheless, Goktepe *et al.* (2008) stated that the results had failed to achieve the expected accuracy for the problem analyzed, and so another learning algorithm was used. With this in mind, the architecture 2 x 30 x 2 was chosen as the optimal, reaching $R^2 = 0.99$.

Figures 26 to 28 present the scatter graphs measured *vs* calculated for the regression analysis and ANN models. A significant improvement in generalization and accuracy is noticeable in Figure 28 when compared to the other two models, which is explained for the non-linear and complex relationship between the soil shear strength and its index parameters.

In conclusion, Goktepe *et al.* (2008) stated that the ANN model trained with the Lavenberg-Marquardt method achieved a significantly good performance in Antalya normally consolidated clays. In addition, the authors highlighted the importance of choosing a proper learning algorithm for the problem, which resulted in reasonable differences in performance of the MLP. However, the study was limited to the Antalya clays and may be unable to make good generalization for prediction of shear strength parameters for all clayey soils.

Figure 26 – Scatter graphs by soil index parameter for linear regression models: (a) ϕ x moisture content; (b) ϕ x plasticity index; (c) c x moisture content; (d) c x plasticity index

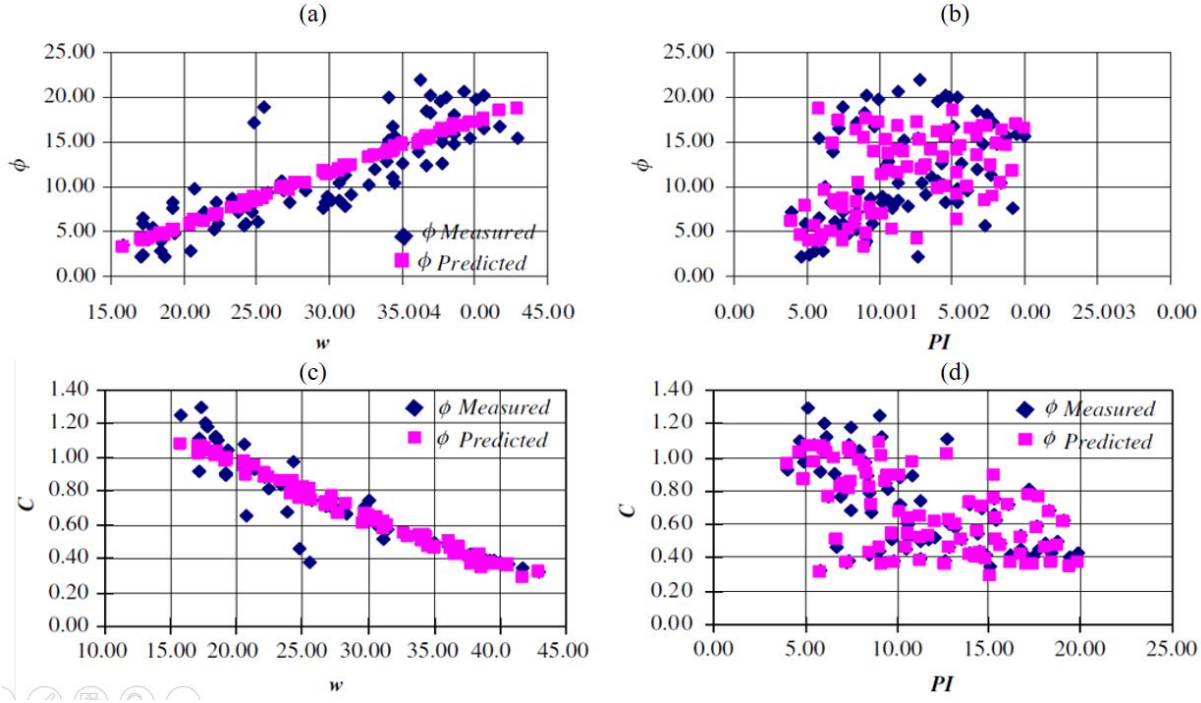

Source: Adapted from Goktepe *et al.* (2008)

Figure 27 – 3D scatter graphs by predicted variable for non-linear regression models

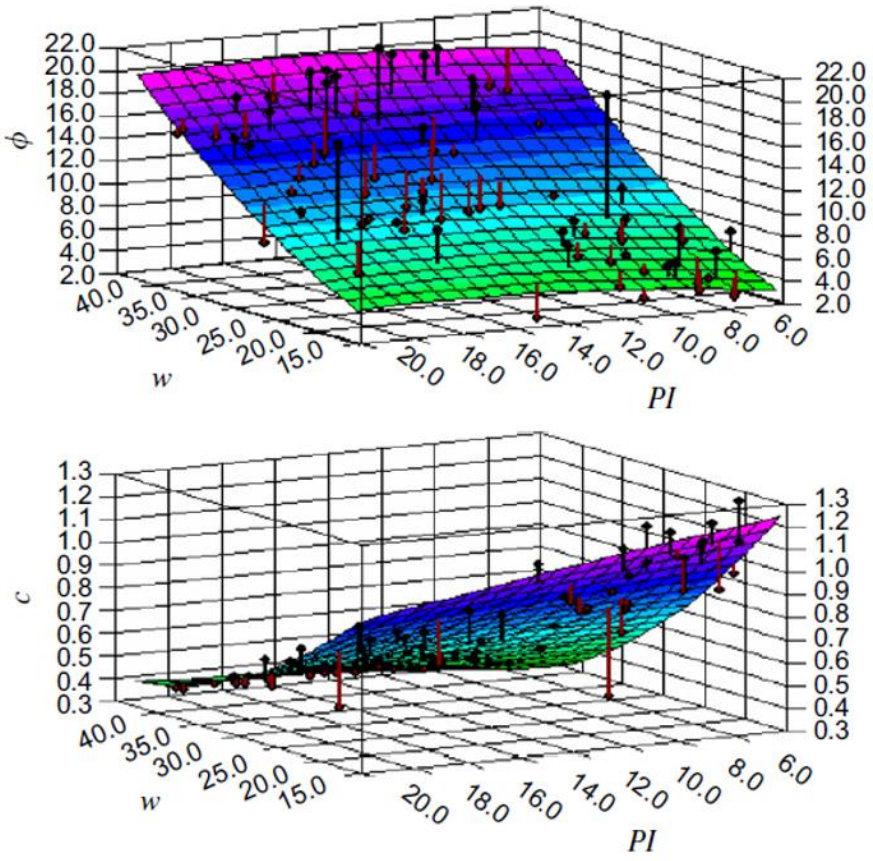

Source: Adapted from Goktepe *et al.* (2008)

Figure 28 – Scatter graphs for ANN models with different learning algorithms: (a) c prediction for ANN using gradient descent algorithm; (b) ϕ prediction for ANN using gradient descent algorithm; (c) c prediction for ANN using Lavenberg-Marquardt algorithm; (d) ϕ prediction for ANN using Lavenberg-Marquardt algorithm;

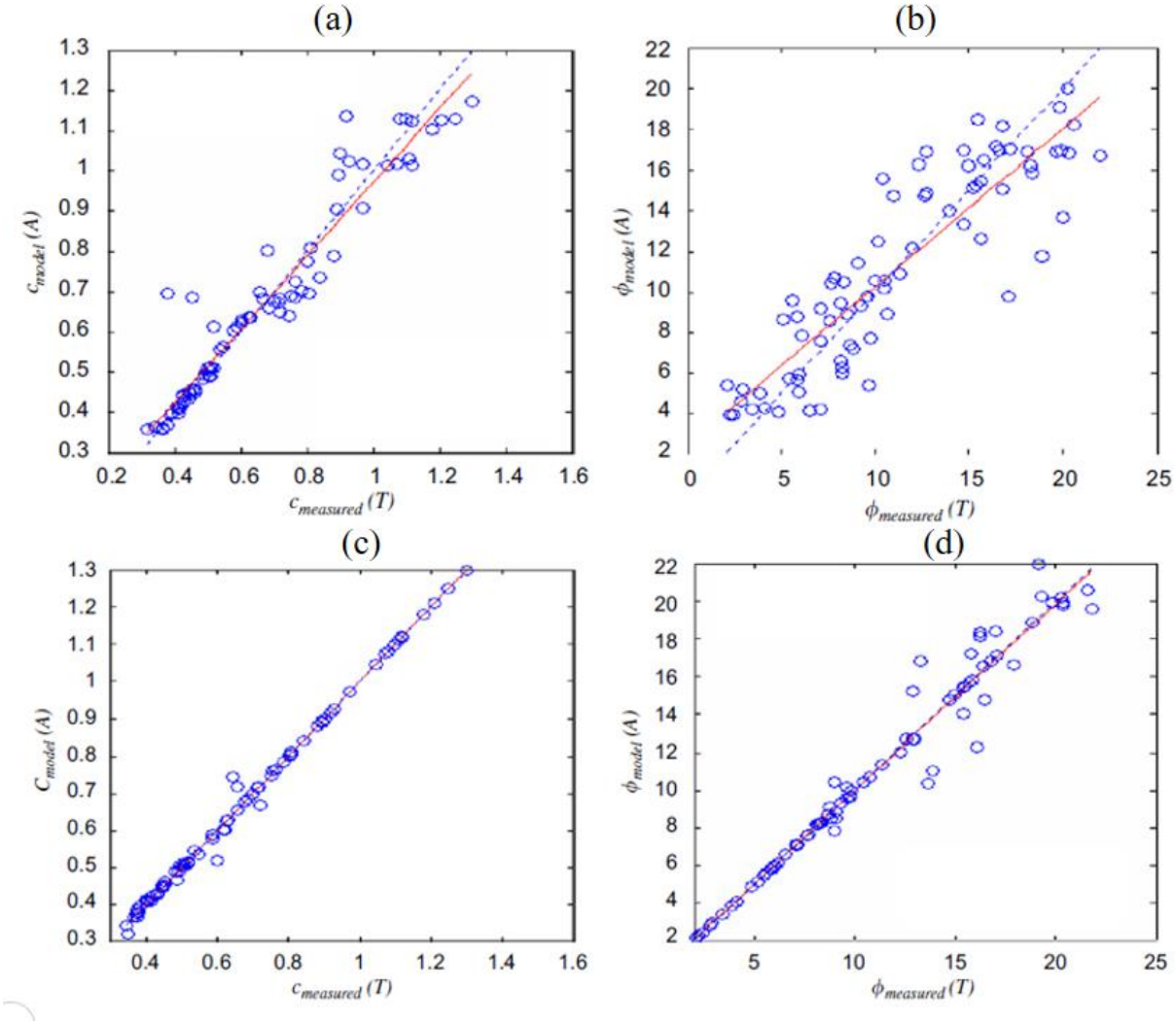

Source: Adapted from Goktepe *et al.* (2008)

In the same year, a study on the residual shear strength of clays prediction with ANN was produced by Das and Basudhar (2008). In their study they proposed various MLP with different input in order to estimate the residual friction angle of clays, since soil cohesion in a residual state is very low or inexistent, and its resistance is given in terms of residual friction angle (ϕ_r). For that matter, a total of 54 samples of volcanic ash clay (39 for training and 15 for testing), along with triaxial and soil characterization test results, were used for building an artificial neural network. Furthermore, the authors used the Bayesian regularization method looking to improve the generalization capacity of the model.

In their work, Das and Basudhar (2008) proposed a sensitivity analysis of input parameters by building four different models based on LL, CF (clay fraction), PI and ΔPI, which represents the deviation from the A-line in classification chart and is given by Equation 25. The proposed models and their results are displayed in Table 8, from which Model 4 was chosen as being the optimal for reaching the highest coefficients of correlation during both training (R^2 = 0.906) and testing (R^2 = 0.942). Moreover, the results showed that ϕ_r and ΔPI as well as ϕ_r and CF are indirectly correlated, meaning that increases in residual friction angle are caused by decreases in ΔPI and CF.

$$\Delta PI = PI - 0.73(LL - 20) \tag{25}$$

Table 8 – Das and Basudhar (2008) - Statistical performance of the models

Model	**Input parameter**	**Coefficient of correlation**	
		Training	**Testing**
Model 1	LL, CF	0.851	0.829
Model 2	LL, PI, CF	0.902	0.883
Model 3	LL, PI, CF, ΔPI	0.926	0.885
Model 4	CF, ΔPI	0.906	0.942

Source: Adapted from Das and Basudhar (2008)

Later, a study for friction angle correlation was performed with the use of a GMDH (Group Method for Data Handling) artificial neural network by Shooshpasha, Amiri and MolaAbasi (2014). The authors pointed to the option for GMDH neural networks because of its good performance when modeling complex systems in which the relationships between the variables are unknown.

Accordingly, they gathered 195 soil samples (120 used for training, 50 for testing and 25 for validation of the model) from Turkey and Taiwan after two earthquakes in 1999. The data collected were later tested in laboratory for shear strength and the results run by a GMDH ANN, which consisted of a multivariate analysis method based on analytical function in a feed-forward network. Furthermore, the input variables were chosen to represent the soil mechanical behavior: N_{60}, σ_{v0}' and FC (Fine Content). Then, various ANN were generated one after the other by means of GMDH, resulting in much complex networks at each stage.

Figures 29 and 30 provided graphs in which measured and predicted values were plotted for training and testing stages, respectively. As may be seen in those figures, the adjustment of the predicted to the measured values was satisfactory and correlations obtained were high and equal to 0.998 for training and 0.997 for testing. From these figures it may also

be found that the models underestimated ϕ' rather than overestimated it in a few cases, which favors safety. Hence, the models were simplified to the polynomial representation, which is shown in Equations 26 and 27.

$$\phi' = -3.574 - 0.183 \cdot \mathrm{FC} + 1.346 \cdot Y_1 + 0.00111 \cdot FC^2 - 0.0056 \cdot Y_1^2 + 0.00127 \cdot Y_1 \cdot FC \quad (26)$$

$$c' = 0.0006\omega^2 - 0.0737\omega - 0.0002\mathrm{PI}^2 - 0.0282\mathrm{PI} + 0.001\ \omega\ \mathrm{PI} + \varepsilon \quad (27)$$

Figure 29 – Training measured and predicted values for ϕ' prediction in a GMDH

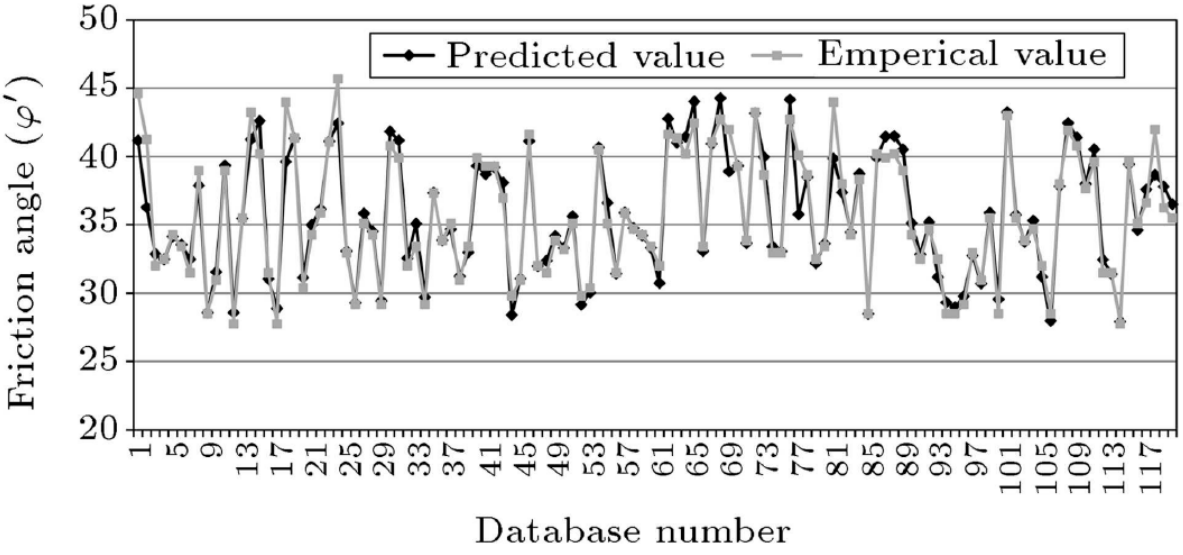

Source: Shooshpasha, Amiri and MolaAbasi (2014)

Figure 30 – Testing measured and predicted values for ϕ' prediction in a GMDH

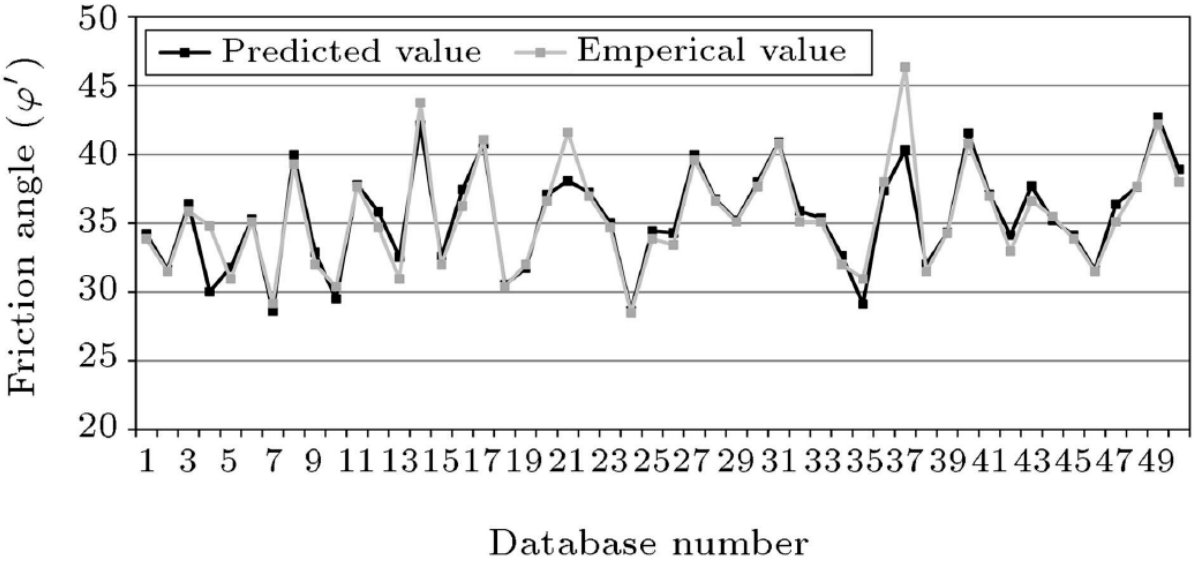

Source: Shooshpasha, Amiri and MolaAbasi (2014)

The model was then validated by running unforeseen data and comparing them to the results of commonly used correlations. Some of those results are displayed in Figure 31, from which the efficiency of the proposed ANN can be attested.

Figure 31 – Comparison of Shooshpasha, Amiri & MolaAbasi proposed ANN for ϕ' prediction with some existing correlations

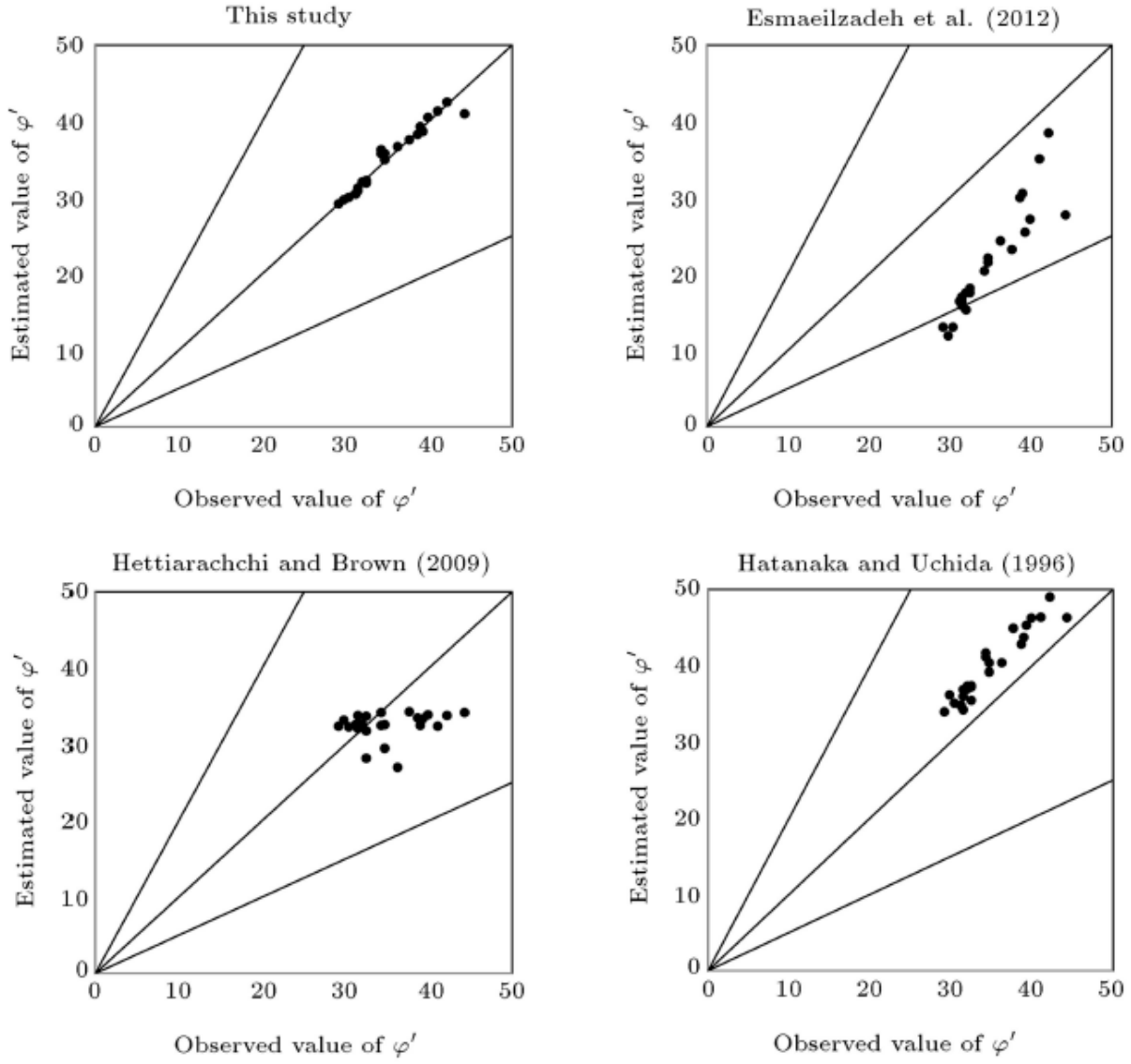

Source: Adapted from Shooshpasha, Amiri and MolaAbasi (2014)

A work on prediction of cohesion and friction angle using ANN was proposed by Braga (2014). In the work, some multiple regression-based models (RLM) and artificial neural networks (ANN) were proposed from the following input: clay (Arg), sand (Are) and silt (Sil) content, clay+silt content (arg+sil) limit of plasticity (LP), liquid limit (LL), plasticity index (PI), relative density (Ds) and moisture content (ω). In order to do so, six models were developed by arranging the input variables as shown below:

- RLM 1 and ANN 1: Arg, Sil, Are, IP and Ds.
- RLM 2 and ANN 2: Arg+sil, Are, IP and Ds.
- RLM 3 and ANN 3: Arg, Sil, Are, LL and Ds.
- RLM 4 and ANN 4: Arg+sil, Are, LL and Ds.
- RLM 5 and ANN 5: Arg+sil, Are, LL, Ds and ω.
- RLM 6 and ANN 6: Arg+sil, Are, LL, Ds and ω.

Accordingly, the data base gathered was divided into 70% samples for training and 30% for testing of the networks. The training process was carried out using the Lavemberg-Marquadt routine reaching up to 15 iterations in the process. The models were then analyzed under the responses in r (coefficient of correlation), c (Wilmont concordance index), R^2 (coefficient of determination), ME (mean error), RMSE (root mean square error) and Id (performance index, Id = r x c).

Results of the regression modelling showed a fair performance of the RLM models, which reached maximum R^2=0.58 for cohesion (model 3) and R^2=0.64 for friction angle (model 5), as shown in Table 9. In addition, Figure 32 shows the low fitting of the predicted to the measured values for c', meanwhile the results for ϕ' showed a slight improvement. Furthermore, Figure 32 illustrates that the number of samples used for c' prediction was low, which may result in good performance for the data used during development of the RLM, but also in low generalization capacity. This was highlighted in the development of the other models that used a greater number of specimen, such as RLM 2 shown in Figure 33. Similarly, model 2 for ϕ' prediction achieved very unsatisfactory results when using a wider training group, as shown in Figure 33.

Table 9 – Correlations of the models proposed by Braga (2014)

Model	**RLM**		**ANN**			
	c' R^2	**ϕ' R^2**	**c' R^2**	**Architecture**	**ϕ' R^2**	**Architecture**
Model 1	0.38	0.07	0.50	5-30-1	0.30	5-50-1
Model 2	0.39	0.06	0.54	4-50-1	0.23	4-50-1
Model 3	0.58	-	0.87	4-50-1	0.86	4-40-1
Model 4	0.23	-	0.47	4-40-2	0.25	4-40-2
Model 5	-	0.64	-	-	0.78	5-10-1
Model 6	0.27	0.32	0.69	5-20-2	0.76	5-50-1

Source: Adapted from Braga (2014)

Figure 32 – Best regression-based models proposed by Braga (2014) for c' and ϕ' prediction: (a) cohesion prediction model results; (b) friction angle prediction results

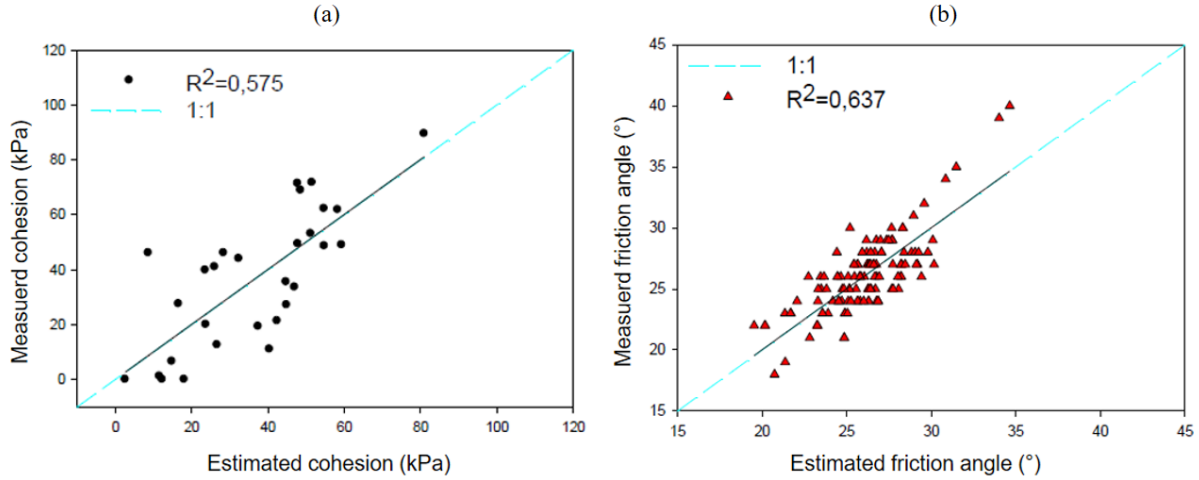

Source: Adapted from Braga (2014)

Figure 33 – Model 2 for c' and ϕ' prediction proposed by Braga (2014): (a) cohesion prediction model results; (b) friction angle prediction results

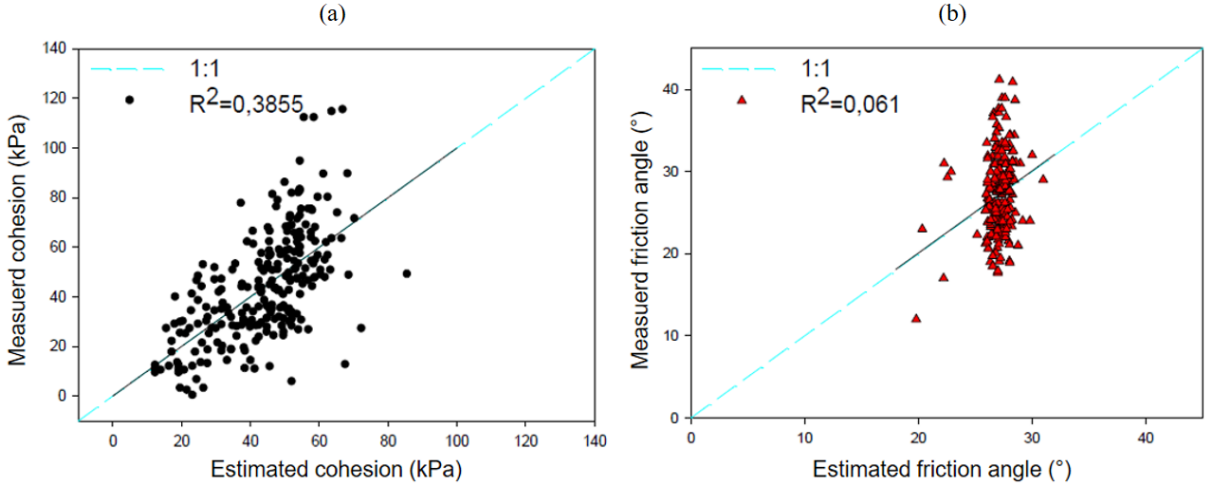

Source: Adapted from Braga (2014)

Otherwise, ANN models presented an overall better performance on shear strength parameters prediction. Table 9 shows that the best ANN models reached correlations up to 0.87 and 0.86 for c' and ϕ' prediction (model 3), respectively, overcoming the results obtained in regression modelling. However, the artificial neural networks suffered from the same generalization problem encountered in RLM when using a wider training and testing data. That is illustrated in Figures 34 and 35, as correlation decreases from model 3 to 6 from 0.87 to 0.69, for cohesion, and 0.86 to 0.76, for friction angle prediction, when widening the sample group. Haykin (2001) had already presented the influence of the size of the training and testing groups in the ANN modelling.

Figure 34 – ANN 3 results versus measured values for model proposed by Braga (2014): (a) adjustment of values for cohesion prediction; (b) adjustment of values for friction angle prediction

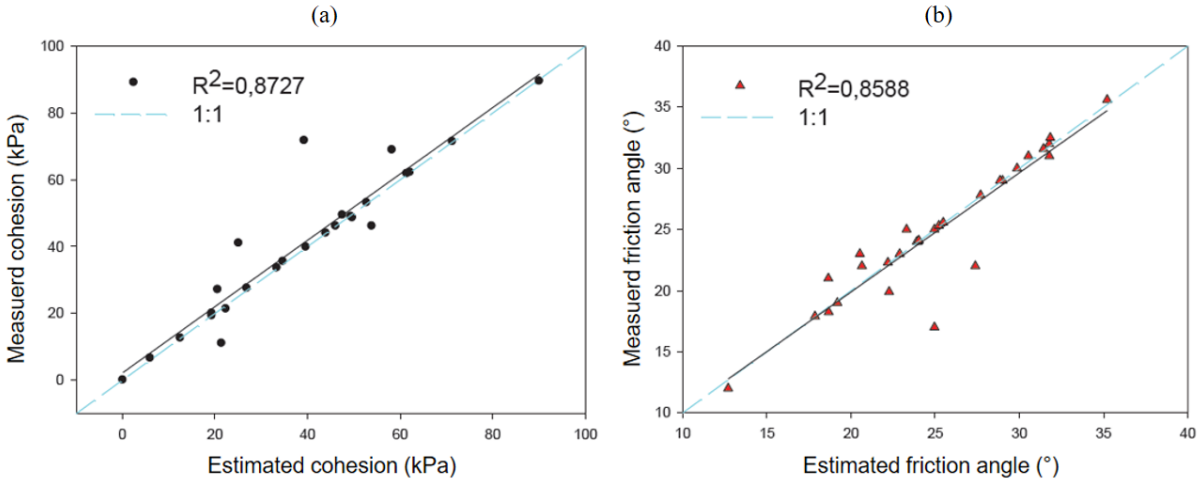

Source: Adapted from Braga (2014)

Figure 35 – ANN 6 results versus measured values for model proposed by Braga (2014) : (a) adjustment of values for cohesion prediction; (b) adjustment of values for friction angle prediction

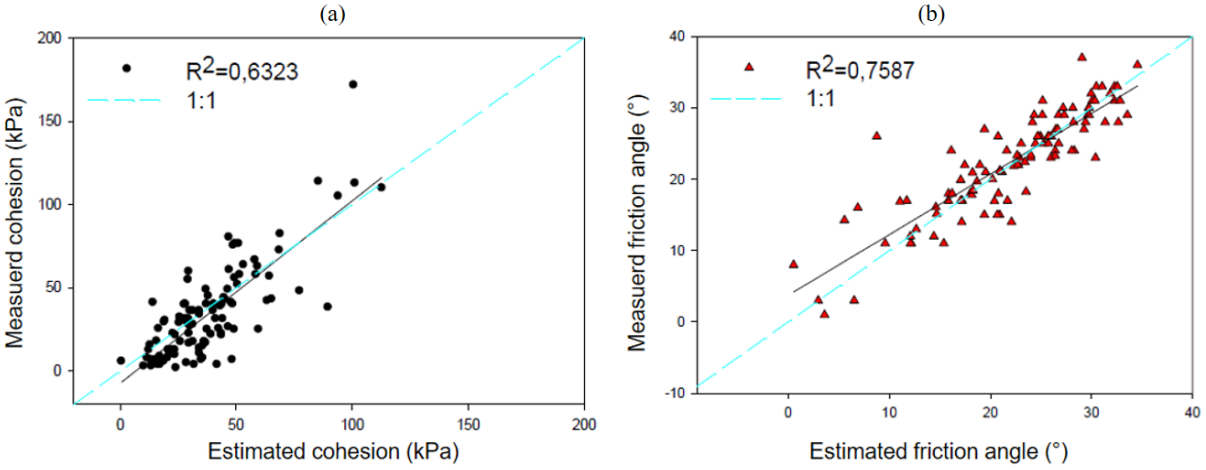

Source: Adapted from Braga (2014)

Lastly, Braga (2014) compared the performances of the models under the statistical parameters previously presented. By doing that, the models were classified as presented in Table 10 proposed by Costa (2004) *apud* Braga (2014). The results are shown in Table 11.

Table 10 – Statistical performance of the models proposed by Braga (2014)

Id	Performance
> 0.85	Great
0.76 ≥ Id ≥ 0.85	Very good
0.66 ≥ Id ≥ 0.75	Good
0.61 ≥ Id ≥ 0.65	Regular
0.51 ≥ Id ≥ 0.60	Weak
0.41 ≥ Id ≥ 0.50	Very weak
< 0.41	Poor

Source: Adapted from Braga (2014)

Table 11 – Performance of the models proposed by Braga (2014)

Model	Predicted parameter	c	r	Id	Performance
RLM 1	c'	0.9147	0.6167	0.5641	Weak
	ϕ'	0.3488	0.2722	0.0950	Poor
RLM 2	c'	0.7374	0.6229	0.4593	Very weak
	ϕ'	0.2968	0.2478	0.0735	Poor
RLM 3	c'	0.8537	0.7581	0.6472	Regular
	ϕ'	-	-	-	-
RLM 4	c'	0.5813	0.4796	0.2788	Poor
	ϕ'	-	-	-	-
RLM 5	c'	-	-	-	-
	ϕ'	0.8751	0.7935	0.6944	Good
RLM 6	c'	0.6216	0.5182	0.3221	Poor
	ϕ'	0.6846	0.5689	0.3895	Poor
ANN 1	c'	0.8074	0.7114	0.5744	Weak
	ϕ'	0.6765	0.5471	0.3701	Poor
ANN 2	c'	0.8899	0.7362	0.6551	Regular
	ϕ'	0.9338	0.4829	0.4509	Very weak
ANN 3	c'	0.9742	0.9369	0.9127	Great
	ϕ'	0.9627	0.9294	0.8948	Great
ANN 4	c'	0.8143	0.6881	0.5603	Weak
	ϕ'	0.6668	0.5098	0.3399	Poor
ANN 5	c'	-	-	-	-
	ϕ'	-	-	-	-
ANN 6	c'	0.8625	0.7974	0.69	Good
	ϕ'	0.932	0.8724	0.813	Very good

Source: Adapted from Braga (2014)

From the results in Table 11 Braga (2014) stated that the RLM did not present good enough performance, being the results obtained from the ANN superior. The results of RLM presented regular to poor performances, being model 5 the only that showed good performance in ϕ' prediction, meaning that regression-based models may not be proper for prediction of

shear strength parameters due to the behavior of data. However, the modelling using artificial neuronal networks presented results that were much more consistent with soil behavior and better generalization capacity.

3 METHODOLOGY

The following section will explain the steps taken in this study, also revealing the difficulties encountered throughout the research. Figure 36 show the stages of the work done, which were designed to obtain soil strength parameters cohesion and friction angle by creating and validating an artificial neural network based on triaxial and direct shear test results found in the literature.

Figure 36 shows that first, during data collection, a database was created by gathering data from the literature without judgment of reliability. Then, the Data Analysis and Treatment step took place by removing unreliable data and analyzing the remaining data in order to verify the input and output range so that the models' interval of confidence could be understood. Unreliable data was removed by analyzing test results and verifying if the soil classification and mechanical behavior were consistent with each other, for instance, thereby avoiding the cases where cohesionless soils were classified as clayey. Once the database was set up, the Definition of Input Parameters step was relevant because the input variables were chosen from the available parameters in a database that could represent soil mechanical behavior. With this in mind, the input variables were chosen to also guarantee their easy collection in day-to-day work. Afterwards, during ANN model implementation and regression models, the models were implemented under different network architectures and input variables followed by the proposal of a correction factor by submitting the best models to an unknown set of data in order to reduce the total quadratic errors. Then, the generated results were analyzed in the Results Analysis step by making a comparison of coefficient of correlation and match to the real results. Coupled with it, a comparison with the existing models for soil mechanical parameter prediction was made. At last, the best model was chosen in the model proposal step.

Figure 36 – Steps of model development

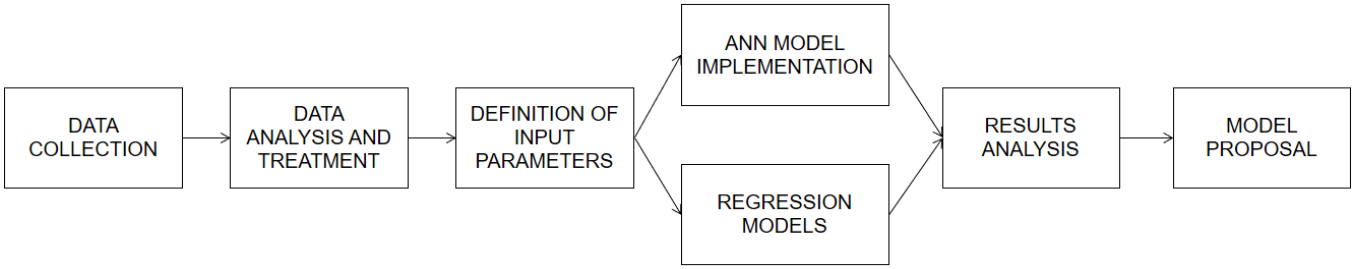

Source: Author

3.1 Data collection

Initially, a database was created based on various articles, dissertations and theses, (Dias, 1987; Coutinho, 2000; Souza Neto & Costa, 2000; Lima, 2002; Gomes, 2003; Suzuki, 2004; Lafayette, 2006; Marques, 2006; Santos, 2007; Santana, 2016; Silva, 2007; Ribeiro *et al.*, 2012; Souza, 2012; Magalhães, 2013; Abdelsalam, Suleiman & Sritharan, 2014; Souza, 2014; Camelo, Lopera & Perez, 2017); Menezes, 1990 *apud* Carvalho, 1991; Agnelli, 1997 *apud* Peixoto, 2001; Menezes, 1997 and Segantini (2000) *apud* Peixoto, 2001; Machado, 1998 *apud* Moraes, 2010; Pérez, 2014; and Gon, 2011). Appendix A lists a total of 118 samples, which were gathered for training and, in Appendix B, 50 subjects are stored for correction factor implementation, the data having been classified and treated in order to avoid false results and set input parameters.

During this study, the following premises were set:

- The database gathered is representative of the population distribution for all the variables;
- Cohesion and Friction Angle have a minimum value of 0;
- Friction angles of soils classified simply as silt or clay were adjusted to 0;
- Soils classified simply as sand had their cohesion set at 0.

Also, there were some limitations to building the database and application of the method, listed as follows:

- The database was limited to the information found in the literature;
- The collected data may not clearly represent the conditions for soils from countries other than Brazil, since most of the database consists of Brazilian data;
- It could not be checked if all information found in the literature is true, rather than just analyzing to check if the collected data had consistent results;
- The database was built on drained test data and may not represent clearly the soil behavior under undrained conditions;
- The proposed models might not predict good values outside the database range.

3.2 Definition of input variables

In order to propose adequate variables that could be used as input for soil shear strength parameters (c’ and ϕ’) prediction even when extraction of undisturbed samples and

performing field resistance tests were not feasible, there were chosen as input variables for RNA the following variables:

- x_1: N_{SPT};

- x_2: σ_{v0}';

- x_3: soil type (defined as a discrete variable, following classifications proposed in Table 14)

The choice of the N_{SPT} value as input variable was based on the possibility of its measurement at great depths and on various works that proposed correlations to obtain soil shear strength parameters, such as Decourt (1989) and Terzaghi. & Peck (1967). These authors validated the use of N_{SPT} value, attesting its efficiency as input for prediction of cohesion and friction angle as long as added it is not much influenced by changes in soil plasticity in fine-grained soils. The efficiency of using it on an ANN model was also presented in the work of Shooshpasha, Amiri & MolaAbasi (2015), achieving great results.

The overburden stress, σ_{v0}', was also chosen as entry in the model for its known influence on the shear strength of soils, which consists on a direct correlation between these variables (Lambe & Whitman 1969). This behavior is noticed during laboratory tests such as triaxial compression, in which a direct relationship between the confining stress and soil shear strength is apparent. Moreover, on ANN modelling for c' and ϕ' prediction the use of this variable was validated by Penumadu & Zhao (1999) and Shooshpasha, Amiri & MolaAbasi (2015).

However, unlike previously realized studies, an important variable was added as input for the model. Soil type was used as entry in order to give information about differences in soil mechanical behavior in a simple way. Furthermore, Morh-Coulomb criterion points to two parts governing mechanical behavior: a cohesive part, which is characteristic of fine-grained soils; and a frictional part, which is much related to coarse-grained soils. Thus, using soil type as input on soil c' and ϕ' could enhance the model efficiency.

Even though these variables are known to effect on shear strength, none of them alone can fully represent soil mechanical behavior. Figures 38, 39, 40 and 41 show that large scatters are obtained when trying to correlate any of the input variables alone with c 'or ϕ', meaning that soil shear strength is a very complex phenomenon that is affected by many soil characteristics. Thus, the ANN proposed in this work could be represented as a simplified formulation, shown in Equation 28, in which f represents the architecture, synaptic weights and bias of all neurons of the network.

$$c', \phi' = f(N_{SPT}, \sigma_{v0}', \text{soil type}) \quad (28)$$

3.3 Data statistics

It is important to have a vast database for the proper working of an Artificial Neural Network, since a higher number of training subjects results in a better generalization and helps to prevent overtraining (Haykin, 2006). For that reason, the first stage of this research was the gathering of direct shear and triaxial test results along with soil and site characterization that could be found in the literature. In order to provide a source for an ANN that could be easily implemented, the input parameters for the method were chosen so this premise is true, as shown in Figure 37.

Regarding soil characterization, some authors have proposed many formulae to predict soil behavior from various data as shown in section 2. Most of these models have assured the efficiency of using in situ test results and, for instance, Penumado and Zhao (1999) used confining effective pressure to predict mechanical behavior of cohesionless soils. Coupled with it, Lambe and Whitman (1986) added that field stress is also very important for tensile strength of soils, it is of a frictional nature. For this reason, the input variables chosen were N_{SPT}, field stress and soil type, since these features are easily collected. Figure 37 shows the diagram for input and output data of the models proposed.

Figure 37 – Input to output scheme

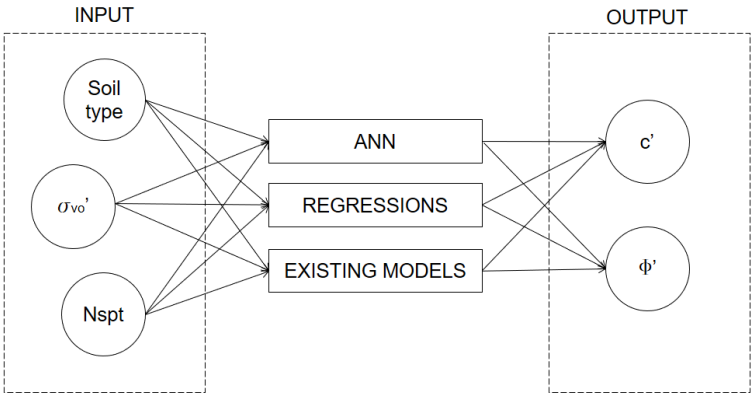

Source: Author

In order to validate the input variables, scatter graphs were plotted showing each input versus each output for all saturations, saturated and unsaturated data. However, since the results were hardly affected despite saturation, the graphs shown were plotted with data for all

saturations. Figures 38, 39, 40 and 41 show the scatter for N_{SPT} x c', σ_{v0} x c', N_{SPT} x ϕ' and σ_{v0} x ϕ', respectively.

Figures 38 and 39 show a concentration of data near the origin of the graph although a direct correlation between the variables cannot be assured for the data spreads as N_{SPT} and σ_{v0} rises. Similar behavior is seen in Figures 40 and 41 although the friction angle database does not include near zero values and most data found above is 20°, which may result in limitation for low values of ϕ' prediction. Hence, from those graphs it may be stated that each input variable alone is not enough to predict c' and ϕ'.

Figure 38 – N_{SPT} x c'

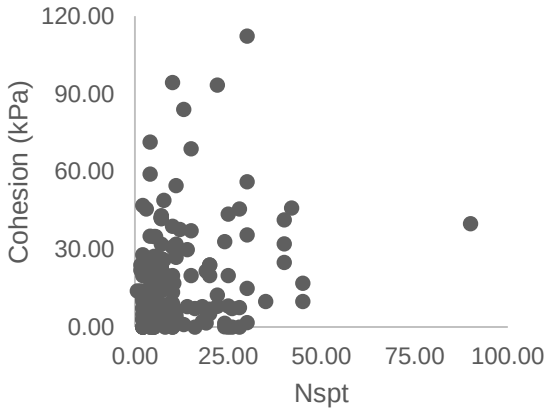

Source: Author

Figure 39 – σ_{v0} x c'

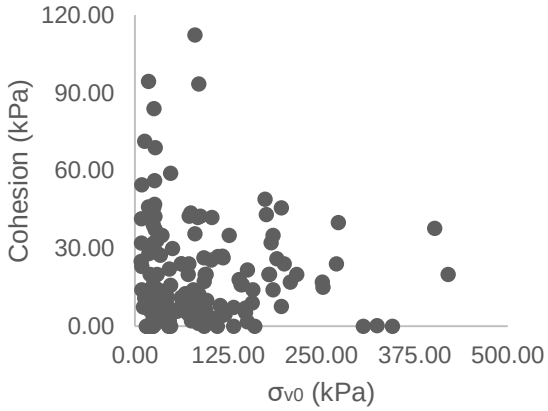

Source: Author

Figure 40 – N_{SPT} x ϕ'

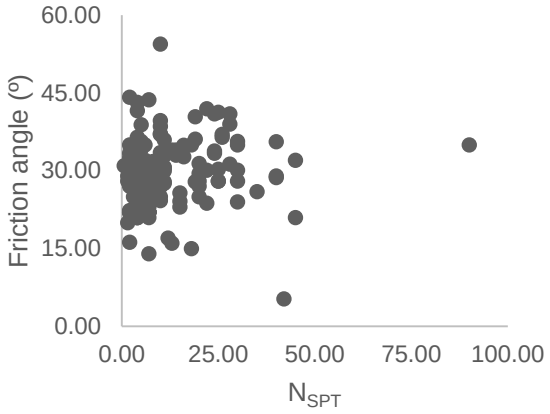

Source: Author

Figure 41 – σ_{v0} x ϕ'

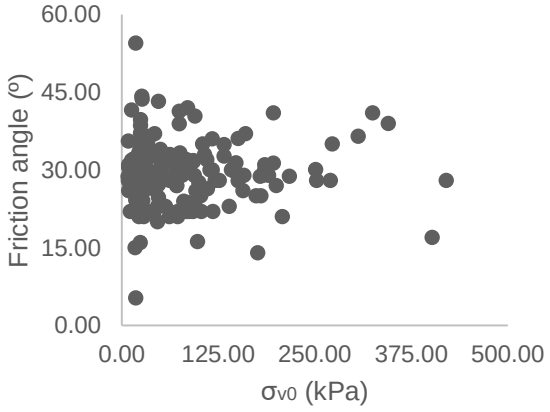

Source: Author

Thus, Figure 42 shows that the data was examined in order to assure its coverage of a wide range of soil type, and input/output variables so it could be representative and validate the model. Also, in order to understand soil content and classification interference in shear strength parameter prediction, the input data for soil type was set as "complete", defining soils for the two most abundant fractions, or "simplified", when soil was classified by its grain size that was more abundant. By doing so, complete models were used to understand whether the soil fractions of least quantity could represent relevant changes in shear strength behavior. On the other hand, simplified models were created to identify the trends for each soil group (clayey, silty or sandy). However, lateritic soil test results were excluded from the database since they have atypical behavior.

Figure 42 – Soil type distribution: (a) for soil type input defined as complete; (b) for soil type input defined as simplified

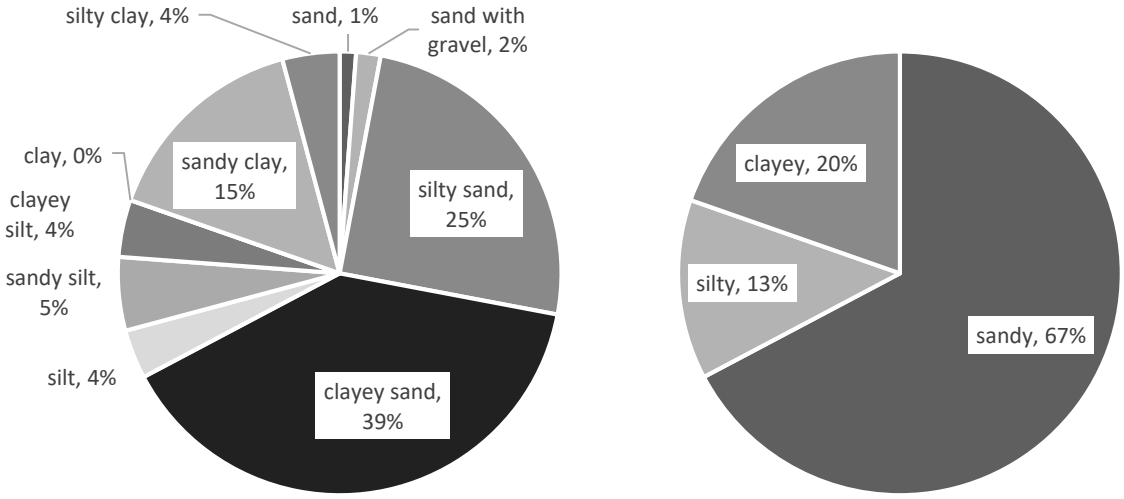

Source: Author

The statistics of the collected data show that the sampling followed the established premises and had several types of soil represented, from purely cohesive to purely frictional, also containing a large amount of mixed soils that have c' and ϕ' different to 0, which are lack in other prediction models. The histograms of the database are shown in Figures 43 to 46.

From the cohesion histogram presented in Figure 43 it may be noted that the distribution of the values had a mean of 18.39 kPa and high standard deviation of 19.69 kPa, resulting in spread of the data, which could also be noticed on the great amplitude (A = 112.3 kPa). Meanwhile, friction angle statistics presented in Figure 44 show lower scatter even though the distribution gathered values in a range of 21° to 35°. That might represent a limitation on the prediction of values outside this range.

For field stress, Figure 45 shows that approximately 90% of the data ranged from 0 kPa to 191.15 kPa. The reason for this is the difficulty to extract undisturbed samples of soils from greater depths, which might also result in a limitation on the accuracy for the models created.

For an ANN it was important to note that scatter in the database would be favorable for the research, since it would give the models better generalization capacity. However, most variables collected showed concentration around the mean, meaning that either the soils have a natural trend or that the sample was flawed. For sake of this research and based on experience, the premise was established that the database was representative of the population.

In addition, the database of the specific weight and the N_{SPT} data showed in Appendix A reveal that it contains soils of varying compactness and with organic matter content. Also, the depth and the field stress represent a large range of stress and site condition. Therefore, it may be assumed that the database may represent several field conditions and may be able to generalize the conditions of a real construction site. The complete data used for this work and their sources might be found in Appendix A.

Figure 43 – Cohesion histogram

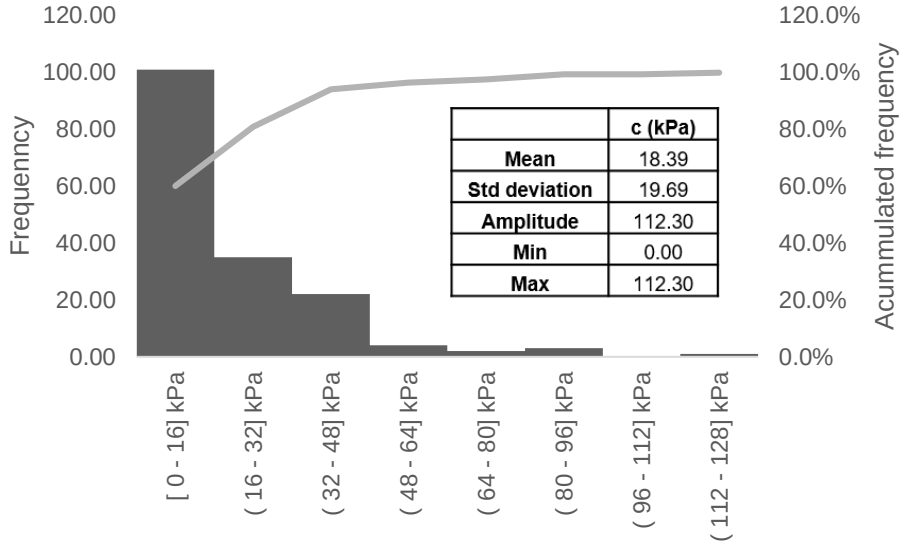

Source: Author

Figure 44 – Friction angle histogram

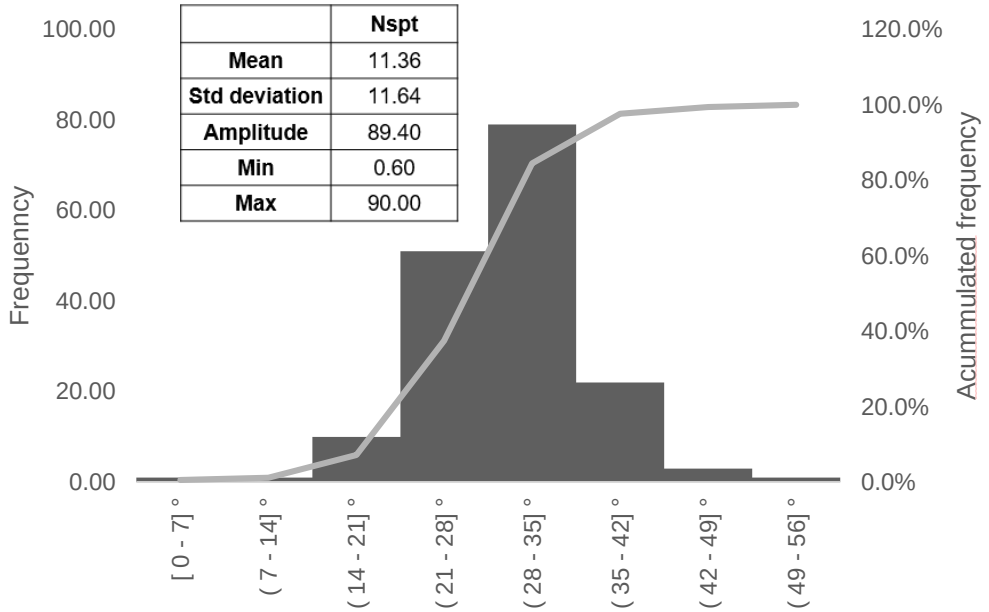

Source: Author

Figure 45 – Field stress histogram

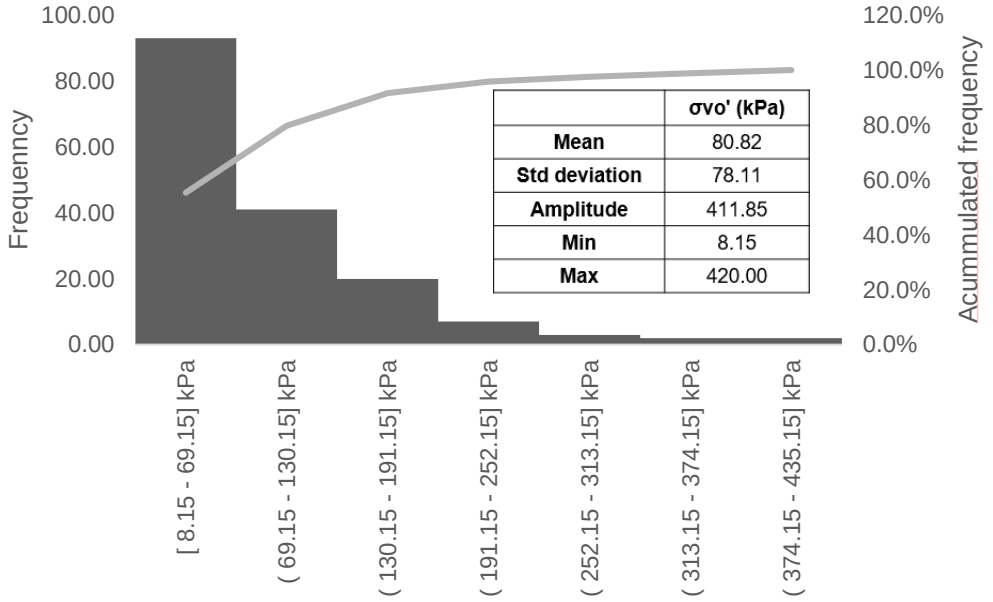

Source: Author

Figure 46 – N_{SPT} histogram

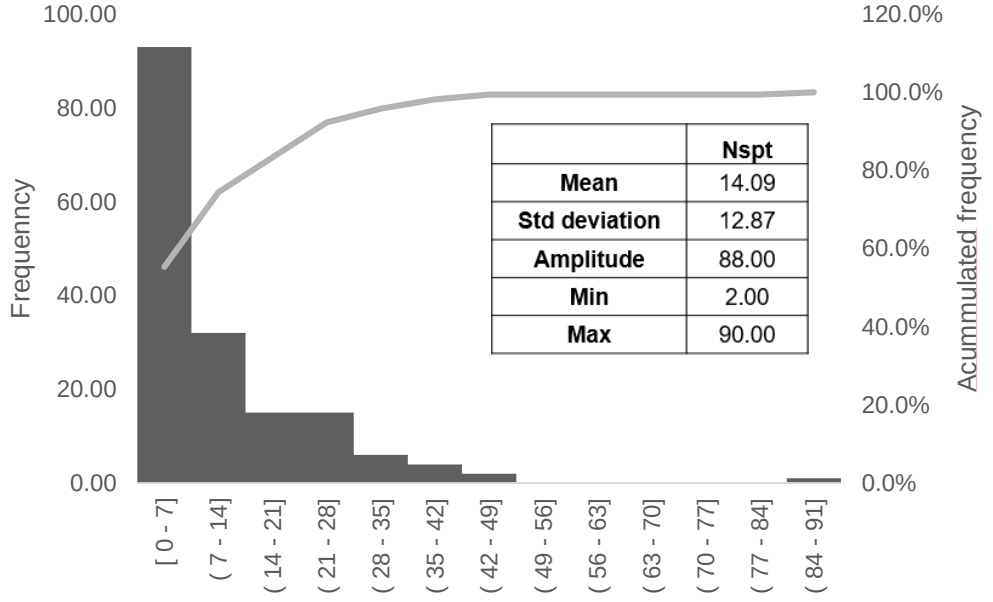

Source: Author

3.4 Model development

Networks developed by QNET are multi-layered feed-forward perceptrons, which means that the ANN built had at least one hidden layer and had a feed-forward type of error

backpropagation. The building of the ANN on QNET was made by separating data for training and validation, setting the architectures and configuring the training parameters.

The training and testing was done using a partial database, setting a total of 118 subjects (85% for training and 15% for testing) under various neural networks. Next, the best models were chosen and then used for testing the remaining 50 unknown subjects in order to set a correction factor for each soil type. The option for that distribution of data between training and testing was taken bearing in mind similar works on ANN, for example, Araujo, Dantas Neto and Souza Filho (2015), Tizpa (2014) and Samui (2012). The data was separated randomly but once completed, it was analyzed to ensure there were no flaws.

Coupled with it, two types of models were proposed from the database in order to check whether the saturation of the test results would interfere in the accuracy of the ANN prediction. Another relevant point for using various saturations was the need to verify if natural soil site conditions could be representative of the saturated test results, provided that the saturated condition is used for designing, since it is most adverse when considering the mechanical behavior. Table 12 presents the separation of examples, which was also carried out per saturation in order to develop two kinds of models. The first model, called Saturated, was developed with a database that consisted only of samples that were saturated during triaxial compression or direct shear tests; the second model, called All Saturations, included soil samples that were tested after being saturated but also specimen that were testes at natural moisture content.

Table 12 – Examples per saturation

Saturation	**Nº of training examples**	**Nº of test examples**	**Total examples**
Saturated	68	12	80
All saturations	100	18	118
Correction factor	-	-	50

Source: Author

In addition, the weights and errors were memorized and the network was automatically tested on an unknown set of data previously chosen by random sorting. Overtraining and memorization were checked through analyzing the RMS plots.

When it came to the construction of the ANN model, it began by choosing the architectures to be tested and which parameters were to be predicted at a time. For a better match, as shown in Table 13, it was decided that ANN would be modeled for prediction of c’

and ϕ’ separately by different networks, and those expected to bring the best results. In one single network, both variables were predicted at once, also testing the following characteristics:

- Number of iterations: 1,000; 10,000; 100,000; 500,000 or 1,000,000 iterations;
- Activation function: sigmoid or hyperbolic tangent;
- Soil saturation during shear strength or triaxial tests: saturated, unsaturated or all saturations;
- Type of soil classification.

Table 13 shows the summary of the tested architectures and the parameters predicted at each time, which were chosen by following the recommendation that, since the number of training cases was not large enough, the number of hidden layers and nodes should not be great because the result may imply difficulties during network memorization (Haykin, 2006). The data shown in the Architecture column in Table 13 represents the amount of neurons in each layer; for instance, a 3-5-3-1 network has three input neurons, five in the first hidden layer, three in the second hidden layer and one output neuron. Moreover, it was proposed that the neurons would be fully connected to each other on an adjacent layer in order to let the training provide the proper weights for the relevant connections, since it could not have been previously verified.

Table 13 – Architectures tested and predicted parameters

Architecture	**Output**
3-2-2	c' and ϕ’
3-3-2	c' and ϕ’
3-5-2	c' and ϕ’
3-3-3-2	c' and ϕ’
3-5-3-2	c' and ϕ’
3-2-1	c'
3-3-1	c'
3-5-1	c'
3-3-3-1	c'
3-5-3-1	c'
3-2-1	ϕ’
3-3-1	ϕ’
3-5-1	ϕ’
3-3-3-1	ϕ’
3-5-3-1	ϕ’

Source: Author

The last characteristic quoted in the previous paragraph refers to the type of classification used as entry in the model, which could be one of the two categories defined below:

- Complete: the soil was classified as specified in ABNT NBR 7250/1982 (see Figure 42 a). The models using this type of classification were expected to bring the best results.
- Simplified: classification was set due to the predominant fraction in soil, (see Figure 42 b).

Furthermore, soil classification could not be established directly as input for QNET does not support string data. For that reason, the classification was converted to numeric data, as shown in Table 14, being the input for simplified models 1, for sandy soils; 2, for silty soils; or 3, for clayey soils. On the other hand, models that used the variable soil type as complete had as input 1, for sand; 2, for sand with gravel; 3, for silty sand; and so on, as shown in Table 14.

Table 14 – Soil classification type

Simplified	**Description**	**Complete**	**Description**
1	Sandy	1	sand
		2	sand with gravel
		3	silty sand
		4	clayey sand
2	Silty	5	silt
		6	sand silt
		7	clayey silt
3	Clayey	8	clay
		9	sandy clay
		10	silty clay

Source: Author

Next, the training parameters of the neural network were set to the default configuration of QNET, in which the learning rate could vary in between the range of $0.001 < \eta < 0.300$ and the momentum was set to $\alpha = 0.800$. Another network configuration was part of the software's default configuration. For that matter, QNET automatically performed the normalization of data between the limits of 0.15 and 0.85 by adopting Equation 29.

$$\frac{X'-0.15}{0.85-0.15} = \frac{X-X_{min}}{X_{max}-X_{min}} \tag{29}$$

where X' represents the normalized variable; X is the variable to be normalized; X_{max} is the maximum value for the variable database; and X_{min} is the minimum value for the variable database.

Next, the ANN was trained by using an error correction algorithm to adjust the weight vectors of the multilayer perceptron. The algorithm in Equation 30 shows that the weights of each node were corrected by a value of Δw_{kj} resulting in a new weight for iteration in time of t+1. In its turn, the correction factor was defined by Equation 31, resulting in the combination of momentum, previous correction factor, learning rate, local gradient and output for the neuron.

$$w_{kj}(t+1) = w_{kj} + \Delta w_{kj} \tag{30}$$

$$\Delta w_{kj} = \alpha \cdot \Delta w_{kj}(t-1) + \eta \cdot \delta_k \cdot y_k \tag{31}$$

As presented by Rumelhart *et al.* (1986) *apud* Haykin (2001), the momentum acts on the previous weight correction error in order to stabilize the algorithm, while the learning rate is applied over the local gradient so the right direction is set on the error correction algorithm. Moreover, Haykin (2001) stated that the use of momentum in learning algorithms along with the learning rate is beneficial because oscillations around a minimum are avoided and the configurations are likely to achieve one of the three cases below:

- Case 1: a local minimum on the error surface is achieved after a low number of epochs;
- Case 2: the global minimum of the error surface is achieved after a low number of epochs;
- Case 3: the network converges to a configuration with good generalization capacity in a low number of epochs.

All things considered, the goal of the error correction algorithm is to achieve the weight vector configuration that stands for the minimum RMS (Root-Mean-Square) error, which is defined by the algorithm in Equation 32.

$$RMS = \sqrt{\sum \frac{(d_k - y_k)^2}{n-k}} \tag{32}$$

where n is the number of input cases and k ~~is~~ the number of output nodes.

From Equation 32 it may be stated that RMS represents a standard deviation such as behavior for the network, which is why minimizing its value may result in a lower scatter in the error distribution. Nonetheless, an RMS analysis during training may not be enough to decide on the best network for prediction of shear strength parameters. Haykin (2001) proposed that the number of epochs ran that would result in the best generalization capacity was not necessarily the one with the lower RMS during training, but rather the combination of its value for training and validation cases. Figure 47 shows the early stopping method, which consists of stopping the ANN training if a minimum global RMS is reached for validation and its value is close to the minimum for training cases.

Figure 47 – Early stopping criterion for ANN optimization

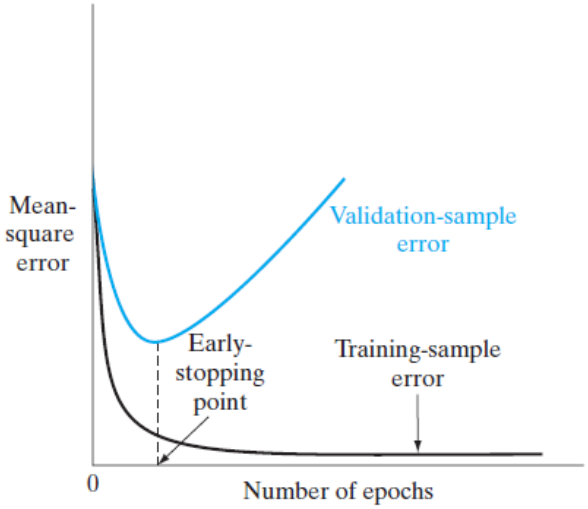

Source: Haykin (2009)

Lastly, the best model was chosen as the architecture and number of iterations resulted in the highest R^2 without overfitting. Coupled with that, the occurrence of overfitting was verified from the coefficient of correlation for training and testing so that it would happen when R^2 increased for training and decreased for testing.

3.5 Statistical regression models

In order to check the efficiency of the use of ANN to solve this problem, it was also necessary to build regression models from the same database, which resulted in simpler but less accurate analytic functions. For sake of the research, two models were proposed built on the same input variables, shown in Equations 33 and 34:

- Linear regression:

$$f(x) = \sigma'_{vo} \cdot a + N_{spt} \cdot b + SoilType \cdot c + d \quad (33)$$

- Non-linear regression:

$$f(x) = a \cdot {\sigma'_{vo}}^{\alpha} + b \cdot {N_{spt}}^{\beta} + c \cdot SoilType^{\theta} + d \quad (34)$$

where a, b, c, d, α, β and θ were the coefficients of the proposed equations and were rational numbers, while f (x) represents the output value of the model (c' or ϕ'). The goal of the built regression models was to set the coefficients proposed to achieve the maximum R^2 and minimum quadratic error.

The regression models were built on a 95% confidence level and were also used for checking the dependency of the input variables with the output values. Hence, four models were built for every output and regression type by removing the variables one at a time, as proposed by Tizpa *et al.* (2014). However, the regression models could not predict both c' and ϕ' simultaneously, and for that reason the results obtained were only compared to the ANN that predicted the same variables.

Also, existing models were used so the results could be compared to the ones obtained from using ANN. For prediction of cohesion, no drained models were used since they were lacking in the literature and instead were compared to undrained cohesion prediction models, so it was ensured that the proposed ANN could not be used under that condition. The methods tested for friction angle were Dunham (1954), Godoy (1983) and Hatanaka & Uchida (1996), meanwhile for undrained cohesion prediction the correlations compared were the ones proposed by Decourt (1989) and Terzaghi & Peck (1996). The limitations of each method were shown in section 2 of this work.

4 ANALYSIS AND DISCUSSION OF RESULTS

This chapter addresses the results of the research. At first, the results will be given for the linear and non-linear regression models created, also indicating the relevance of each input variable and choosing the best fitting model.

Next, the results of pre-trained with partially gathered data neural networks will be presented and run with the remaining set of data, so that the correction factors are generated. Then, the ANN models generated by training and testing with the full set of data will be presented, analyzed and compared to each other, so the one with the highest correlation is chosen for prediction of c' and ϕ' and both parameters simultaneously. The architecture, weights and biases will be presented and then the best results from regression and ANN will be compared.

Lastly, the results of the existing models will be compared to the best ANN models, showing their efficiency in the prediction of the strength parameters for soil mixtures.

4.1 Regression

Linear and non-linear regression models were built and tested from the database in Appendix A and will be addressed in the following sections. The results will show the accuracy of the models and data behavior. Firstly, the models were tested in a previous database that was randomly set, and then the generalization capacity of the regression models was tested with the addition of new subjects to the modeling process.

4.1.1 Linear regression

The linear regression was taken in different saturation conditions, first being made for all saturation data, showing low R^2 independently of the various input and output used. Figures 48 to 51 show, for linear regression models on c' prediction, the scatter and x=y line for functions that used different input, while Table 17 presents a summary of the results for those models. In addition, only the complete results presented in Figure 48 will be analyzed, since that was the model to reach the highest coefficient of correlation and considered all the input variables proposed.

The results of Table 17 and Figures 48 to 51 show that the removal of N_{SPT} data from the equations caused abnormal behavior in the capacity of cohesion prediction, since R^2

decreases for training and increases significantly for testing process. That information may lead to the conclusion that this variable is important on cohesion prediction models. Furthermore, there is a concentration of calculated data around a horizontal line that crosses the y-axis approximately on c'=20 kPa, showing little capacity of generalization. The results also showed a similar behavior for soil type although the increase in the coefficient of correlation happened during training while its decrease occurred during testing. This is why this variable was also set as relevant for cohesion prediction. It is also important to note that even though there was a drop in R^2 for training, testing results showed little change as the field stress was removed from the equation, although every model was unsatisfactory for c' prediction.

Table 15 – Linear regression for c' prediction for all saturations

Function	**Equation**	**Training R^2**	**Test R^2**
$c' = f(\sigma_{v0}', N_{SPT}, \text{soil type})$	$c' = -0.031\sigma'_{vo} + 0.420N_{spt} + 0.475SoilType + 13.648$	0.07	0.04
$c' = f(N_{SPT}, \text{soil type})$	$c' = 0.460N_{spt} + 1.915SoilType + 2.539$	0.05	0.04
$c' = f(\sigma_{v0}', \text{soil type})$	$c' = 0.028\sigma'_{vo} + 2.451SoilType + 3.711$	0.00	0.13
$c' = f(\sigma_{v0}', N_{SPT})$	$c' = -0.008\sigma'_{vo} + 0.644N_{spt} + 7.376$	0.05	0.01

Source: Author

Another point to be highlighted in the model proposed in Figure 48 is that the standard deviation of the absolute error is equal to 21.19 kPa, which is high especially when compared to the mean of cohesion database, $\bar{x}$ = 19.50 kPa. Thus, the lack of accuracy made this model inefficient and it could not, therefore, be used for cohesion prediction.

Figure 48 – $c' = f(\sigma_{v0}', N_{SPT}, \text{soil type})$ for all saturations

Source: Author

Figure 49 – c' = f(N_{SPT}, soil type) for all saturations

Source: Author

Figure 50 – c' = f($\sigma_{v0}^{'}$, soil type) for all saturations

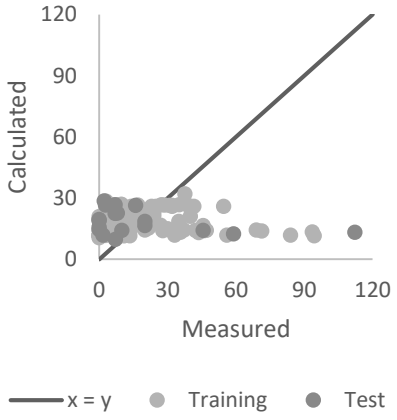

Source: Author

Figure 51 – c' = f($\sigma_{v0}^{'}$, N_{SPT}) for all saturations

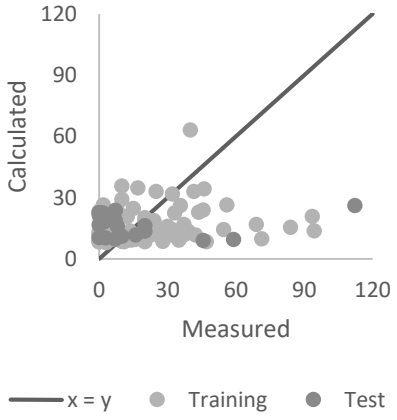

Source: Author

For friction angle, Table 18 and Figures 52 to 55 illustrate the scatter of measured versus calculated. It could be stated from Table 18 that field stress and N_{SPT} had little correlation with friction angle since R^2 for training did not change much and increased for testing when these variables were removed from the model. Also, the coefficients for σ_{v0}' in every model were low, having little influence on the output, what was questionable considering that the shear strength of soils is of frictional nature, Lambe (1969). However, it could be a result of the database characteristics, which has both saturated and unsaturated test data.

From Figure 52, it may be said that the linear regression models for friction angle prediction proposed could not generalize the data behavior since the calculated data remains around ϕ'=30º and has a high standard deviation of the absolute errors approximately equal to 6.39 kPa. However, Figures 52 to 55 showed better generalization capacity and spread of data. Moreover, the coefficients of correlation obtained from the models were 0.03 or lower for training, which show that they are unfit for the analyzed phenomena. Thus, the use of these models should be discarded for they are unreliable.

Table 16 – Linear regression for ϕ' prediction for all saturations

Function	**Equation**	**Training R^2**	**Test R^2**
$\phi' = f(\sigma_{v0}', N_{SPT}, \text{soil type})$	$\phi' = -0.006\sigma'_{vo} - 0.027N_{spt} - 0.440SoilType + 33.794$	0.03	0.09
$\phi' = f(N_{SPT}, \text{soil type})$	$\phi' = 0.293N_{spt} + 3.245SoilType + 7.343$	0.02	0.24
$\phi' = f(\sigma_{v0}', \text{soil type})$	$\phi' = 0.050\sigma'_{vo} + 3.367SoilType + 7.144$	0.03	0.11
$\phi' = f(\sigma_{v0}', N_{SPT})$	$\phi' = 0.046\sigma'_{vo} + 0.409N_{spt} + 14.405$	0.01	0.10

Source: Author

Figure 52 – $\phi' = f(\sigma_{v0}', N_{SPT}, \text{soil type})$ for all saturations

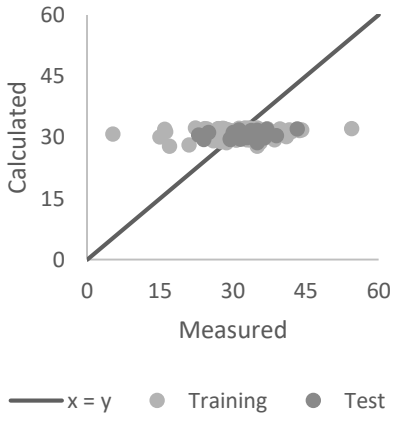

Source: Author

Figure 53 – ϕ' = f(N_{SPT}, soil type) for all saturations

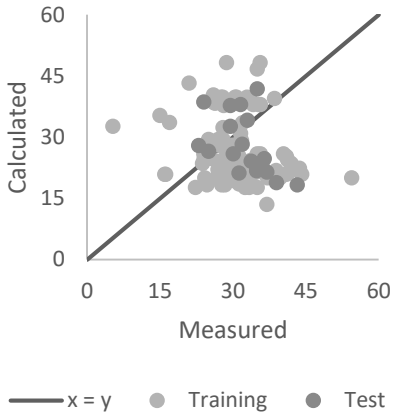

Source: Author

Figure 54 – ϕ' = f(σ_{v0}', soil type) for all saturations

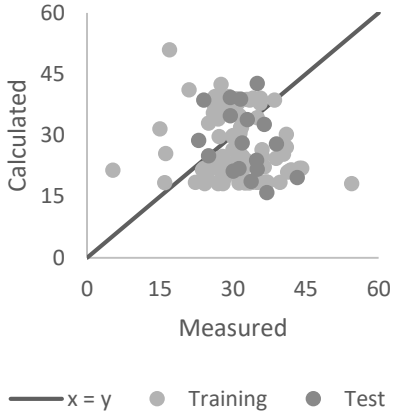

Source: Author

Figure 55 – ϕ' = f(σ_{v0}', N_{SPT}) for all saturations

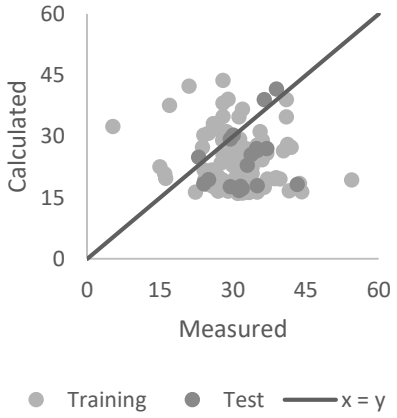

Source: Author

Yet, when using linear regression on saturated data separately for mechanical parameter prediction, the results showed greater consistency with the measured results. Nevertheless, greater improvement occurred for cohesion models, reaching R^2=0.24 during training, while for friction angle prediction all the models presented $R^2 \leq 0.04$ for the training process and $R^2 \leq 0.27$ during testing, which still makes them unreliable in both cases. For comparison purposes, Tables 19 and 20 show the summary of these results and only the scatter graphs of the best results were presented.

From Tables 19 and 20 it may be said that the field stress had little relevance on friction angle prediction since the coefficient of correlation remained stable during training when removed from the equations. Likewise, for cohesion prediction model there was no decrease of R^2 when removing this variable, which did not match the behavior of shear strength of soils claimed by Lambe (1969). By contrast, the removal of N_{SPT} from the regression equations had great interference over coefficient of correlation, being the greatest increase for the cohesion model. On the other hand, in those models shown in Table 19, removing soil type from the regression equations resulted in an improvement from R^2 = 0.11 to R^2 = 0.19 for training. Meanwhile, for friction angle model in Table 20, its removal had no effect on R^2 although it was expected that this input parameter would result in better generalization capacity. In spite of this, the use of soil type showed consistency in all models, assuring its relevance on shear strength parameters prediction.

Table 17 – Linear regression for c' prediction for saturated data

Function	**Equation**	**Training R^2**	**Test R^2**
c' = f(σ_{v0}', N_{SPT}, soil type)	$c' = 0.012\sigma'_{vo} + 0.334N_{spt} + 1.318SoilType - 0.282$	0.24	0.00
c' = f(N_{SPT}, soil type)	$c' = 0.366N_{spt} + 1.264SoilType + 0.505$	0.24	0.02
c' = f(σ_{v0}', soil type)	$c' = 0.035\sigma'_{vo} + 1.401SoilType + 2.423$	0.11	0.00
c' = f(σ_{v0}', N_{SPT})	$c' = 0.008\sigma'_{vo} + 0.341N_{spt} + 5.942$	0.19	0.10

Source: Author

Table 18 – Linear regression for ϕ' prediction for saturated data

Function	Equation	Training R^2	Test R^2
ϕ'= f(σ_{v0}', N_{SPT}, soil type)	$\phi' = 0.002\sigma'_{vo} - 0.063N_{spt} - 0.457SoilType + 31.987$	0.04	0.24
ϕ'= f(N_{SPT}, soil type)	$\phi' = -0.057N_{spt} - 0.466SoilType + 32.117$	0.04	0.20
ϕ' = f(σ_{v0}', soil type)	$\phi' = -0.002\sigma'_{vo} - 0.472SoilType + 31.479$	0.02	0.27
ϕ'= f(σ_{v0}', N_{SPT})	$\phi' = 0.003\sigma'_{vo} - 0.065N_{spt} + 29.830$	0.02	0.20

Source: Author

The scatter graphs for the best saturated models for cohesion and friction angle prediction are presented in Figures 56 and 57, respectively. From those graphs it may be found that although there was an improvement in the coefficient of correlation, the models were still inefficient since they could barely generalize data, especially when it came to friction angle prediction, resulting in roughly constant and equal to 30º output values as Figure 57 shows. Also, for ϕ' prediction, standard errors were up to 5.97º, which represents a considerable change in soil behavior.

Yet, cohesion prediction showed a better but nonetheless unreliable generalization of data, as shown in Figure 56. Saturated data presented revealed that the model did not calculate values above 15 kPa well, and had an excessive standard error of 10.67 kPa, to the extent that it results in a considerable change in soil mechanical behavior. Bearing this in mind, none of these equations obtained from linear regression could be implemented in practical uses for they could not be precise and would result in unreliable data.

Figure 56 – c' = f(σ_{v0}', N_{SPT}, soil type) for saturated data in linear regression

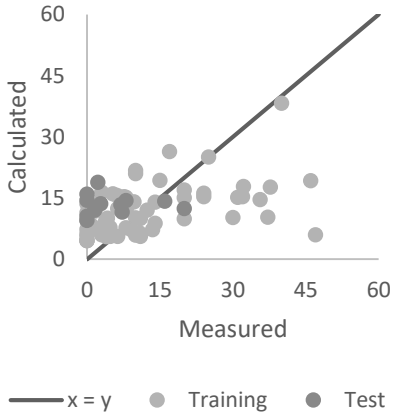

Source: Author

Figure 57 – $\phi' = f(\sigma_{v0}', N_{SPT}$, soil type) for saturated data in linear regression

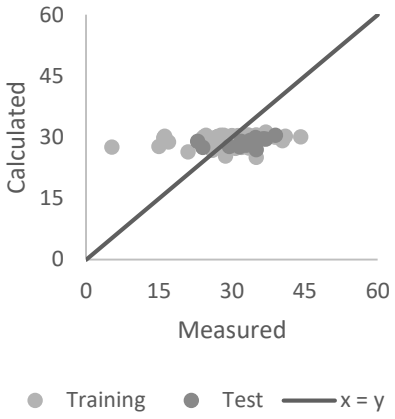

Source: Author

4.1.2 Non-linear regression

Likewise, non-linear regression was first set over saturated and all saturations data by using all the input variables proposed, and then removing one at a time. The resulting equations, their coefficient of correlation and other parameters for the models built will be addressed in this section. For simplicity's sake, only the graphs of the best fitting models will be presented.

First, the non-linear regression modeling was implemented by using the same contour conditions proposed for the previously illustrated models. Table 21 shows that all models resulted in a low coefficient of correlations, reaching a maximum of 0.12 for the training process. It can also be found from the results that the variable soil type had negative relevance on cohesion prediction, since its removal resulted in a significant increase in coefficient of correlation for the regression, which changed from 0.01 to 0.12 during training for all saturations results. On the other hand, N_{SPT} removal resulted in a drop in R^2 value from 0.07 to 0.01, although removing field stress from equations showed no effect. Keeping that in mind, it may be said that N_{SPT} is of great relevance in shear resistance parameters prediction, provided that a similar result was obtained for linear regression. This validates the use of this variable as input for the models.

Table 19 – Non-linear regression for c' prediction for all saturations

Function	Equation	Training R^2	Test R^2
c' = f(σ_{v0}', N_{SPT}, soil type)	$c' = -1.421 \cdot {\sigma'_{vo}}^{-30.453} + 1028.562 \cdot {N_{spt}}^{0.005} - 19.976 \cdot SoilType^{-18.341} - 1021.459$	0.07	0.01
c'= f(N_{SPT}, soil type)	$c' = -322.923 \cdot {N_{spt}}^{-0.019} - 22.268 \cdot SoilType^{-2.152} + 330.630$	0.07	0.00
c' = f(σ_{v0}', soil type)	$c' = -4.505 \cdot {\sigma'_{vo}}^{-73.8} - 20.059 \cdot SoilType^{-3.394} + 19.971$	0.01	0.02
c'= f(σ_{v0}', N_{SPT})	$c' = 74.197 \cdot {\sigma'_{vo}}^{-0.544} - 331.535 \cdot {N_{spt}}^{-0.023} + 324.000$	0.12	0.00

Source: Author

For friction angle prediction, results presented in Table 22 have also shown agreement with linear regression models. In both models, field stress, N_{SPT} and soil type had little influence on the predicted output, causing a drop of R^2 from 0.03, 0.03 and 0.01, respectively. Despite this, it is important to observe that none of these variables alone is able to very accurately predict soil shear strength behavior, provided that authors such as Lambe (1969) showed that the nature of shear strength of soils has many factors influencing it. In conclusion, all the models presented a low coefficient of correlation since the highest value encountered was $R^2 = 0.05$ for training.

Table 20 – Non-linear regression for ϕ' prediction for all saturations

Function	Equation	Training R^2	Test R^2
ϕ' = f(σ_{v0}', N_{SPT}, soil type)	$\phi' = -3.211 \cdot 10^{-5} \cdot {\sigma'_{vo}}^{1.962} + 50.293 \cdot {N_{spt}}^{-0.006} + 11.172 \cdot SoilType^{-0.960} - 21.423$	0.05	0.27
ϕ'= f(N_{SPT}, soil type)	$\phi' = -2712.425 \cdot {N_{spt}}^{-11.401} + 10.439 \cdot SoilType^{-0.884} + 27.850$	0.03	0.29
ϕ' = f(σ_{v0}', soil type)	$\phi' = 2.675 \cdot {\sigma'_{vo}}^{-12.880} + 10.232 \cdot SoilType^{-0.953} + 28.066$	0.03	0.28
ϕ'= f(σ_{v0}', N_{SPT})	$\phi' = -3.150 \cdot {\sigma'_{vo}}^{-59.063} - 0.137 \cdot {N_{spt}}^{0.702} + 31.615$	0.01	0.03

Source: Author

Figures 58 and 59 show the plotted scatter graphs "measured *versus* calculated" for the models for all saturations data. These figures show the behavior previously presented by linear regression models, in which there had been a low generalizing capacity. For instance, the results obtained for cohesion prediction show a high error standard deviation of 21.23 kPa, and that the proposed model has little capacity for predicting values since the predicted values remained under 40 kPa. Likewise, the friction angle prediction struggles when calculating ϕ'

out of the range of approximately 30º±2º and has an error standard deviation of 6.27. That said, none of these models is reliable for predicting shear strength parameters.

Figure 58 – c' = f(σ_{v0}', N_{SPT}, soil type) for all saturations in non-linear regression

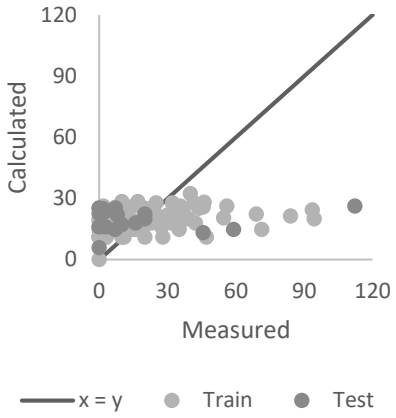

Source: Author

Figure 59 – ϕ' = f(σ_{v0}', N_{SPT}, soil type) for all saturations in non-linear regression

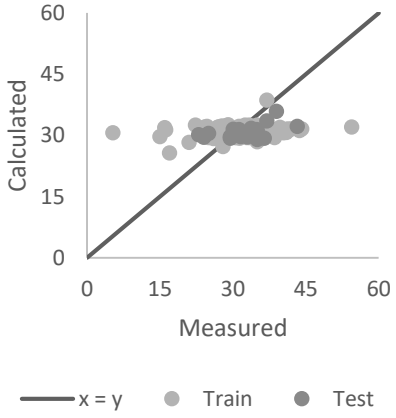

Source: Author

For saturated models, results are shown in Tables 23 and 24. Similarly, to linear regression, Table 23 shows that the removal of field stress on saturated results for cohesion prediction caused no diminishment of R^2. By contrast, N_{SPT} demonstrated great interference in saturated models, having the coefficient of correlation decreased by its removal from 0,24 to 0,05. On the other hand, the use of soil type did not show much relevance provided that its removal from equations showed improvement on coefficient of correlation. Figure 60 shows the poor adjustment of cohesion predicted data to the x = y, therefore the model is unreliable for the proposed purpose.

Table 21 – Non-linear regression for c' prediction for saturated data

Function	Equation	Training R^2	Test R^2
c' = f(σ_{v0}', N_{SPT}, soil type)	$c' = -276.191 \cdot {\sigma'_{vo}}^{-15.936} + 0.293 \cdot {N_{spt}}^{1.052} - 31.691 \cdot SoilType^{-0.320} + 26.844$	0.24	0.07
c'= f(N_{SPT}, soil type)	$c' = 0.291 \cdot {N_{spt}}^{1.055} - 32.344 \cdot SoilType^{-0.310} + 27.558$	0.24	0.07
c' = f(σ_{v0}', soil type)	$c' = 4.066 \cdot {\sigma'_{vo}}^{-6.513} - 31.778 \cdot SoilType^{-0.312} + 32.360$	0.05	0.12
c'= f(σ_{v0}', N_{SPT})	$c' = 8.871 \cdot {\sigma'_{vo}}^{-1.027} + 4.890 \cdot 10^{-4} \cdot {N_{spt}}^{2.488} + 10.237$	0.14	0.15

Source: Author

In their turn, friction angle prediction models presented an overall coefficient of correlation up to 0.10, for saturated data. Those results show low capacity of generalization, what may be verified in Figure 61 as for the calculated data remained roughly constant around 30º. In addition to that, from the results in Table 24 it may be stated that the removal of any of the proposed input from the equations resulted in less accurate models, showing diminishment of R^2 from 0.10 to 0.05.

Table 22 – Non-linear regression for ϕ' prediction for saturated data

Function	Equation	Training R^2	Test R^2
ϕ' = f(σ_{v0}', N_{SPT}, soil type)	$\phi' = 3.302 \cdot {\sigma'_{vo}}^{-6.664} + 9.082 \cdot {N_{spt}}^{-0.320} + 11.009 \cdot SoilType^{-1.324} + 22.629$	0.10	0.23
ϕ'= f(N_{SPT}, soil type)	$\phi' = 29.661 \cdot {N_{spt}}^{-19.369} + 10.785 \cdot SoilType^{-1.164} + 26.808$	0.05	0.36
ϕ' = f(σ_{v0}', soil type)	$\phi' = 2.885 \cdot {\sigma'_{vo}}^{-5.275} + 10.769 \cdot SoilType^{-1.163} + 26.798$	0.05	0.36
ϕ'= f(σ_{v0}', N_{SPT})	$\phi' = 42.509 \cdot {\sigma'_{vo}}^{-9.589} + 8.717 \cdot {N_{spt}}^{-0.342} + 24.947$	0.05	0.28

Source: Author

Figures 60 and 61 show that all the models generated from non-linear regression had low generalization capacity. Moreover, the cohesion prediction model and friction angle model in Figures 60 and 61, respectively, showed that both models failed to generalize data. However, even though the results obtained in non-linear regression appeared to be better than those obtained in linear regression, the models remained unreliable for the coefficient of correlation of $R^2 \leq 0.24$.

Figure 60 – c' = f(σ_{v0}', N_{SPT}, soil type) for saturated data in non-linear regression

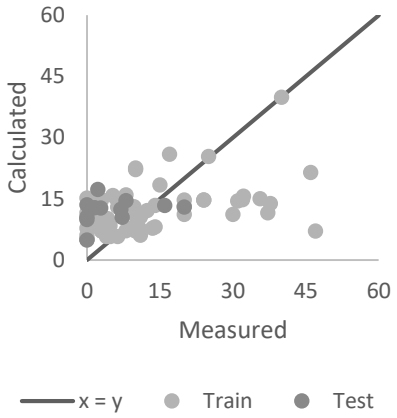

Source: Author

Figure 61 – ϕ' = f(σ_{v0}', N_{SPT}, soil type) for saturated data in non-linear regression

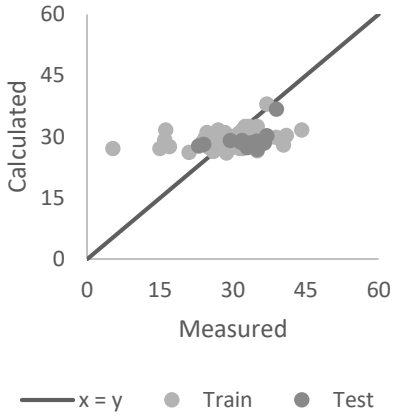

Source: Author

4.2 ANN model implementation

This section will discuss the modeling using artificial neural networks, which was done in two phases: training and testing, in which some different networks were run; and the correction factor proposal, in which the best models from the previous step were run under a new set of data in order to verify the generalization capacity, the influence of the dataset on the modeling, and to propose a correction factor to reduce the quadratic errors.

4.2.1 ANN Training and testing

The ANN training and testing using QNET consisted of adjusting the weight and biases for each networks proposed. From the overall results it was observed that the coefficients of correlation obtained from this modeling were better than those from regression models, reaching R^2 up to 0.91.

First, the networks were run under the complete and simplified soil type data to predict cohesion and friction angle simultaneously for both all saturations and saturated data. Tables 25 to 28 show the summary of the correlations obtained during training and testing per architecture, activation function, epochs and saturation of data. From the results it can be stated that the prediction of both variables was more efficient when removing the data in which the specimen was not saturated for the complete description of the soil, which was to be expected since saturated and unsaturated data have different behavior under shear strength prediction. Furthermore, the results showed improved correlation during training as the number of epochs increases, although some architectures had the testing correlation decrease simultaneously, which indicates overtraining, Haykin (2009).

From the presented tables it may be stated that the best model for prediction had the sigmoid activation function and the architecture 3-5-3-2 as shown in Table 25. However, although the overall correlation calculated by the program was approximately equal to 0.91, the individual R^2 for cohesion and friction angle was 0.75 and 0.43, respectively, which makes the model better than the regression models, but still unreliable for ϕ' prediction. Moreover, the input node interrogator showed the percentage of contribution of each variable on the output, all input having relevance on the prediction since the contributions were NI (σ'_{v0})= 36.02%, NI (N_{SPT}) = 48.22% and NI (soil type) = 15.76%. That said, the correlations and RMS versus epochs were plotted in order to check the presence of overtraining, shown in Figure 62. From the results, it may be claimed that there had not been overtraining since both R^2 for training and testing increased along with the increment in the number of epochs. In addition, comparison of model results shown in Figure 62 illustrate that the choice for simplified or complete soil type entry do not effect prediction behavior, meaning models are equivalent.

Table 23 – c' and ϕ' prediction from complete soil type using sigmoid function

	Network	Iterations	ALL SATURATIONS		SATURATED	
			Training	Testing	Training	Testing
SIGMOID	3-2-2	1,000	0.732	0.720	0.675	0.905
		10,000	0.750	0.733	0.727	0.907
		100,000	0.759	0.704	0.745	0.827
		500,000	0.763	0.660	0.746	0.744
		1,000,000	0.764	0.657	0.746	0.743
	3-3-2	1,000	0.734	0.720	0.680	0.911
		10,000	0.750	0.734	0.723	0.896
		100,000	0.767	0.709	0.776	0.846
		500,000	0.775	0.706	0.778	0.851
		1,000,000	0.775	0.688	0.781	0.899
	3-5-2	1,000	0.734	0.720	0.689	0.902
		10,000	0.749	0.737	0.724	0.900
		100,000	0.786	0.733	0.793	0.827
		500,000	0.800	0.711	0.807	0.839
		1,000,000	0.803	0.713	0.820	0.867
	3-3-3-2	1,000	0.732	0.720	0.640	0.915
		10,000	0.732	0.720	0.722	0.885
		100,000	0.775	0.701	0.784	0.856
		500,000	0.809	0.649	0.851	0.494
		1,000,000	0.816	0.638	0.864	0.597
	3-5-3-2	1,000	0.732	0.720	0.640	0.915
		10,000	0.740	0.716	0.722	0.886
		100,000	0.792	0.693	0.795	0.821
		500,000	0.817	0.686	0.885	0.895
		1,000,000	0.824	0.657	0.907	0.907

Source: Author

Table 24 – c' and ϕ' prediction from complete soil type using hyperbolic function

Networks		Iterations	ALL SATURATIONS		SATURATED	
			Training	Testing	Training	Testing
HYPERBOLIC TANGENT	3-2-2	1,000	0.747	0.723	0.721	0.884
		10,000	0.756	0.730	0.739	0.906
		100,000	0.763	0.662	0.746	0.747
		500,000	0.764	0.655	0.746	0.747
		1,000,000	0.764	0.655	0.746	0.749
	3-3-2	1,000	0.746	0.720	0.722	0.891
		10,000	0.756	0.730	0.742	0.905
		100,000	0.774	0.732	0.757	0.732
		500,000	0.776	0.711	0.767	0.739
		1,000,000	0.776	0.704	0.768	0.725
	3-5-2	1,000	0.748	0.733	0.722	0.893
		10,000	0.763	0.727	0.749	0.892
		100,000	0.792	0.716	0.806	0.872
		500,000	0.797	0.706	0.828	0.717
		1,000,000	0.799	0.696	0.839	0.587
	3-3-3-2	1,000	0.734	0.722	0.642	0.916
		10,000	0.765	0.726	0.771	0.863
		100,000	0.800	0.621	0.803	0.851
		500,000	0.814	0.676	0.826	0.362
		1,000,000	0.819	0.686	0.833	0.352
	3-5-3-2	1,000	0.733	0.720	0.689	0.904
		10,000	0.756	0.734	0.774	0.868
		100,000	0.808	0.741	0.833	0.856
		500,000	0.824	0.724	0.859	0.897
		1,000,000	0.828	0.738	0.870	0.866

Source: Author

Table 25 – c' and ϕ' prediction from simplified soil type using sigmoid function

Networks		Iterations	ALL SATURATIONS		SATURATED	
			Training	Testing	Training	Testing
SIGMOID	3-2-2	1,000	0.734	0.722	0.652	0.918
		10,000	0.749	0.736	0.717	0.883
		100,000	0.758	0.703	0.724	0.881
		500,000	0.763	0.671	0.733	0.845
		1,000,000	0.765	0.656	0.761	0.856
	3-3-2	1,000	0.735	0.717	0.686	0.909
		10,000	0.748	0.734	0.718	0.892
		100,000	0.762	0.730	0.757	0.882
		500,000	0.765	0.717	0.783	0.908
		1,000,000	0.766	0.713	0.785	0.911
	3-5-2	1,000	0.736	0.718	0.689	0.911
		10,000	0.749	0.735	0.718	0.895
		100,000	0.782	0.720	0.781	0.857
		500,000	0.794	0.704	0.789	0.853
		1,000,000	0.795	0.697	0.809	0.879
	3-3-3-2	1,000	0.732	0.720	0.640	0.915
		10,000	0.740	0.713	0.717	0.883
		100,000	0.761	0.704	0.782	0.918
		500,000	0.795	0.729	0.858	0.751
		1,000,000	0.805	0.730	0.860	0.857
	3-5-3-2	1,000	0.732	0.720	0.640	0.916
		10,000	0.733	0.721	0.717	0.883
		100,000	0.766	0.712	0.778	0.897
		500,000	0.794	0.696	0.847	0.559
		1,000,000	0.798	0.727	0.852	0.370

Source: Author

Table 26 – c' and ϕ' prediction from simplified soil type using hyperbolic function

Networks		Iterations	ALL SATURATIONS		SATURATED	
			Training	Testing	Training	Testing
HYPERBOLIC TANGENT	3-2-2	1,000	0.747	0.733	0.718	0.891
		10,000	0.752	0.730	0.724	0.885
		100,000	0.763	0.673	0.731	0.852
		500,000	0.765	0.650	0.766	0.859
		1,000,000	0.765	0.650	0.769	0.862
	3-3-2	1,000	0.748	0.734	0.717	0.888
		10,000	0.760	0.717	0.746	0.860
		100,000	0.772	0.698	0.772	0.882
		500,000	0.775	0.681	0.782	0.853
		1,000,000	0.779	0.712	0.782	0.852
	3-5-2	1,000	0.747	0.731	0.717	0.892
		10,000	0.768	0.724	0.730	0.881
		100,000	0.793	0.731	0.791	0.883
		500,000	0.794	0.710	0.811	0.891
		1,000,000	0.795	0.702	0.812	0.890
	3-3-3-2	1,000	0.733	0.723	0.714	0.878
		10,000	0.748	0.739	0.742	0.851
		100,000	0.788	0.701	0.823	0.929
		500,000	0.807	0.711	0.850	0.835
		1,000,000	0.811	0.712	0.853	0.733
	3-5-3-2	1,000	0.734	0.719	0.704	0.891
		10,000	0.760	0.722	0.741	0.900
		100,000	0.803	0.677	0.858	0.867
		500,000	0.812	0.689	0.873	0.746
		1,000,000	0.840	0.721	0.879	0.806

Source: Author

Figure 62 – Training and testing for model Sigmoid 3-5-3-2 for c’ and ϕ’: (a) training; (b) testing

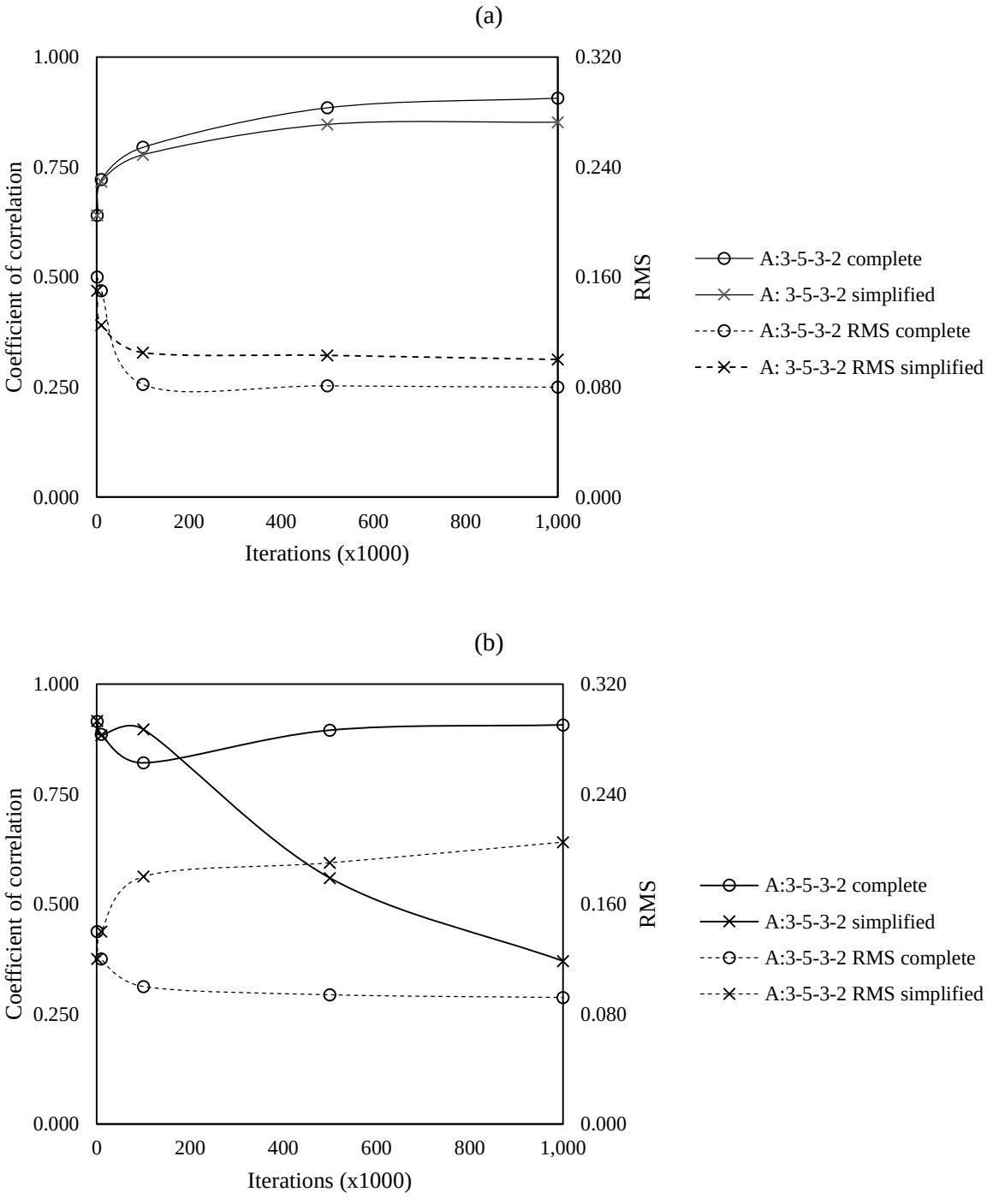

Source: Author

Another key to observe in the model was its capability to predict the shear strength parameters for all soil types. This may be verified in Table 29, which shows the coefficient of correlation for each soil type prediction, the proposed model having shown good agreement

with sandy, silty and clayey soils for cohesion prediction while friction angle prediction showed poor results, not to mention that errors reached up to 31.19 kPa and 13.25° for cohesion and friction angle, respectively, as shown in Figures 63 and 64. Nevertheless, the mean errors for the model were considerably low, making it partially reliable on prediction, although Table 29 also shows that the model completely failed to predict the friction angle for clayey soils, achieving $R^2 = 0.01$, and having unsatisfactory results for silty and sandy soils, reaching errors up to 9 kPa, consisting of considerable change in mechanical behavior.

Table 27 – c' and ϕ' prediction R^2 per soil type for network Sigmoid 3-5-3-2

Soil type	**R^2**		**Mean error**	
	c'	**ϕ'**	**c' (kPa)**	**ϕ' (°)**
All types	0.75	0.43	3.71	3.44
Sandy	0.80	0.48	3.12	3.40
Silty	0.59	0.51	5.08	3.04
Clayey	0.69	0.01	4.26	4.22

Source: Author

Figures 63 and 64 show adjustment of friction angle and cohesion prediction to measured values, respectively, from which it was found that the ANN model was more accurate than all the linear and non-linear regression models. Figures 63 and 64 also show that the proposed ANN was able to understand and predict soil mechanical behavior, as observed in the concentration of data around the x=y line, whereas the best regression models had data clustered around a constant value.

Next, the correction factor was proposed from an unknown database of 50 samples that had not been used for training and testing. Results of correction factor proposal did not represent an overall improvement for the proposed ANN model for c' and ϕ', having shown better agreement only for sandy soils when predicting the friction angle. Figure 65 shows the raw data and application of a correction factor of CF = 1.08 for sandy soils during the ϕ' prediction, resulting in a drop in the quadratic errors for both the data used for training and testing, having Σe^2 reduced from 1139.52 to 269.68, and the correction factor database. Moreover, there was also a decrease in error standard deviation of training and testing dataset from 4.76 to 0.33 and increase of the mean error, although R^2 remained equals to 0.48 despite this. The summary of the results for training and testing dataset is shown in Table 30, but the correction for silty and clayey soils resulted in loss of generalization capacity for the friction angle prediction and none of the results showed improvement for c' prediction.

Table 28 – ϕ' prediction statistics for sandy soils before and after CF implementation for network Sigmoid 3-5-3-2

Error Statistics	Raw	Corrected
$\bar{e}$	0.39	2.28
σ	4.76	0.33
Σe^2	1.139.52	269.68
CF	1.00	1.08

Source: Author

Figure 63 – Adjustment of data for model Sigmoid 3-5-3-2 on friction angle prediction

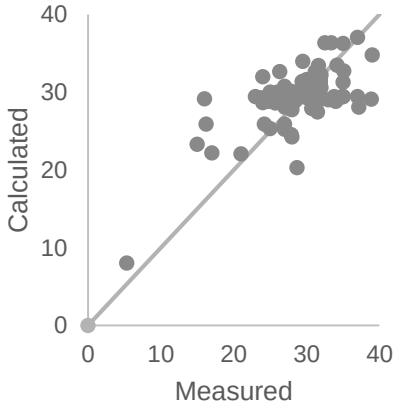

Source: Author

Figure 64 – Adjustment of data for model Sigmoid 3-5-3-2 on cohesion prediction

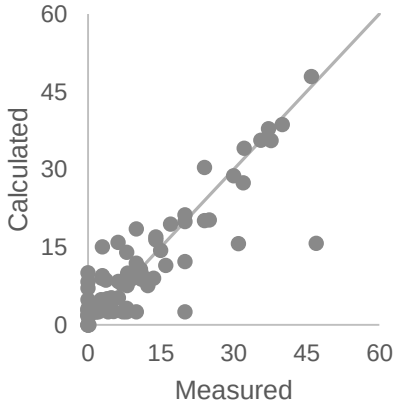

Source: Author

All things considered, even though the model proposed resulted in low mean errors, it failed to achieve satisfactory correlation for prediction of friction angle based on the data, which may prejudice its practical use. However, its use on prediction of cohesion achieved good

results. Bearing this in mind, the accuracy for predicting both variables simultaneously was questioned, making it necessary to build new models.

Figure 65 – Adjustment of corrected values of sandy soils for model Sigmoid 3-5-3-2 on friction angle prediction

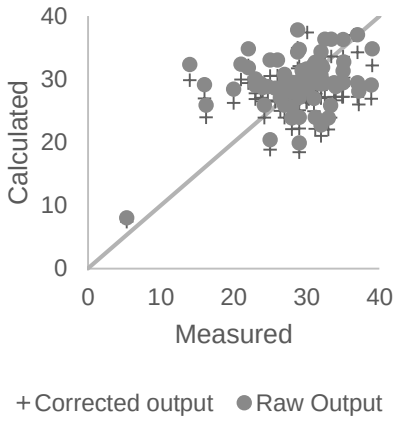

Source: Author

Accordingly, artificial neural networks were built, in which the cohesion and friction angle were predicted separately in an attempt to obtain better results than those obtained from a single ANN. Firstly, the general correlation results obtained at each ANN built for cohesion prediction are presented in Tables 31 to 34, showing that the overall results with complete soil description were much better than those with simplified soil type input, and the best correlation was obtained by network that used the saturated database, had the 3-3-3-1 architecture, hyperbolic function and complete description of the soil type. From the tables presented it could be claimed that the neural networks built with the sigmoid function failed to generalize during testing, to the extent that the correlations dropped from 0.77 to 0.02 for the same architecture and number of iterations. In addition, the results for a simplified soil type also showed a rough decrease, reaching correlations down to 0.47 for a 3-3-3-1 architecture using hyperbolic activation function and saturated data. However, results from a single network for prediction of both cohesion and friction angle simultaneously showed better accuracy and generalization capacity by using sigmoid functions, thus the option for an activation function is not deterministic but rather depends on the simulated problem.

Table 29 – c' prediction from complete soil type using sigmoid function

	Networks	Iterations	ALL SATURATIONS		SATURATED	
			Training	Testing	Training	Testing
SIGMOID	3-2-2	1,000	0.253	0.132	0.462	0.079
		10,000	0.258	0.208	0.491	-0.036
		100,000	0.359	-0.051	0.556	0.140
		500,000	0.384	-0.275	0.561	0.069
		1,000,000	0.385	-0.279	0.561	0.067
	3-3-2	1,000	0.205	-0.114	0.454	-0.039
		10,000	0.260	0.201	0.492	-0.027
		100,000	0.430	0.158	0.639	0.046
		500,000	0.453	0.163	0.646	0.061
		1,000,000	0.461	0.134	0.649	0.049
	3-5-2	1,000	0.235	-0.042	0.464	-0.092
		10,000	0.259	0.233	0.491	-0.034
		100,000	0.429	0.184	0.658	0.046
		500,000	0.483	0.101	0.755	0.163
		1,000,000	0.511	0.223	0.767	0.247
	3-3-3-2	1,000	0.048	-0.213	0.442	0.000
		10,000	0.145	-0.219	0.489	-0.063
		100,000	0.385	-0.064	0.641	0.044
		500,000	0.502	0.061	0.652	-0.063
		1,000,000	0.520	0.152	0.798	0.024
	3-5-3-2	1,000	0.240	-0.008	0.407	0.096
		10,000	0.249	0.010	0.490	-0.039
		100,000	0.427	0.172	0.663	0.042
		500,000	0.546	-0.037	0.826	0.378
		1,000,000	0.568	0.078	0.845	0.154

Source: Author

Table 30 – c' prediction from complete soil type using hyperbolic function

	Networks	Iterations	ALL SATURATIONS		SATURATED	
			Training	Testing	Training	Testing
HYPERBOLIC TANGENT	3-2-2	1,000	0.258	0.201	0.490	-0.045
		10,000	0.294	0.146	0.526	0.249
		100,000	0.384	-0.268	0.560	0.074
		500,000	0.385	-0.275	0.561	0.073
		1,000,000	0.386	-0.273	0.561	0.077
	3-3-2	1,000	0.256	0.210	0.490	-0.044
		10,000	0.331	0.130	0.519	0.193
		100,000	0.449	0.166	0.640	0.040
		500,000	0.463	0.116	0.650	0.042
		1,000,000	0.464	0.109	0.650	0.040
	3-5-2	1,000	0.257	0.173	0.492	-0.035
		10,000	0.337	0.105	0.636	0.048
		100,000	0.479	0.025	0.726	0.047
		500,000	0.509	-0.005	0.791	0.199
		1,000,000	0.535	-0.059	0.803	0.190
	3-3-3-2	1,000	0.110	-0.294	0.324	0.372
		10,000	0.327	0.143	0.523	0.235
		100,000	0.511	0.042	0.649	-0.012
		500,000	0.545	0.084	0.851	0.794
		1,000,000	0.562	0.056	0.854	0.774
	3-5-3-2	1,000	0.120	-0.178	0.086	0.371
		10,000	0.273	0.083	0.631	0.077
		100,000	0.511	-0.107	0.852	0.236
		500,000	0.686	0.043	0.862	0.225
		1,000,000	0.707	0.044	0.863	0.285

Source: Author

Table 31 – c' prediction from simplified soil type using sigmoid function

	Network	Iterations	ALL SATURATIONS		SATURATED	
			Training	Testing	Training	Testing
SIGMOID	3-2-2	1,000	0.140	-0.123	0.434	0.039
		10,000	0.257	0.238	0.480	-0.055
		100,000	0.349	-0.008	0.564	0.030
		500,000	0.380	-0.211	0.566	0.079
		1,000,000	0.384	-0.252	0.566	0.081
	3-3-2	1,000	0.224	-0.126	0.441	0.043
		10,000	0.257	0.235	0.479	-0.055
		100,000	0.382	-0.031	0.570	0.137
		500,000	0.419	0.072	0.590	0.217
		1,000,000	0.423	0.047	0.612	0.297
	3-5-2	1,000	0.174	-0.146	0.436	0.108
		10,000	0.256	0.245	0.479	-0.053
		100,000	0.384	0.021	0.609	0.043
		500,000	0.446	0.069	0.664	0.240
		1,000,000	0.462	0.020	0.679	0.370
	3-3-3-2	1,000	0.099	-0.242	-0.346	0.000
		10,000	0.154	-0.305	0.479	-0.066
		100,000	0.380	-0.041	0.575	0.142
		500,000	0.489	0.358	0.761	0.021
		1,000,000	0.526	0.472	0.794	-0.014
	3-5-3-2	1,000	0.157	-0.127	0.139	-0.398
		10,000	0.186	-0.192	0.480	-0.058
		100,000	0.372	-0.068	0.571	0.135
		500,000	0.455	0.016	0.757	-0.189
		1,000,000	0.574	0.328	0.765	-0.177

Source: Author

Table 32 – c' prediction from simplified soil type using hyperbolic function

Network		Iterations	ALL SATURATIONS		SATURATED	
			Training	Testing	Training	Testing
HYPERBOLIC TANGENT	3-2-2	1,000	0.257	0.220	0.479	-0.061
		10,000	0.280	0.182	0.480	-0.065
		100,000	0.378	-0.194	0.538	0.324
		500,000	0.387	-0.284	0.542	0.307
		1,000,000	0.391	-0.288	0.543	0.310
	3-3-2	1,000	0.254	0.235	0.479	-0.061
		10,000	0.299	0.195	0.528	-0.067
		100,000	0.418	0.076	0.580	0.180
		500,000	0.427	0.060	0.618	0.329
		1,000,000	0.431	-0.002	0.635	0.394
	3-5-2	1,000	0.255	0.189	0.479	-0.052
		10,000	0.311	0.179	0.527	0.015
		100,000	0.441	0.076	0.672	0.243
		500,000	0.471	0.008	0.748	0.249
		1,000,000	0.521	0.175	0.757	0.213
	3-3-3-2	1,000	0.205	0.385	0.426	0.089
		10,000	0.292	0.183	0.567	0.055
		100,000	0.690	0.282	0.712	0.476
		500,000	0.557	0.285	0.728	0.481
		1,000,000	0.564	0.318	0.734	0.469
	3-5-3-2	1,000	0.168	-0.311	0.470	-0.061
		10,000	0.325	0.094	0.565	-0.026
		100,000	0.541	0.309	0.787	-0.177
		500,000	0.604	0.376	0.836	-0.303
		1,000,000	0.623	0.381	0.843	-0.356

Source: Author

From the network presented, the coefficient of correlation and the interference of each input over the output were calculated. The results obtained showed a general $R^2 = 0.69$, although for sandy, silty and clayey soils it was equal to 0.66, 0.82 and 0.66, respectively, which represents lower generalization capacity in comparison with network 3-5-3-2, made for prediction of both cohesion and the friction angle together. Yet, the input node interrogator presented similar results, all the input variables having relevant interference on the output: NI (σ'_{v0}) = 25.63%, NI (N_{SPT}) = 55.05% and NI (soil type) = 19.59%. That said, the overall correlation was plotted in Figure 66 to verify overtraining, but from the results it can be said that it failed to occur, since both R^2 for training and testing increased along with the increment of the number of epochs and, at the last stop, it was constant for both training and testing.

Figure 66 – Epochs x R^2 for model Hyperbolic Tangent 3-3-3-1 1,000,000 for cohesion prediction using complete soil type: (a) training; (b) testing

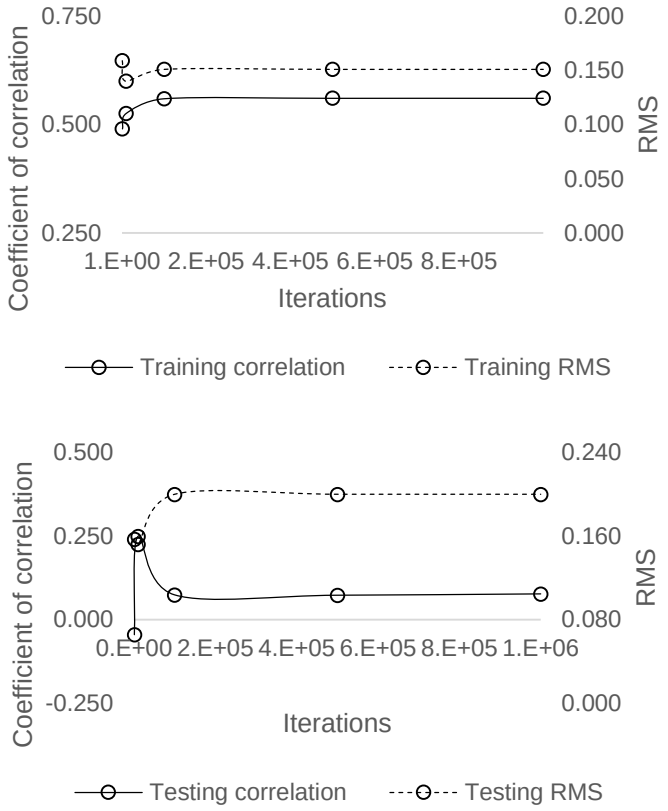

Source: Author

In addition, the coefficients of correlation and mean errors shown in Table 35 offer a view on the soil type accuracy. From Table 35 it may be stated that the mean errors for each soil type had low values, even though correlations were not that high and the maximum errors went as far as 33.44 kPa. However, the distribution of error can be modeled as a normal probability distribution with $\bar{x} = 4.48$ kPa, meaning that the confidence of the prediction models is calculable. In light of this, the confidence for having errors in the interval ±5 kPa was calculated resulting in Conf (e ± 5kPa) approximately equal to 76%, while Table 36 shows the confidence given for other maximum errors.

Table 33 – c' prediction R^2 per soil type for network Hyperbolic Tangent 3-3-3-1 1,000,000

Soil type	**R^2**	**Mean error (kPa)**
All types	0.69	4.48
Sandy	0.66	4.89
Silty	0.82	3.34
Clayey	0.66	4.35

Source: Author

Table 34 – Confidence per threshold for network Hyperbolic Tangent 3-5-3-1 1,000,000

Error	Confidence
< 2	69.12%
< 3	71.45%
< 4	73.77%
< 5	76.09%
< 6	78.41%

Source: Author

In comparison, the confidence for linear and non-linear regression models was calculated. Results of this analysis illustrate that not only R^2 had low variability from the choice of regression model, but also their confidence did not suffer great interference from the selected regression model, being equal to 71.69% for linear and 71.79% for Conf (e ± 5kPa). This is equivalent to having Conf (e ± 3kPa) for the proposed neural network, and so its improvement on accuracy may be attested.

Subsequently, the correction factor was calculated by reducing the total quadratic error of the unknown dataset. Table 37 provides the statistics of the error distribution for the training data on cohesion prediction for sandy soils after the implementation of CF = 0.88, showing that, although the mean error increased, there was a decrease in the standard deviation and a severe drop in the quadratic errors, also resulting in stronger confidence for the model. Table 38 stages that the confidence per maximum acceptable error increases after CF is implemented to correct the ANN outputs, for instance, showing improvement, reaching Conf (e ± 5 kPa) = 85.11%. However, a correction factor was not applied to silty soils because it did not result in a better fit. In turn, it was not applied to clayey soils in the final model because there was only a small improvement in standard deviation, meaning there was no diminishment in the total quadratic error.

Table 35 – c' prediction statistics for sandy soils before and after CF implementation for network Hyperbolic Tangent 3-3-3-2 1,000,000

Error Statistics	Raw	Corrected
$\bar{e}$	4.48	5.42
σ	5.34	5.05
Σe^2	2640.37	180.27
CF	1.00	0.88

Source: Author

Table 36 – Confidence per threshold for network Hyperbolic Tangent 3-5-3-1 1,000,000 after CF implementation

Error	Confidence
<2	72.73%
<3	76.86%
<4	80.98%
<5	85.11%
<6	89.23%

Source: Author

Figures 67 and 68 display the data behavior before and after the inclusion of the correction factor for cohesion prediction. Coupled with coefficient of correlation, the scatter in Figure 67 elucidates the improvement of the ANN model in comparison with the regression models proposed in the previous section once the data had a better fit around the x=y line. Similarly, Figure 68 displays the result of the improvement obtained by using CF = 0.88 for sandy soils, which was expressive since the majority of the output values was below the x=y line. In short, the use of the proposed ANN showed great reliability and for that reason its practical use in engineering is attested.

Figure 67 – Adjustment of data for model Hyperbolic Tangent 3-3-3-1 1,000,000 on cohesion prediction

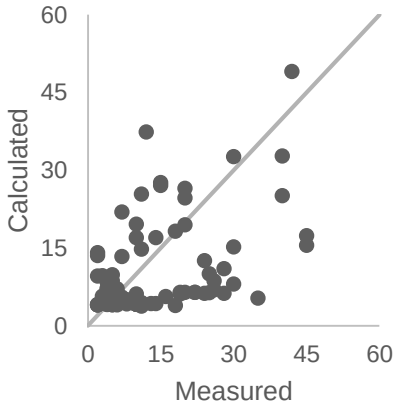

Source: Author

Figure 68 – Adjustment of corrected values for model Hyperbolic Tangent 3-3-3-1 1,000,000 on cohesion prediction over sandy soils

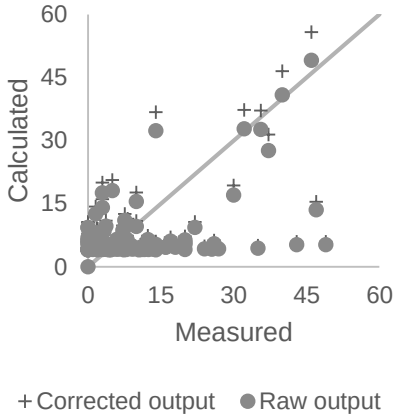

Source: Author

Similarly, in order to predict friction angle, some neural networks were proposed based on both saturated and all saturation data. Unlike the results obtained for cohesion prediction, the overall correlations presented in Tables 39 to 42 show that the best model is the one with the architecture 3-5-3-1, sigmoid activation function and simplified soil type. Furthermore, even though the chosen architecture did not reach a great correlation for testing, its results showed better consistence than the ones obtained from a single ANN for prediction of c' and ϕ' simultaneously. However, as well as the results obtained from the input node interrogator for cohesion prediction, the influence of each input variable over the output was approximately equal, NI (σ'_{v0}) = 29.80%, NI (N_{SPT}) = 36.35% and NI (soil type) = 33.85%, showing that the choice for the input parameters was correct. After the general correlation obtained for train and test was plotted in Figure 69, from which no occurrence of overtraining is detected since the correlations increased to a maximum at the last stop, which happened at 1,000,000 epochs. Figure 69 also illustrates that the model reached R^2 as far as 0.83 for training and 0.66 for testing, which showed better adjustment than network Sigmoid 3-5-3-2 1,000,000 for prediction of cohesion and friction angle.

Figure 69 – Overall correlations for network Sigmoid 3-5-3-1 1,000,000 on friction angle prediction: (a) training; (b) testing

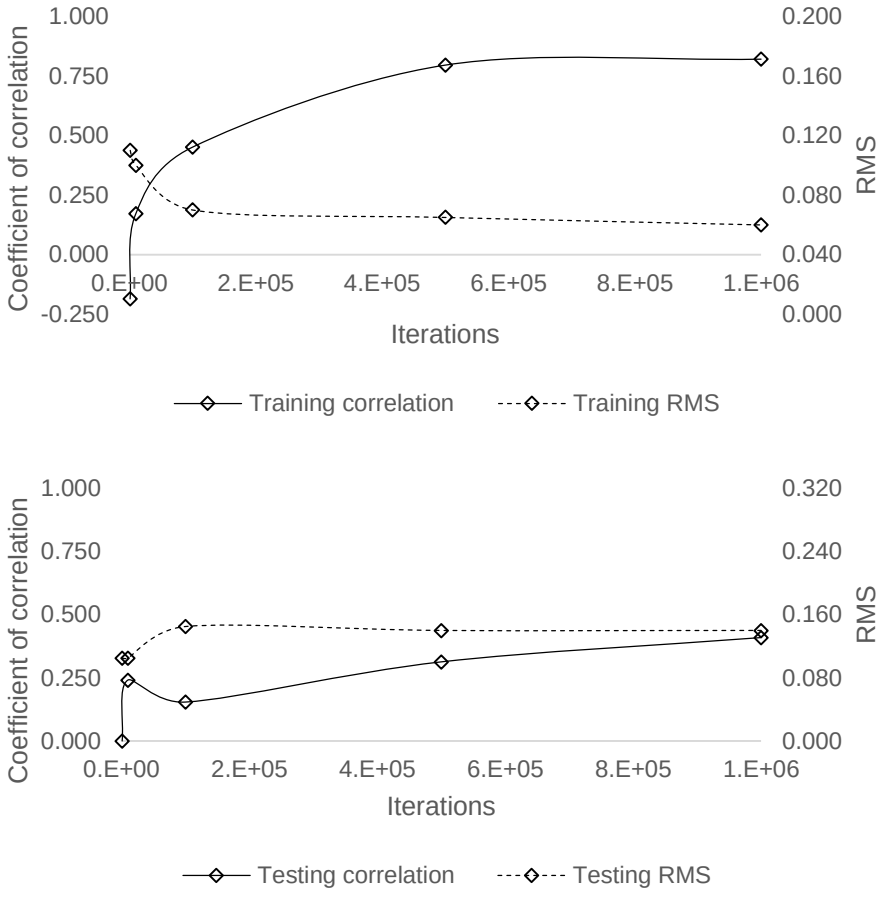

Source: Author

Table 37 – ϕ' prediction from complete soil type using sigmoid function

	Network	Iterations	ALL SATURATIONS		SATURATED	
			Training	Testing	Training	Testing
SIGMOID	3-2-2	1,000	0.165	0.415	-0.079	0.000
		10,000	0.172	0.326	0.218	0.488
		100,000	0.329	0.546	0.385	-0.154
		500,000	0.365	0.584	0.513	-0.143
		1,000,000	0.457	0.449	0.531	-0.010
	3-3-2	1,000	0.149	0.488	0.200	0.507
		10,000	0.171	0.311	0.213	0.475
		100,000	0.384	0.507	0.422	0.451
		500,000	0.436	0.328	0.458	0.443
		1,000,000	0.481	0.309	0.465	0.487
	3-5-2	1,000	0.171	0.300	0.191	0.458
		10,000	0.173	0.327	0.212	0.476
		100,000	0.330	0.496	0.425	0.447
		500,000	0.443	0.105	0.442	0.366
		1,000,000	0.521	-0.139	0.634	0.303
	3-3-3-2	1,000	0.084	0.207	0.105	-0.362
		10,000	0.150	0.413	0.140	-0.545
		100,000	0.327	0.513	0.344	0.425
		500,000	0.512	0.190	0.598	0.363
		1,000,000	0.553	0.417	0.728	0.118
	3-5-3-2	1,000	0.148	0.000	-0.186	0.000
		10,000	0.162	0.451	0.171	0.241
		100,000	0.329	0.508	0.451	0.154
		500,000	0.676	0.086	0.795	0.313
		1,000,000	0.713	-0.071	0.820	0.409

Source: Author

Table 38 – ϕ' prediction from complete soil type using hyperbolic tangent function

	Network	Iterations	ALL SATURATIONS		SATURATED	
			Training	Testing	Training	Testing
HYPERBOLIC	3-2-2	1,000	0.167	0.323	0.202	0.514
		10,000	0.179	0.317	0.263	0.585
		100,000	0.341	0.430	0.426	0.383
		500,000	0.341	0.426	0.428	0.369
		1,000,000	0.341	0.422	0.429	0.354
	3-3-2	1,000	0.168	0.279	0.202	0.529
		10,000	0.175	0.317	0.445	0.304
		100,000	0.427	0.388	0.545	0.236
		500,000	0.491	0.037	0.579	0.370
		1,000,000	0.528	0.260	0.593	0.355
	3-5-2	1,000	0.172	0.309	0.211	0.504
		10,000	0.322	0.489	0.414	0.361
		100,000	0.433	0.281	0.569	0.311
		500,000	0.586	0.011	0.716	0.302
		1,000,000	0.587	0.021	0.731	0.339
	3-3-3-2	1,000	0.141	0.521	0.160	0.575
		10,000	0.317	0.492	0.246	0.515
		100,000	0.519	0.456	0.433	0.372
		500,000	0.534	0.372	0.768	0.282
		1,000,000	0.535	0.356	0.790	0.244
	3-5-3-2	1,000	0.143	0.614	0.139	-0.400
		10,000	0.196	0.425	0.408	0.345
		100,000	0.510	-0.180	0.694	0.067
		500,000	0.691	-0.104	0.819	0.177
		1,000,000	0.693	-0.187	0.841	0.320

Source: Author

Table 39 – ϕ' prediction from simplified soil type using sigmoid function

	Network	Iterations	ALL SATURATIONS		SATURATED	
			Training	Testing	Training	Testing
SIGMOID	3-2-2	1,000	-0.026	0.864	0.129	-0.479
		10,000	0.144	0.217	0.202	0.440
		100,000	0.310	0.558	0.401	-0.126
		500,000	0.330	0.554	0.517	0.670
		1,000,000	0.354	0.490	0.526	0.698
	3-3-2	1,000	0.118	0.465	0.150	0.650
		10,000	0.143	0.227	0.190	0.471
		100,000	0.311	0.563	0.525	0.185
		500,000	0.477	0.352	0.518	0.314
		1,000,000	0.497	0.536	0.607	0.466
	3-5-2	1,000	0.140	0.359	0.151	0.107
		10,000	0.144	0.249	0.192	0.464
		100,000	0.317	0.572	0.537	0.311
		500,000	0.518	0.394	0.662	0.410
		1,000,000	0.556	0.452	0.691	0.477
	3-3-3-2	1,000	0.003	0.000	-0.004	-0.030
		10,000	0.131	0.315	0.156	0.141
		100,000	0.303	0.533	0.512	0.152
		500,000	0.531	0.503	0.714	0.352
		1,000,000	0.574	0.488	0.757	0.259
	3-5-3-2	1,000	0.025	0.000	-0.092	0.000
		10,000	0.143	0.389	0.013	0.000
		100,000	0.305	0.538	0.410	0.377
		500,000	0.467	0.548	0.760	0.663
		1,000,000	0.558	0.500	0.829	0.655

Source: Author

Table 40 – ϕ' prediction from simplified soil type using hyperbolic tangent function

Network		Iterations	ALL SATURATIONS		SATURATED	
			Training	Testing	Training	Testing
HYPERBOLIC	3-2-2	1,000	0.136	0.405	0.155	0.554
		10,000	0.158	0.253	0.230	0.384
		100,000	0.327	0.561	0.513	0.652
		500,000	0.445	0.437	0.531	0.705
		1,000,000	0.467	0.402	0.534	0.706
	3-3-2	1,000	0.140	0.292	0.187	0.553
		10,000	0.157	0.182	0.366	0.288
		100,000	0.478	0.326	0.546	0.365
		500,000	0.507	0.233	0.595	0.581
		1,000,000	0.511	0.388	0.601	0.592
	3-5-2	1,000	0.142	0.288	0.183	0.435
		10,000	0.146	0.239	0.369	0.202
		100,000	0.552	0.442	0.657	0.280
		500,000	0.580	0.496	0.663	0.168
		1,000,000	0.582	0.495	0.663	0.162
	3-3-3-2	1,000	0.127	0.481	0.174	0.431
		10,000	0.144	0.254	0.317	0.386
		100,000	0.495	0.490	0.663	0.302
		500,000	0.570	0.514	0.790	0.040
		1,000,000	0.576	0.519	0.795	0.279
	3-5-3-2	1,000	0.117	0.541	0.020	-0.478
		10,000	0.160	0.381	0.257	0.507
		100,000	0.626	0.595	0.720	0.623
		500,000	0.699	0.525	0.857	0.313
		1,000,000	0.708	0.498	0.864	0.385

Source: Author

After obtaining the best model for friction angle prediction, its limitations were tested. First, the database and its outputs were divided into groups defined by the soil classification in order to check the accuracy of the model on prediction of the shear strength parameters for each soil type. Table 43 presents the results obtained in this analysis, showing that although the overall mean error was little, the maximum error obtained in the modeling was up to 11.18° and the model failed to predict ϕ' for clayey soils. However, results of the confidence analysis in Table 44 revealed that for the proposed maximum acceptable error e = ±5º the confidence obtained was Conf (e ±5º) = 85.93%, meaning that the proposed model is extremely reliable. In comparison, the confidence for the ANN model was greater than the linear and non-linear regression models, which obtained Conf (e ± 5) equal to 77.22% and

77.25%, respectively, meaning that the neural network had developed superior capacity of ϕ' prediction.

Table 41 – ϕ' prediction R^2 per soil type for network Sigmoid 3-5-3-1 1,000,000

Soil type	R^2	Mean error (kPa)
All types	0.66	2.59
Sandy	0.66	2.94
Silty	0.74	1.87
Clayey	0.09	1.79

Source: Author

Table 42 – Confidence per threshold for network Sigmoid 3-5-3-1 1,000,000 on ϕ' prediction

Error	Confidence
<2	73.06%
<3	77.35%
<4	81.64%
<5	85.93%
<6	90.22%

Source: Author

Next, the implementation of a correction factor equal to 1.08 for sandy soils resulted in reduction of the total quadratic error from $\Sigma e^2 = 758.18$ to $\Sigma e^2 = 283.65$. Moreover, results presented in Tables 45 and 46 revealed a sharp drop in the standard deviation, meaning that the accuracy of the model had improved. In its turn, Table 46 displays that, after the CF implementation, a small drop in confidence per maximum acceptable error occurred, although it was not relevant on loss of reliability of the proposed model.

Table 43 – ϕ' prediction statistics for sandy soils before and after CF implementation for network Sigmoid 3-5-3-1 1,000,000

Error Statistics	Raw	Corrected
$\bar{e}$	0.07	2.32
σ	3.89	0.44
Σe^2	758.18	283.65
CF	1.00	1.08

Source: Author

Table 44 – Confidence per threshold for network Sigmoid 3-5-3-1 1,000,000 on ϕ' prediction after CF implementation

Error	Confidence
<2	72.79%
<3	76.94%
<4	81.09%
<5	85.25%
<6	89.40%

Source: Author

Coupled with the presented results, Figures 70 and 71 illustrate the scatter measured x calculated, revealing that the model showed great adjustment of data. In addition, Figure 71 exhibits the improvement obtained by using CF = 1.08 for sandy soils, which was expressive since most of the data was above the x=y line. However, the implementation of CF for silty and clayey soils was not proposed because it would have resulted in loss of accuracy of the model. In short, the use of the proposed ANN showed great reliability, which is why its practical use in engineering is confirmed.

Figure 70 – Data adjustment for model Sigmoid 3-5-3-1 1,000,000 on friction angle prediction

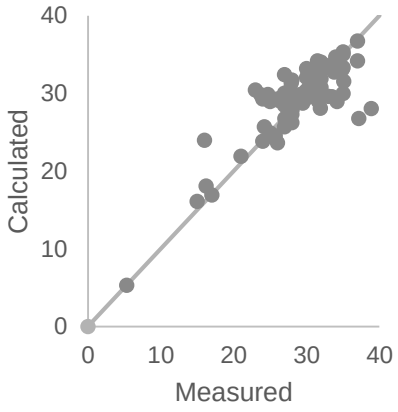

Source: Author

Figure 71 – Data adjustment for model Sigmoid 3-5-3-1 1,000,000 on friction angle prediction

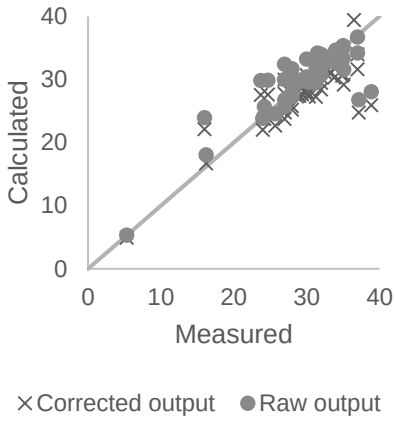

Source: Author

4.2.2 Model comparison

The use of ANN showed better efficiency in shear strength parameters prediction when compared to models generated from statistical regression, yet its performance was tested in comparison with some existing correlations. However, existing correlations that use N_{SPT} for cohesion estimation take into consideration the undrained resistance of purely cohesive soils, and for this matter a significant discrepancy was perceived.

Using artificial neural networks to estimate the cohesion from the effective overburden stress, SPT blow count and soil type for a non-purely cohesive soil resulted in fair accuracy, R^2=0.85 for the whole dataset. This correlation showed a sharp increase in generalization capacity when compared to the best models developed from linear and non-linear multiple regression that had low R^2, as shown in Table 47. Moreover, the use of ANN for c' predictions provided a sharp decrease in the mean error from $\bar{e}$ = 8.2 kPa, for the linear regression-based model, to $\bar{e}$ = 3.5 kPa. Likewise, there was a drop in the standard deviation, as may be noted in Figure 72, which displays a better adjustment of the predicted values to the x=y line for the measured versus calculated scatter graph. Furthermore, data concentration closer to the measured axis for the statistical regression-based correlations shows that these models failed to generalize cohesions above 30 kPa. When compared with the ANN model, the existing models proposed by Decourt (1989) and Terzaghi and Peck (1996) produced results that could not represent the drained cohesion of the soils as expected, since the equations were proposed for undrained conditions, ensuring the need for a correlation that could represent the soil cohesive behavior under drained conditions.

Table 45 – c' prediction statistics per model

Model	R^2	$\bar{e}$ (kPa)	σ (kPa)	Confidence
ANN Hyperbolic Tangent 3-3-3-2 1,000,000	0.76	3.5	4.7	80.93%
Linear regression $c' = 0.366N_{spt} + 1.264SoilType + 0.505$	0.20	8.2	6.8	75.75%
Non-linear regression $c' = -276.191 \cdot {\sigma'_{vo}}^{-15,936} + 0.293 \cdot {N_{spt}}^{1,052} - 31.691 \cdot SoilType^{-0,320} + 26.844$	0.22	8.0	6.8	75.78%
Decourt (1989) $c_u = 12.5\ N_{SPT}$	0.15	180.6	171.3	-
Terzaghi and Peck (1996) $c_u = 4.4\ N_{SPT}$	0.15	57.3	57.4	-

Source: Author

Figure 72 – c' prediction using ANN and regression-based models: (a) comparison of ANN with linear-based model; (b) comparison of ANN with non-linear based model

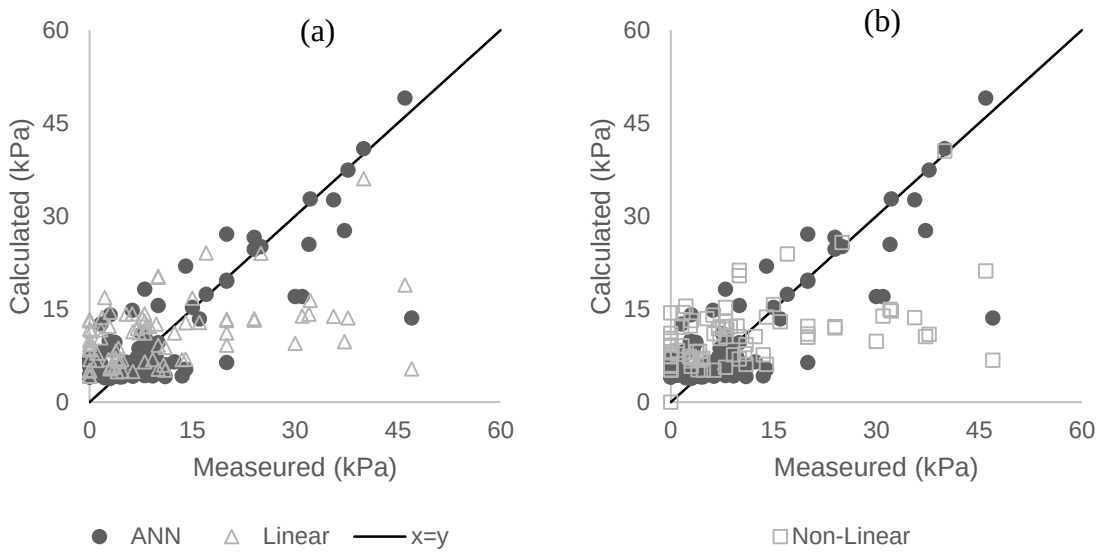

Source: Author

The errors had to be examined in order to calculate the confidence of the models presented in Table 47. In light of this, the error histograms for each model were plotted and the confidence calculated considering the occurrence of $\bar{e} \leq 5$ kPa. From the results showed in Table 47 and Figures 73, 74 and 75, which present the histograms of errors for each model proposed, it may be said that the error dispersions could be modeled as Student's t distributions with confidence up to 80.93% for the ANN model. This means that there is a confidence of 80.93% and that the estimation of cohesion by the proposed network from a random set of unforeseen data presents a mean error of 5 kPa or less, and for that reason the model is highly reliable.

Figure 73 – Error histogram for c’ prediction with ANN

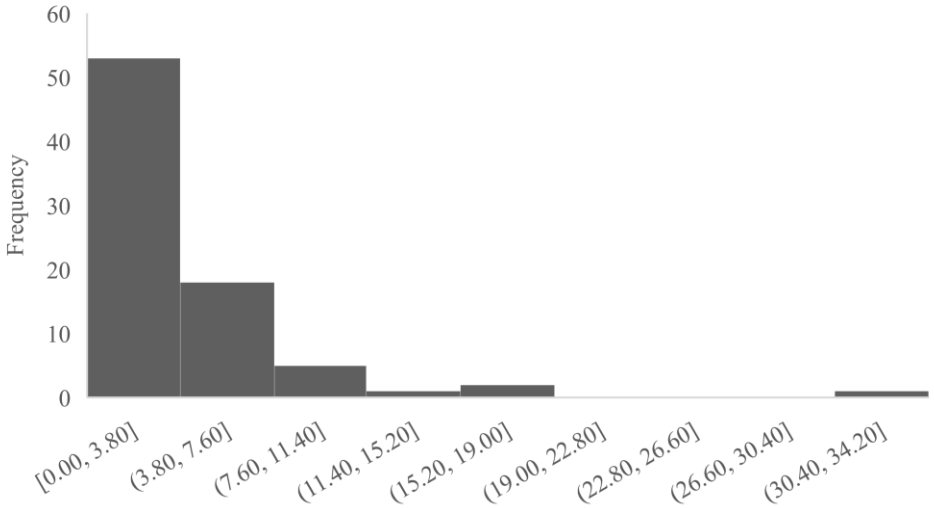

Source: Author

Figure 74 – Error histogram for c’ prediction with linear regression-based model

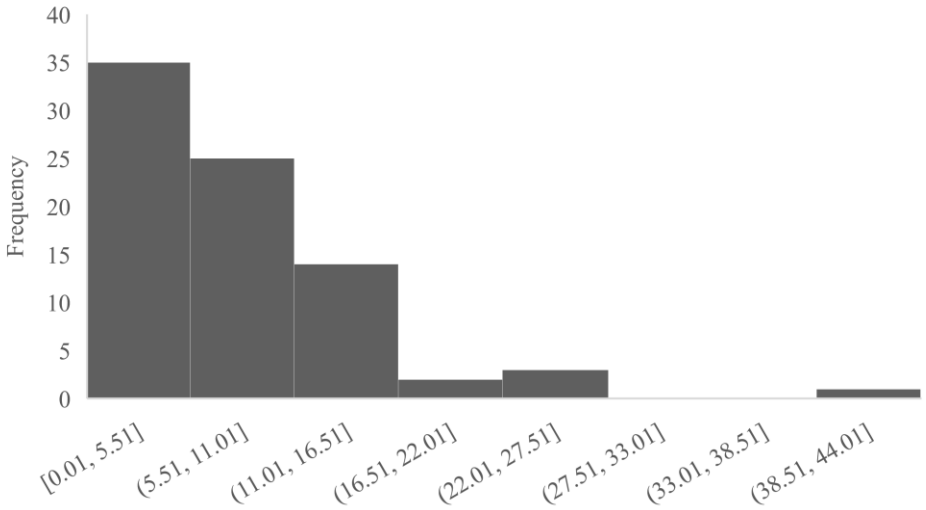

Source: Author

Figure 75 – Error histogram for c' prediction with non-linear regression-based model

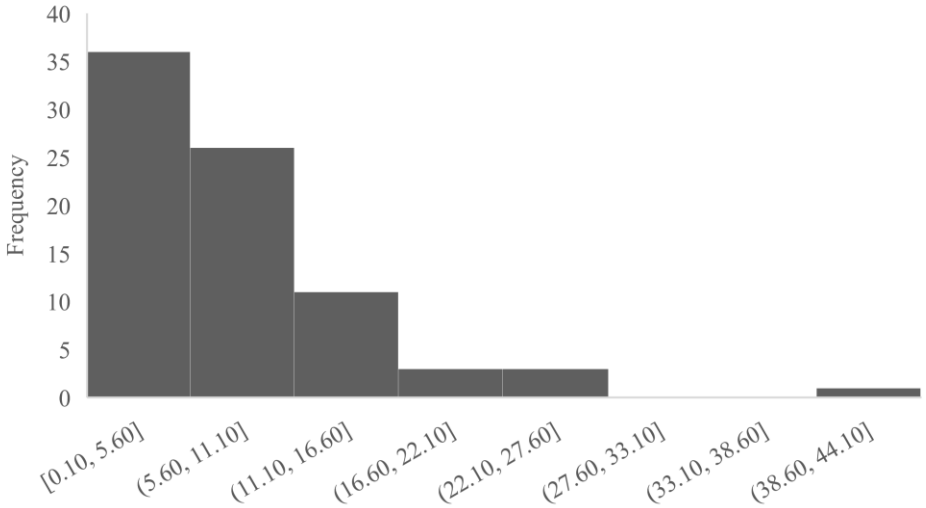

Source: Author

The ANN and regression-based models for the friction angle estimation were also compared to the existing correlations proposed by Dunham (1954), Godoy (1983) and Hatanaka and Uchida (1996). Table 48 presents the statistics for the proposed models and the existing correlations used for comparison matter in this study. From the statistics shown, a better performance may be found of the artificial neural network over coefficient of correlation, mean error, standard deviation and confidence of the model, meaning that this model had the best accuracy and generalization capacity. Furthermore, when compared to the regression-based models, the ANN proposed showed significant improvement in the adjustment of the predicted values to the x=y line in the measured *versus* calculated scatter graph as shown in Figure 76.

Unlike the cohesion prediction, the well-known correlations used for matter of comparison were designed to estimate the soil in drained conditions, although they only took into consideration the frictional portion of the shear strength behavior. As mentioned above, the correlations proposed by Dunham (19954), Godoy (1983) and Terzaghi and Peck (1996) tended to overestimate the friction angle values, as shown in Figures 77, 78 and 79. However, it is important to point out that Dunham (1954) considered the effect of grain size distribution and particle shape on his study, which could not be evaluated in this study for lack of information in the database, while the correlations proposed by Godoy (1983) and Hatanaka and Uchida (1996) had their specificities applied during the modeling.

Figure 76 – ϕ' prediction using ANN and regression-based models: (a) comparison of ANN with linear-based model; (b) comparison of ANN with non-linear based model

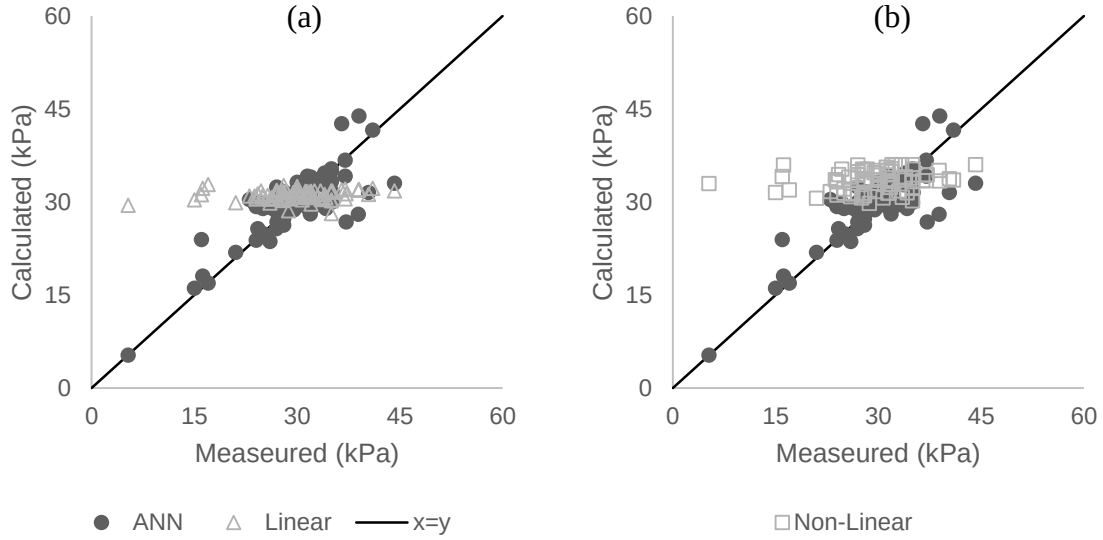

Source: Author

Table 46 – ϕ' prediction statistics per model

Model	R^2	$\bar{e}$ (°)	σ (°)	Confidence
ANN Sigmoid 3-5-3-1 1,000,000	0.64	2.8	2.7	92.56%
Linear regression $\phi' = 0{,}002\sigma'_{vo} - 0{,}063N_{spt} - 0{,}457\text{SoilType} + 31{,}987$	0.04	4.4	4.0	83.49%
Non-linear regression $\phi' = 3{,}302 \cdot \sigma'_{vo}{}^{-6{,}664} + 9{,}082 \cdot N_{spt}{}^{-0{,}320} + 11{,}009 \cdot \text{SoilType}^{-1{,}324} + 22{,}629$	0.11	4.1	4.1	83.41%
Dunham (1954) $\phi' = \sqrt{12 \cdot N_{SPT}} + 25°$	0.01	8.8	7.6	-
Godoy (1983) $\phi' = 0{,}4 \cdot N_{SPT} + 28°$	0.01	6.7	7.0	-
Hatanaka & Uchida (1996) $\phi' = \sqrt{20 \cdot N_{SPT,1}} + 20°$	0.06	10.1	10.0	-

Source: Author

The confidence of each model was then calculated considering the error dispersion as Student's t distribution, being the error histograms for each model presented in Figures 80, 82 and 83. Like the cohesion prediction, the confidence interval was calculated for mean errors equal to or less than 5°, representing little change in soil shear strength behavior. The values obtained from this analysis are shown in Table 48 and display the superiority of the artificial neural networks in the estimation of friction angle and generalization capacity. The 92.56% confidence obtained for the ANN model for estimation of friction angle means that that there

is a confidence of 92.56% that its application on an unforeseen dataset results in $\bar{e} \leq 5$ kP. Thus, the ANN with sigmoid activation function, architecture 3-5-3-1 and 1,000,000 iterations is the best model for estimation of the friction angle.

Figure 77 – Application of Dunham (1954) correlation for ϕ' prediction

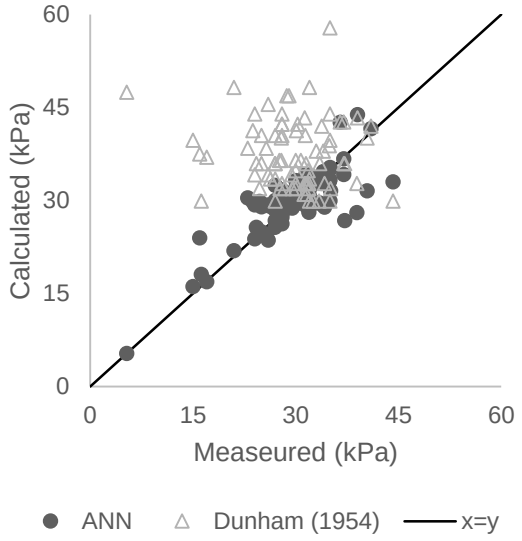

Source: Author

Figure 78 – Application of Godoy (1983) correlation for ϕ' prediction

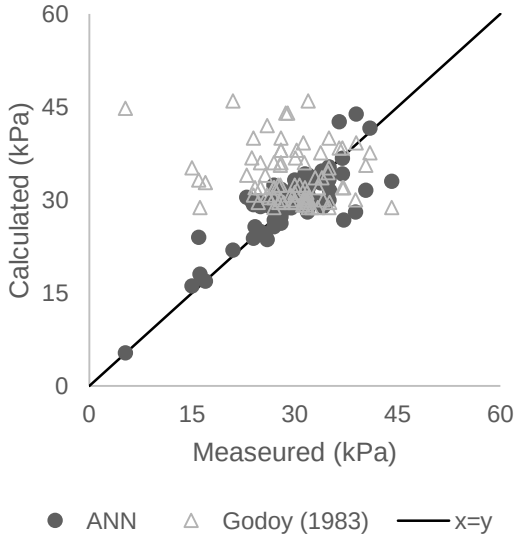

Source: Author

Figure 79 – Application of Terzaghi and Peck (1996) correlation for ϕ' prediction

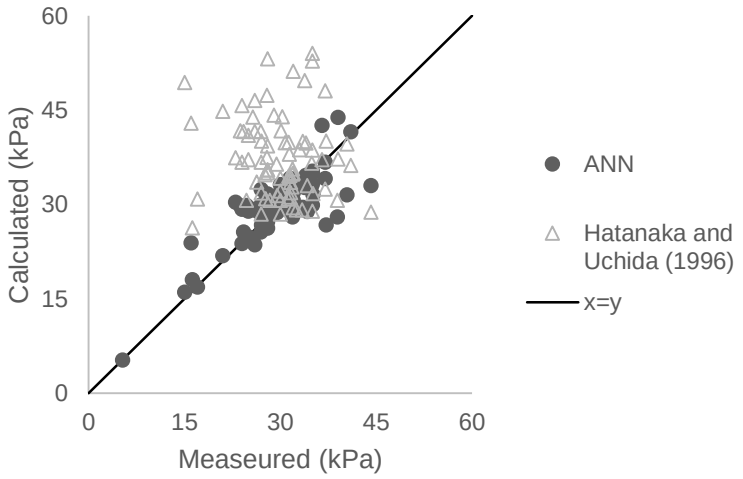

Source: Author

Figure 80 – Error histogram for ϕ' prediction with ANN

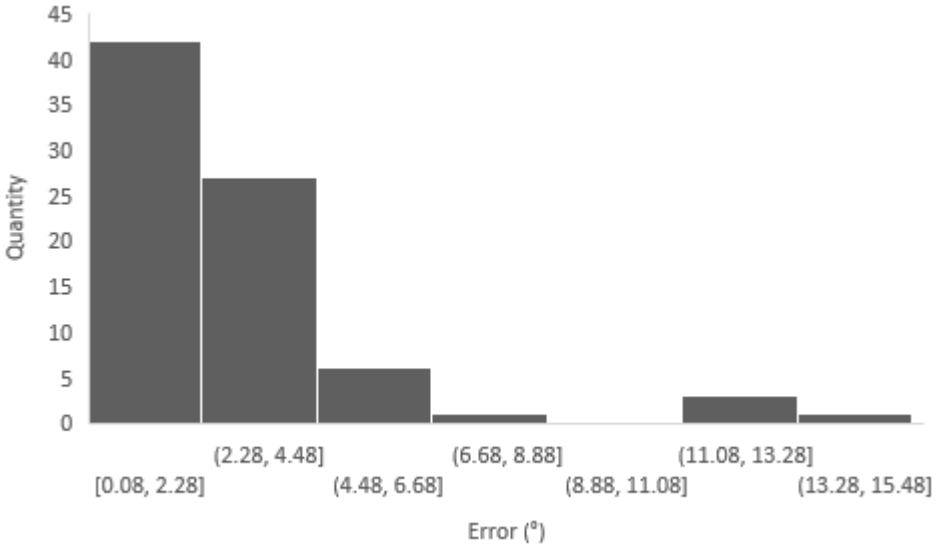

Source: Author

Figure 81 – Error histogram for ϕ’ prediction with linear regression-based model

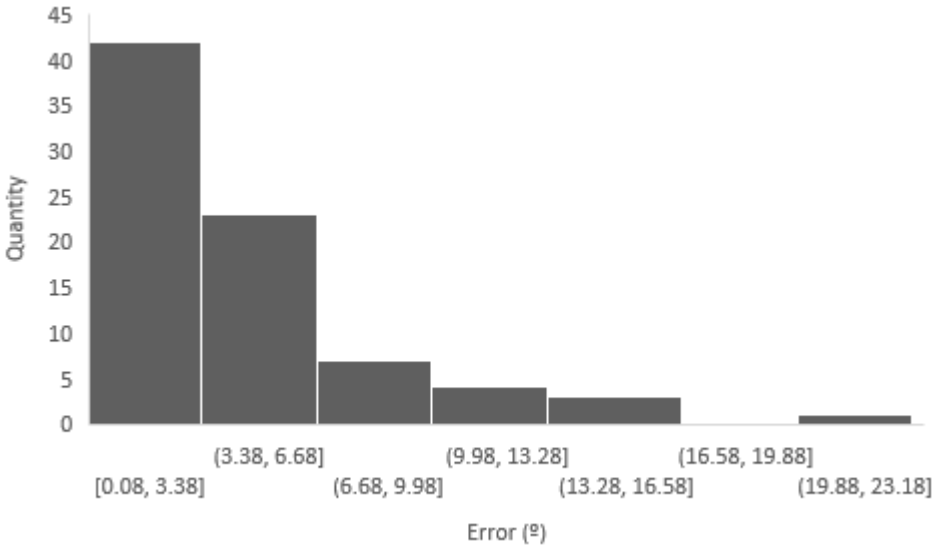

Source: Author

Figure 82 – Error histogram for ϕ’ prediction with non-linear regression-based model

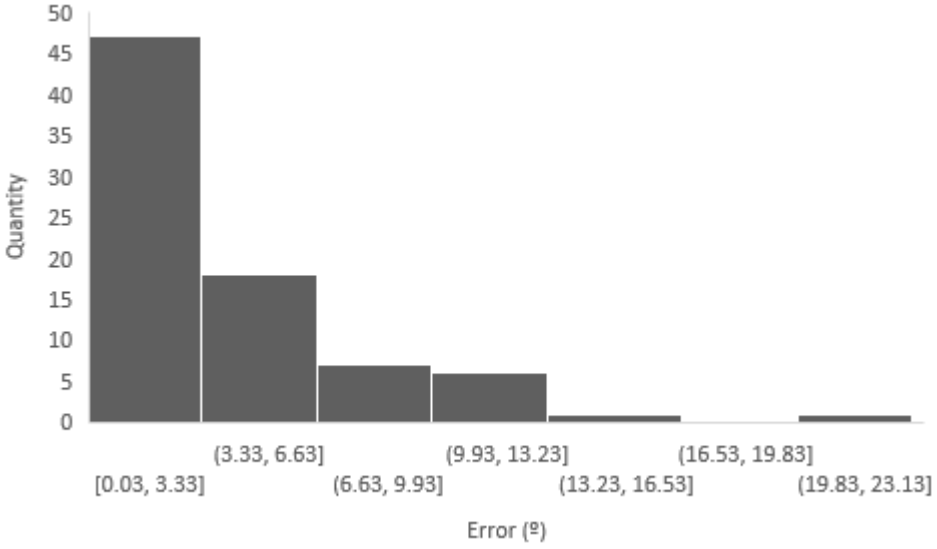

Source: Author

All things considered, the best models for estimation of cohesion and friction angle were the artificial neural networks. However, these results presented lower correlations than those obtained by Göktepe (2008), R^2 up to 0.99, for c’ and ϕ’ estimation. Nevertheless, as mentioned earlier, the higher correlation of his study might be a result of less distinct data, which were collected from a single region in Turkey. Similarly, Das and Basudhar (2008) work resulted in higher correlations, up to 0.906 for training, to predict the residual friction angle for

clayey soils. Another study presented on shear strength parameter prediction proposed by Shooshpasha, Amiri and MolaAbasi (2014) also reached a high correlation of $R^2 = 0.998$ when estimating friction angle of sandy soils from N_{SPT}, σ_{v0}' and fines content, but did not consider the cohesive part of shear strength in soils since the database consisted in pure sands only.

In turn, when comparing to Braga (2014), the results were more consistent since the best models obtained by the author had a much smaller training and testing database than the present study. This means that this work's proposed ANN had a better generalization capacity. Nevertheless, since there was no description of the data used in the development of the models proposed by Braga (2014), the range in which their performances could be assured cannot be verified and compared to this work's models. That said, the present work may be said as more reliable.

Nevertheless, the fair results obtained from the present study may be explained as being the result of the random data collection, which gathered test results from various sites and regions. Thus, the results obtained from the proposed models could be improved for more complex networks and larger database.

4.2.2 ANN model presentation

From the previous results, the ANN that were considered to have the most efficiency for shear strength parameter prediction had the networks are listed below, along with their respective training and test coefficient of correlation. Together with these results, the weights and biases for c' prediction are shown in Tables 49, 50 and 51 and the network architecture is presented in Figure 83. The weights and biases for ϕ' are shown in Tables 52, 53 and 54 and the architecture for the best model is presented in Figure 84. When predicting both parameters simultaneously, the weights and biases are shown in Tables 55, 56 and 57 and the network architecture is illustrated in Figure 84.

- Cohesion prediction best model: Hyperbolic tangent activation function, architecture 3-3-3-1 and 1,000,000 iterations, with R^2 for training and testing equal to 0.854 and 0.774, respectively. This model used a complete soil classification as entry.

Table 47 – Weights and biases for the first hidden layer of network 3-3-3-1 on c' prediction

Hidden Layer 1			
Inputs	1	2	3
x1	2.94269	-10.6871	-18.6528
x2	-3.63808	12.14051	45.13189
x3	-0.05844	-0.10323	7.72295
bias	-0.12452	-3.43988	-5.92382

Source: Author

Table 48 – Weights and biases for the second hidden layer of network 3-3-3-1 on c' prediction

Hidden Layer 2			
Hidden layer 1 outputs	1	2	3
x1	-19.9345	-10.7241	-5.81207
x2	1.44002	-8.52452	-27.2681
x3	-24.6634	-3.53626	12.05468
bias	8.50769	11.10801	-11.5128

Source: Author

Table 49 – Weights and biases for output layer of network 3-3-3-1 on c' prediction

Output Layer	
Hidden layer 2 outputs	1
x1	7.46726
x2	-9.02887
x3	7.29609
bias	8.34813

Source: Author

Figure 83 – Architecture for ANN model on c' prediction

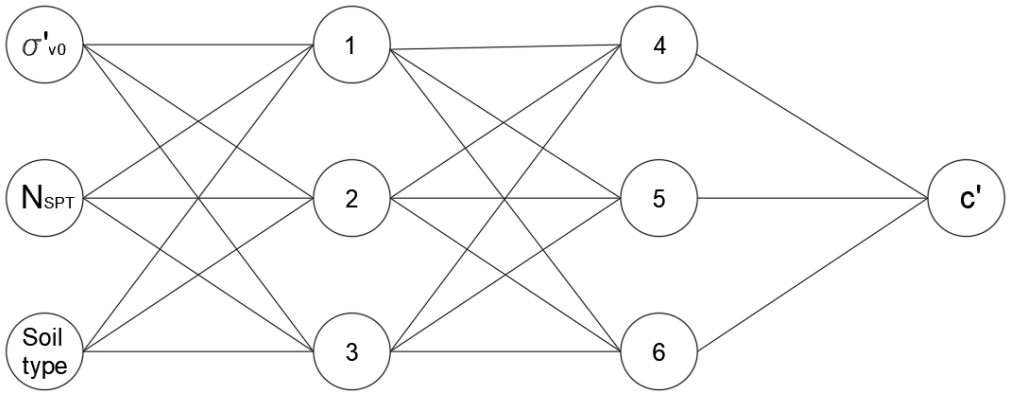

Source: Author

- Friction angle prediction best model: Sigmoid activation function, architecture 3-5-3-1 and 1,000,000 iterations, with R^2 for training and testing equal to 0.829 and 0.655, respectively. This model used a simplified soil classification as entry.

Table 50 – Weights and biases for the first hidden layer of network 3-5-3-1 on ϕ' prediction

Hidden Layer 1					
Inputs	1	2	3	4	5
x1	12.9258	-6.02139	-4.15388	0.42515	-15.4192
x2	-3.98955	-6.03259	-3.58148	-2.05385	5.57072
x3	1.26238	3.56393	-18.5785	10.0399	-13.3855
bias	-2.71222	4.21254	8.54067	-2.34381	7.11163

Source: Author

Table 51 – Weights and biases for the second hidden layer of network 3-5-3-1 on ϕ' prediction

Hidden Layer 2			
Hidden layer 1 outputs	1	2	3
x1	-2.77859	-9.53831	-13.0743
x2	-2.89588	-0.60774	-2.54257
x3	9.07938	8.67639	-13.7442
x4	8.15802	-0.08773	8.6918
x5	-2.87022	-9.56678	0.41626
bias	-5.3424	4.06341	-1.31783

Source: Author

Table 52 – Weights and biases for output layer of network 3-5-3-1 on ϕ' prediction

Output Layer	
Hidden layer 2 outputs	1
x1	-10.8197
x2	15.8379
x3	-10.6528
bias	1.02589

Source: Author

Figure 84 – Architecture for ANN model on ϕ’ prediction

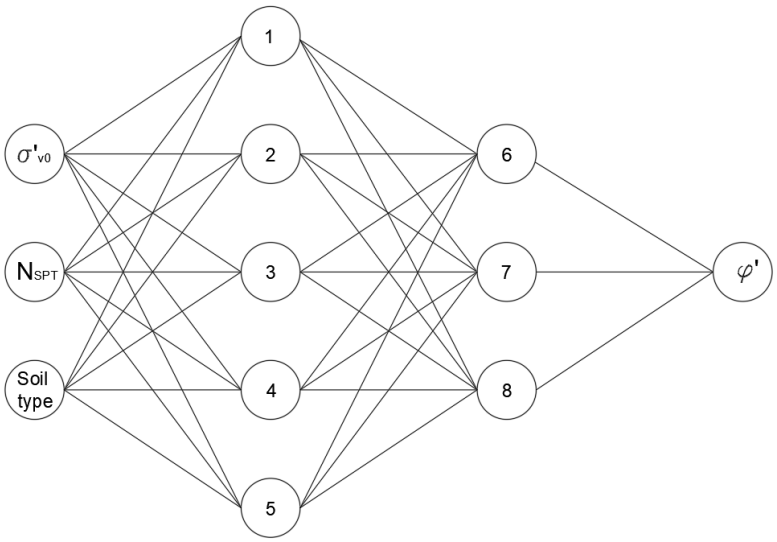

Source: Author

- Prediction of c' and ϕ’ simultaneously: Sigmoid activation function, architecture 3-5-3-2 and 1,000,000 iterations, with R^2 for training and testing equal to 0.907 and 0.907, respectively. This model used a complete soil classification entry.

Table 53 – Weights and biases for the first hidden layer of network 3-5-3-2 on c’ and ϕ’ prediction

Hidden Layer 1					
Inputs	1	2	3	4	5
x1	-1.17973	-1.65795	-0.78733	-7.35028	-3.91777
x2	-0.53958	-2.27637	4.86595	0.80423	0.75441
x3	-0.87106	6.38232	-3.48135	2.47995	-0.21921
bias	0.79406	1.55309	-1.95058	-2.23904	3.76636

Source: Author

Table 54 – Weights and biases for the second hidden layer of network 3-5-3-2 on c’ and ϕ’ prediction

Hidden Layer 2			
Hidden layer 1 outputs	1	2	3
x1	-0.1525	-1.78576	-0.42858
x2	3.0853	0.14302	-3.78402
x3	-2.79359	-0.75782	-5.79142
x4	1.73838	3.57438	-2.95181
x5	1.11837	-1.51168	5.7729
bias	-0.7349	0.06234	0.1625

Source: Author

Table 55 – Weights and biases for output layer of network 3-5-3-2 on c’ and ϕ’ prediction

Output Layer		
Hidden layer 2 oututs	1	2
x1	1.15471	-4.49033
x2	2.2832	2.95612
x3	-6.20171	4.75768
bias	2.42702	0.6111

Source: Author

Figure 85 – Architecture for ANN model on ϕ’ prediction

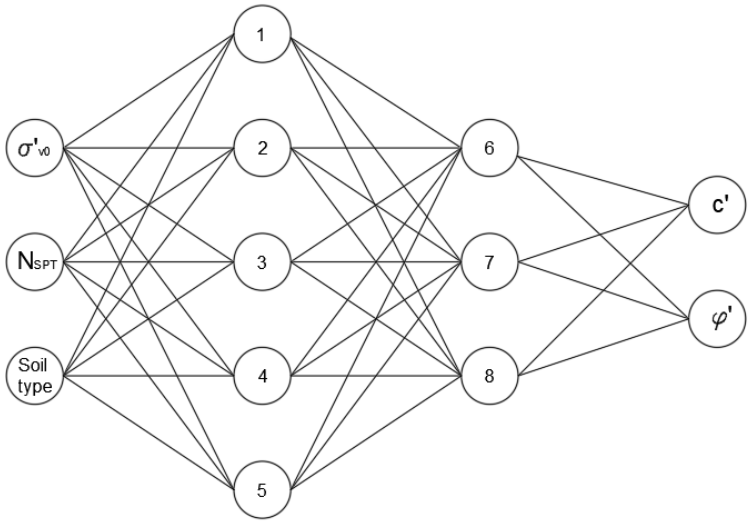

Source: Author

Furthermore, in order to make the estimation of these variables easier, there were proposed nomographs, which consisted of graphs combining the input variables. Examples of nomographs for prediction of c’ and ϕ’ separately are presented in Figures 86 and 87, where anomalies in c’ estimation may be noticed. Likewise, nomographs built from model 3-5-3-2 with a complete soil type entry for c’ and ϕ’ prediction simultaneously have presented analogous anomalies. Thus, it may be stated that these networks might not have generalized soil mechanical behavior but rather statistics of the database.

Figure 86 – Nomograph based on architecture 3-3-3-1 for c’ prediction in sandy soils

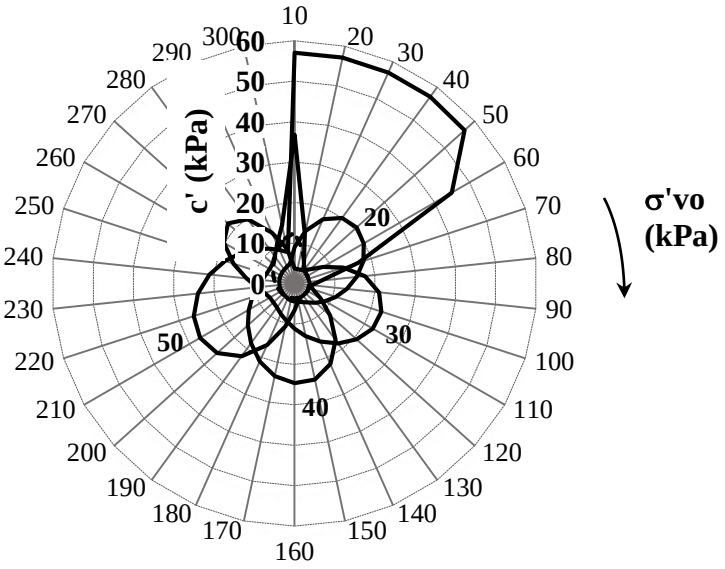

Source: Author

Figure 87 – Nomograph based on architecture 3-5-3-1 for ϕ’ prediction on soil 01

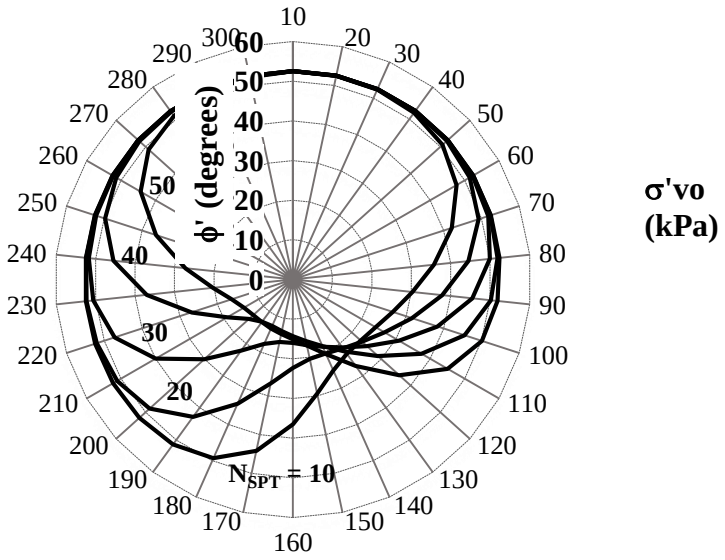

Source: Author

However, ANN model defined by architecture 3-5-3-2 with simplified soil type entry and trained until 100 thousand iterations resulted in reliable nomographs. Even though this model did not achieve the best correlations among the tested architectures, it reproduced soil shear strength behavior more accurately than previously shown nomographs. The nomographs for c’ and ϕ’ prediction are presented in Figures 88, 89, 90, 91, 92 and 93, illustrating that N_{SPT} value might not be so relevant when overburden stress is great. Also, it is important to highlight that the best model is not simply the one with the higher correlations

during training and testing, but rather the one that can understand and reproduce the phenomenon.

Figure 88 – Nomograph based on architecture 3-5-3-2 for c’ prediction in sandy soils

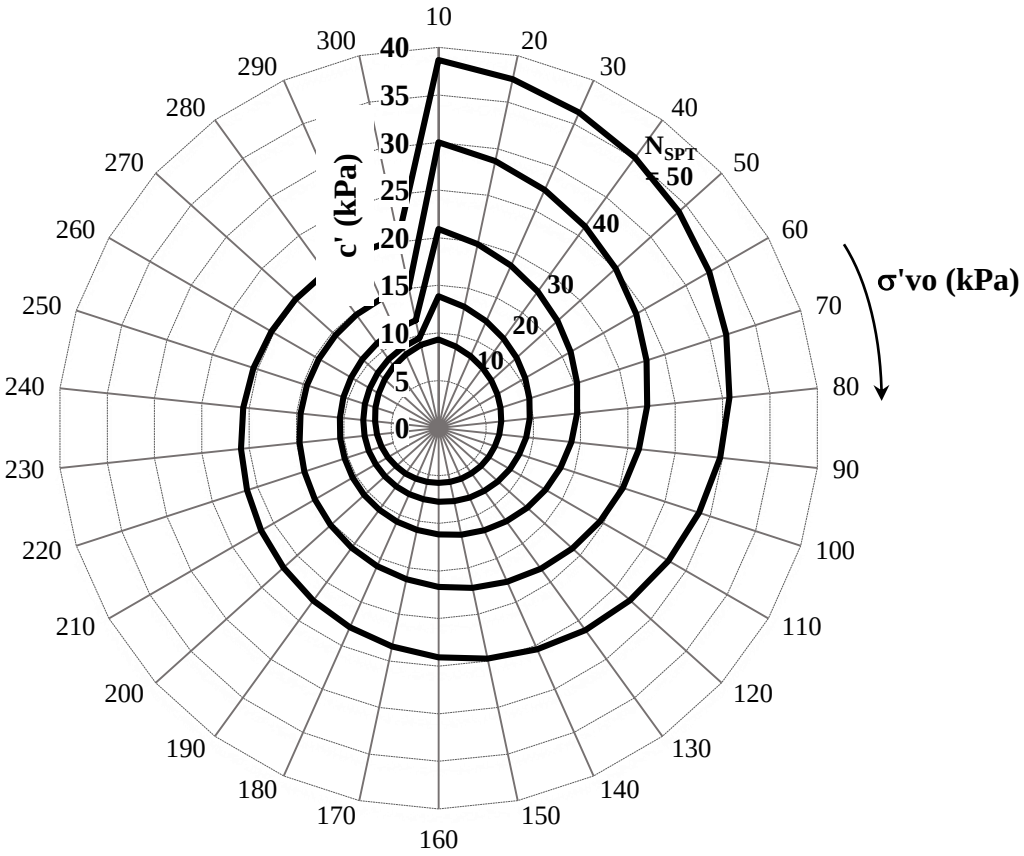

Source: Author

Figure 89 – Nomograph based on architecture 3-5-3-2 for c’ prediction in silty soils

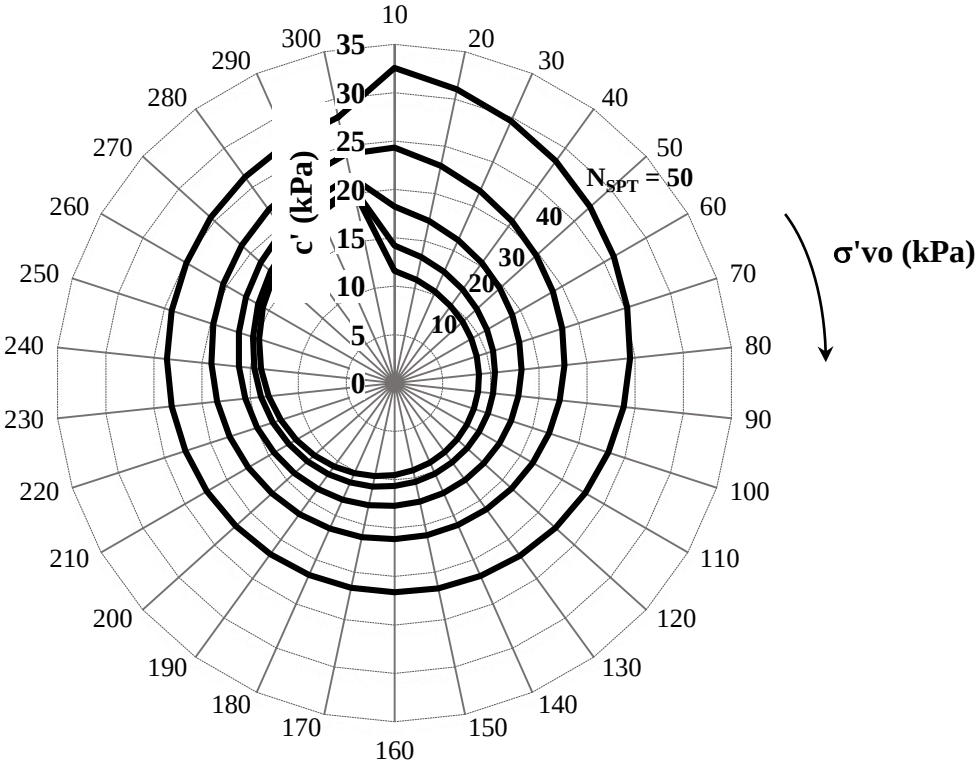

Source: Author

Figure 90 – Nomograph based on architecture 3-5-3-2 for c’ prediction in clayey soils

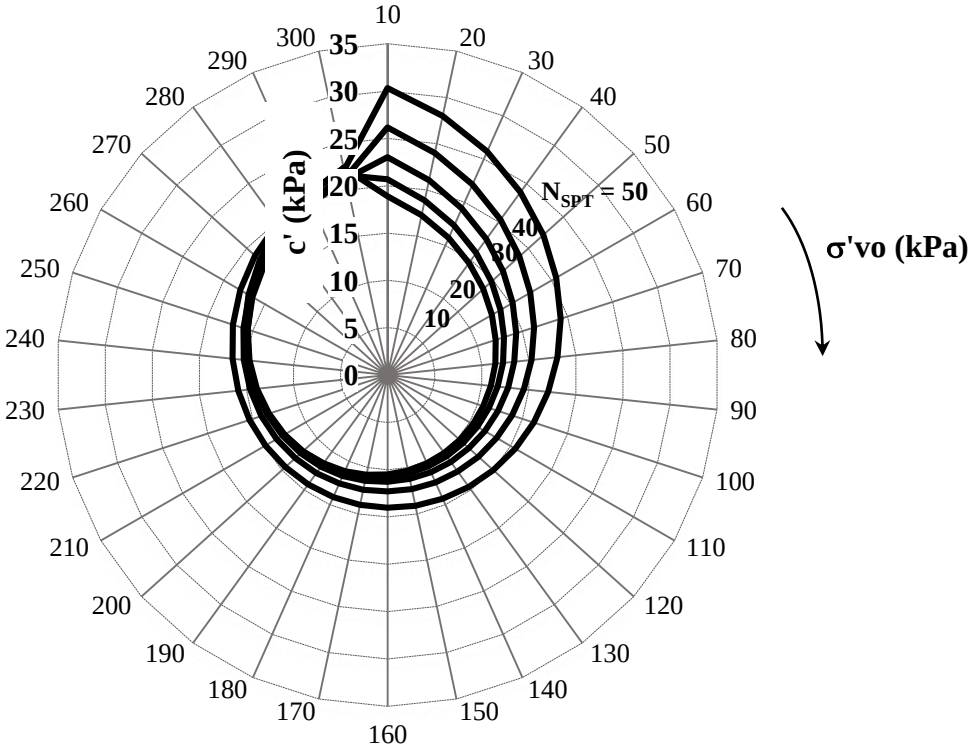

Source: Author

Figure 91 – Nomograph based on architecture 3-5-3-2 for ϕ’ prediction in sandy soils

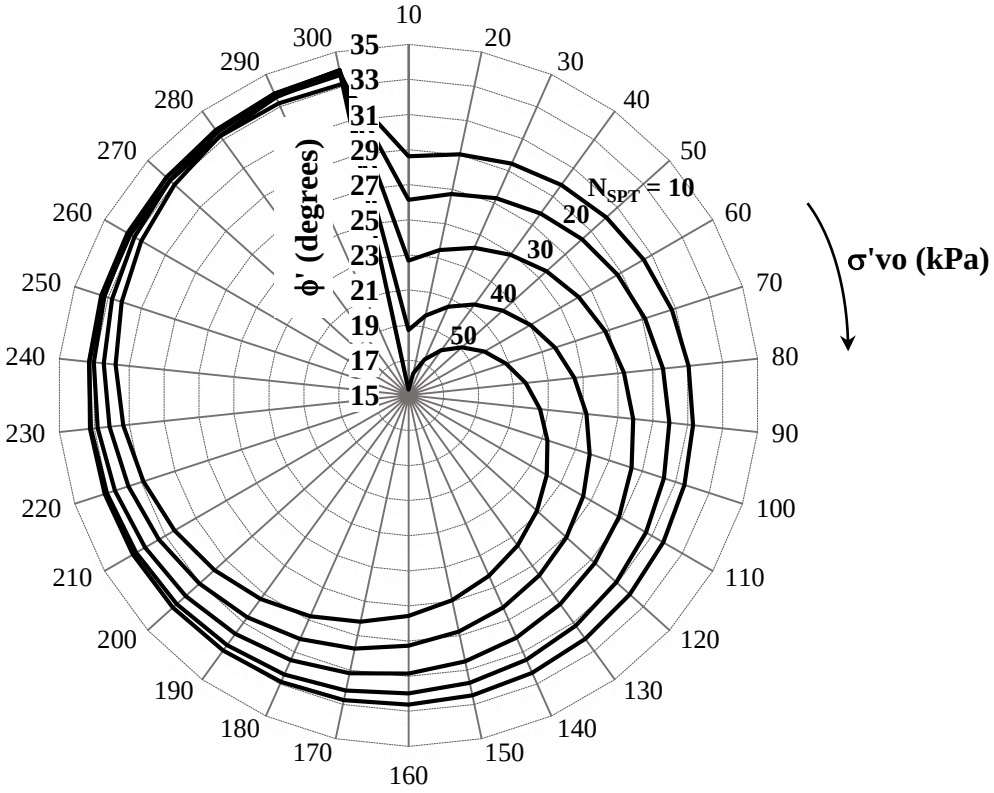

Source: Author

Figure 92 – Nomograph based on architecture 3-5-3-2 for ϕ’ prediction in silty soils

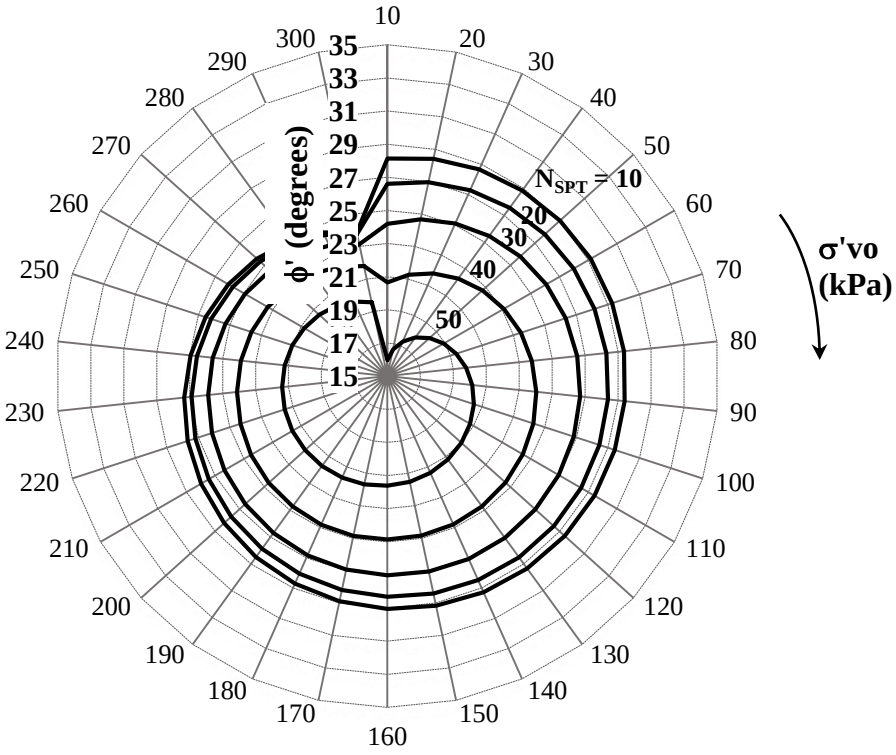

Source: Author

Figure 93 – Nomograph based on architecture 3-5-3-2 for ϕ’ prediction in clayey soils

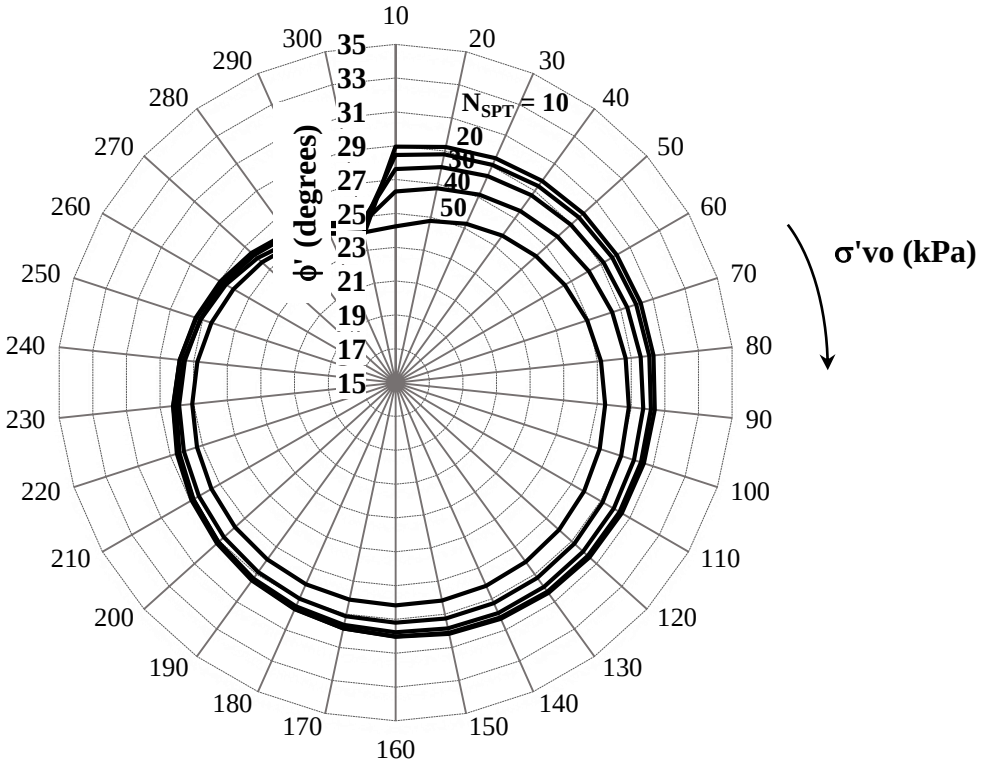

Source: Author

For example, if the input parameters are N_{SPT} = 20, σ_{v0}’ = 70 kPa and soil type = sandy, the combination for effective cohesion and effective friction angle are found in nomograph shown in Figures 88 and 91 respectively, and the outputs are approximately c’ = 10 kPa and ϕ’ = 30°. This application steps are shown in Figures 94, 95 and 96 for cohesion prediction and Figures 97, 98 and 99 for friction angle prediction.

Steps of cohesion prediction by means of nomograph:

- First step (Figure 94): firstly, the input overburden stress (σ_{v0}’) is identified in the radial axis, in which values grow clockwise.
- Second step (Figure 95): once σ_{v0}’ is identified, there should be chosen the N_{SPT} curve the represents the input.
- Third step (Figure 96): finally, the value of c’ is given by identifying which curve represented by the vertical axis correspond to the input coordinates.

Steps of friction angle prediction by means of nomograph:

- First step (Figure 97): firstly, the input overburden stress (σ_{v0}’) is identified in the radial axis, in which values grow clockwise.

- Second step (Figure 98): once σ_{v0}' is identified, there should be chosen the N_{SPT} curve the represents the input.
- Third step (Figure 99): finally, the value of ϕ' is given by identifying which curve represented by the vertical axis correspond to the input coordinates.

Figure 94 – First step on cohesion prediction using nomograph: σ_{v0}' entry

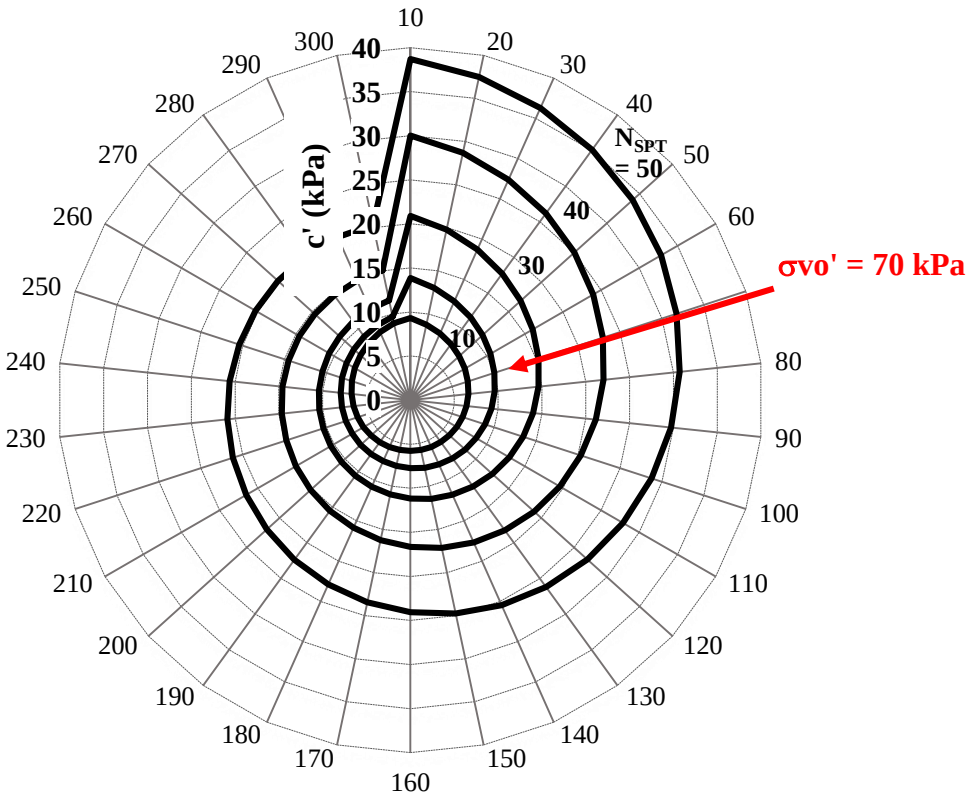

Source: Author

Figure 95 – Second step on cohesion prediction using nomograph: N_{SPT} entry

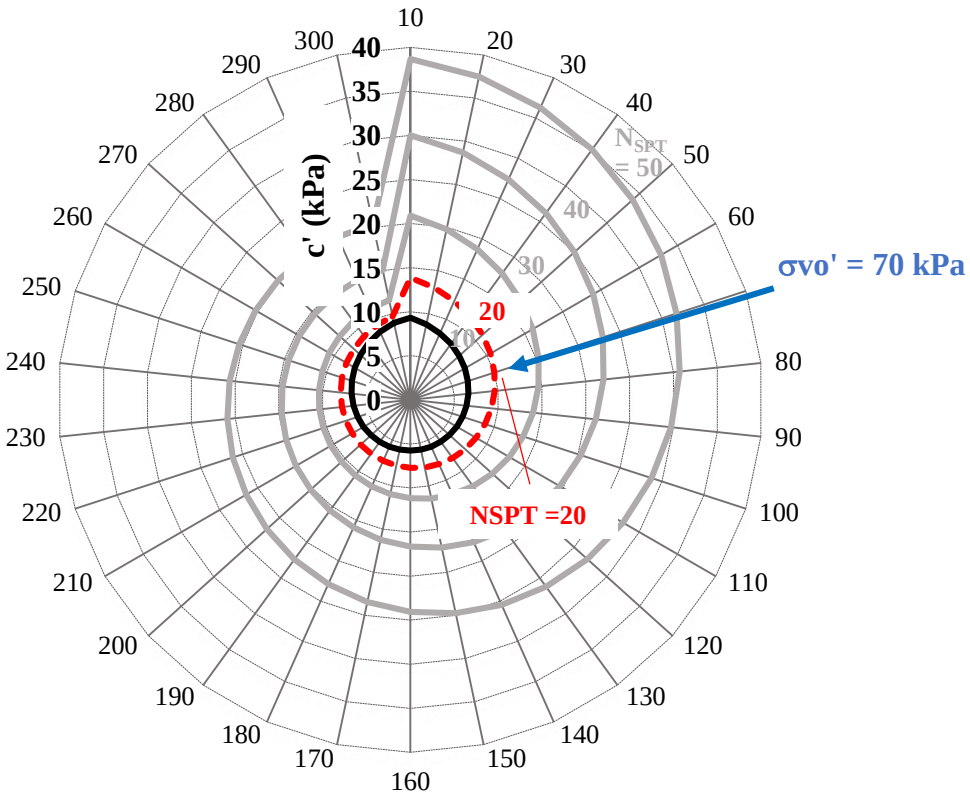

Source: Author

Figure 96 – Third step on cohesion prediction using nomograph: obtaining output

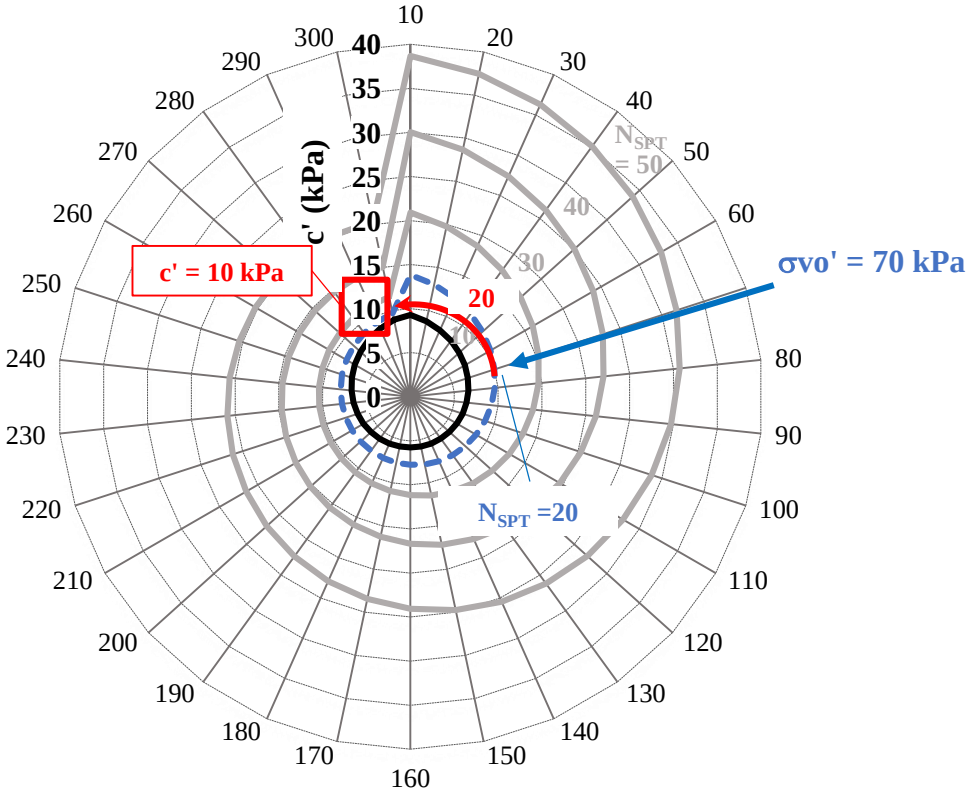

Source: Author

Figure 97 – First step on friction angle prediction using nomograph: σ_{v0}' entry

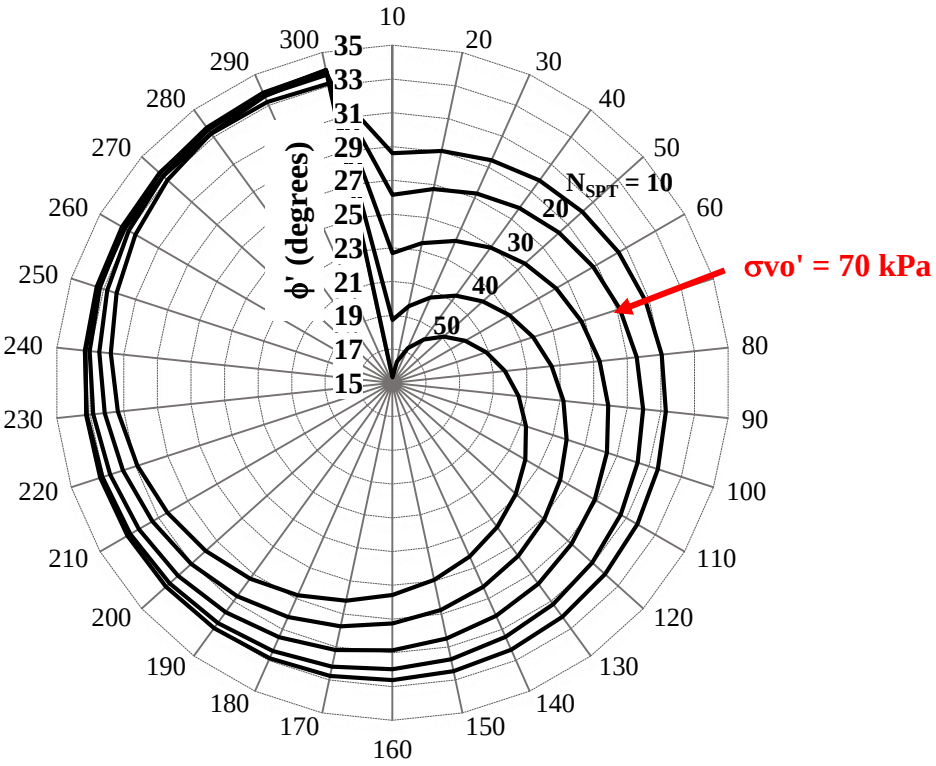

Source: Author

Figure 98 – Second step on friction angle prediction using N_{SPT} entry

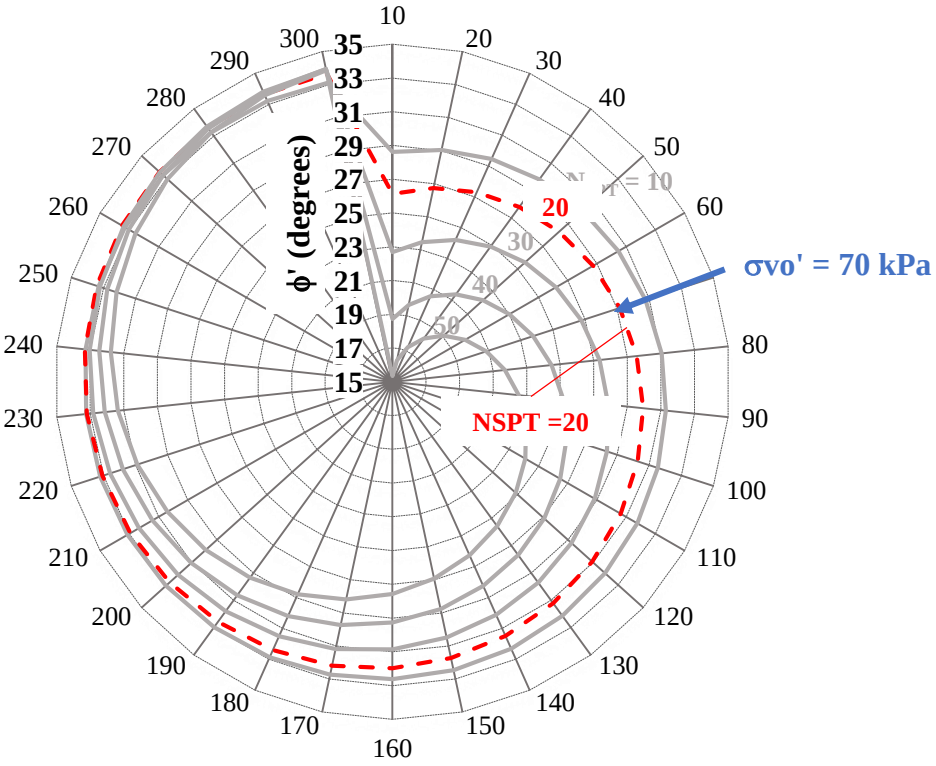

Source: Author

Figure 99 – Third step on friction angle prediction using nomograph: obtaining output

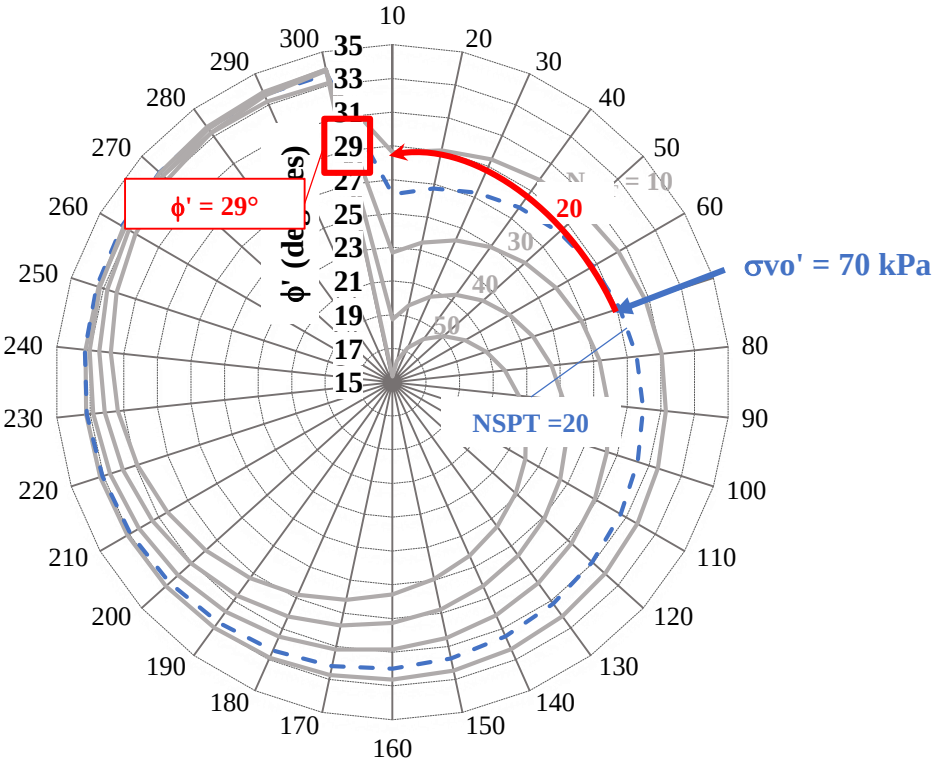

Source: Author

5 CONCLUSIONS AND FURTHER RESEARCH SUGGESTIONS

This chapter will present the conclusions of the work on prediction of soil shear strength parameters, as well as its limitations and suggestions for future studies. Also, the summary of the results and discussion will be provided in order to guide further studies.

5.1 Conclusions

This work looked to study and improve the designing of structures in Geotechnical Engineering by proposing the use of Artificial Neural Networks in the estimation of soil shear strength parameters, cohesion and friction angle. Firstly, from the regression-based models it was concluded that:

- All of the proposed input variables chosen, σ_{v0}', N_{SPT} and soil type, presented significant relation to the predicted outputs and so they were used in the artificial neural networks as well.
- The best regression-based models were obtained for the data that was tested under saturated conditions, representing the most adverse soil state. Furthermore, the non-linear multiple regression models gave better results than those obtained from linear regression.
- The correlations obtained from the regression-based models were low, proving these models unreliable for predicting cohesion and friction angle. This was found in the generalization incapacity these models, for calculated values would concentrate around a constant value.

Once it was attested that the use of correlations based on regression analysis was inefficient, the neural networks were implemented, resulting in the following conclusions:

- The use of triaxial test results that were not saturated before testing along with saturated samples resulted in loss of generalization capacity. Moreover, the use of different architectures and activation functions did not result in great differences in ANN efficiency, although cohesion models responded slightly better to hyperbolic tangent activation function, while friction angle presented better results when using the sigmoid activation function. Thus, the option for an activation function is variable sensitive.
- Results from the input node interrogator displayed significant relationship among the input variables and the predicted data, agreeing with the regression

analysis. However, the NI results for the input variables in friction angle prediction were more equilibrated, meanwhile cohesion estimation presented a greater relationship to N_{SPT} when compared to the other variables.

- The validation stage only resulted in a decrease in total quadratic error for sandy soils for both c' and ϕ' prediction. For cohesion prediction, the CF applied for sandy soils was 0.88, meanwhile, for friction angle CF = 1.08.

Finally, the proposed models were compared to the existing correlations. From the results it was concluded:

- Existing models for cohesion prediction could not be compared with the ANN because they returned the undrained shear strength of soils.
- The artificial neural networks showed better agreement to the predicted data than the existing models proposed by Dunham (1954), Godoy (1983) and Terzaghi and Peck (1996) for friction angle estimation, being able to produce models with good generalization capacity and reliability. The best model for cohesion and friction angle prediction had sigmoid activation function, architecture 3-5-3-2, complete soil type entry and was trained up to 1,000,000 iterations, presenting coefficients of correlation 0.91 and 0.91 for training and testing, respectively.
- The reliability of the neural networks was attested and for the best ANN confidence level tables were set per maximum mean error.
- Although complete soil type entry resulted in greater correlations, the nomographs presented better efficiency on effective cohesion and effective friction angle prediction for the model that had sigmoid activation function, architecture 3-5-3-2, simplified soil type entry and was trained up to 100,000 iterations, presenting coefficients of correlation 0.78 and 0.90 for training and testing, respectively. The nomographs presented great understanding of soil shear strength behavior.

It is also important to point out the limitations of the given research. Hence, since the objective of the work was to propose a model with easily collected input, it is pointed out that the proposed models did not consider consolidation of soils, particle size distribution, particle shape, plasticity nor any other soil characteristic that is known to affect soil shear strength. Also, the database was built on drained test data and may not represent the soil behavior well under undrained conditions, and the models proposed might not predict good

values outside of the database range, suggesting the application within the range of $1 \leq N_{SPT} \leq 48$ and $8.15 \text{ kPa} \leq \sigma'_{v0} \leq 252.15 \text{ kPa}$.

5.2 Further research suggestion

In order to improve the designing of structures in Geotechnical Engineering, the following is proposed for further research:

- The use of different methods for training the neural networks to predict shear strength parameters, such as the methods proposed and used by Göktepe (2008) and Das and Basudhar (2008).
- Including and testing other input variables such as CPT and ground water level in order to verify whether they would result in more accurate models.
- Use a different soil type input type for proposition of ANN.
- Propose ANN for each soil type in order to verify the behavior of shear strength parameters.
- Improvement of the database with test results containing data outside of the database range of this work.
- Implementation of an artificial neural network to estimate the elasticity modulus and Poisson of the soils.

REFERENCES

ABDELSALAM, S. S.; SULEIMAN, M. T.; SRITHARAN, S. Modeling Load-Transfer Behavior of H-Piles using Direct Shear and Penetration Test Results. **Geotechnical Testing Journal**, [s.l.], v. 37, n. 4, p. 20130074-20130091, May 13, 2014.

ARAUJO, C. B. C. **Application of perceptron type artificial neural networks in prediction of displacements** ("*Aplicação das redes neurais artificiais do tipo perceptron na estimativa de recalques*"). 2015. 228 f. Dissertation (Master's) – Master's Course in Geotechnics, Department of Environmental and Hydraulic Engineering, Federal University of Ceará, Fortaleza, 2015.

ARAUJO, C. B. C.; DANTAS NETO, S. A.; SOUZA FILHO, F. A. Streamflow forecasting for the dam Orós/CE from hydrometeorological data using perceptrons. **Revista Brasileira de Meteorologia**, [s.l.], v. 30, n. 1, p.37-46, Mar 2015.

ASSOCIAÇÃO BRASILEIRA DE NORMAS TÉCNICAS. **NBR 7250**: Identificação e descrição de amostras de solos obtidas em sondagens de simples reconhecimento dos solos. Rio de Janeiro: ABNT, 1982.

BRAGA, F. V. A. **Soil shear strength parameters prediction using pedotransfer function** ("Estimativa dos parâmetros de resistência do solo ao cisalhamento através de pedotransferência**").** 2014. 98 f. Thesis (Doctorate) – Agricultural Engineering Course, Universidade Federal de Santa Maria, Santa Maria, 2014.

CAMELO, C. S.; LOPERA, J. F. B.; PEREZ, J. A. R. Slope stabilization Project: Case study San António de Parado – Colombia ("Projeto de Estabilização de Encostas: Caso de Estudo San António de Prado – Colômbia"). In: **Conferencia brasileira sobre estabilidade de encostas**, 12, 2017, Santa Catarina. **Anais.** Santa Catarina: Cobrae, p. 1 - 7. 2017.

CARVALHO, D. **Analysis of last loads to the traction of excavated, instrumented stakes in experimental field of São Carlos - SP** ("Análise de cargas últimas à tração de estacas escavadas, instrumentadas, em campo experimental de São Carlos – SP"). 1991. 227 f. Thesis

(Doctorate) - Civil Engineering Course, Department of Geotechnics, São Carlos College of Engineering, São Carlos, Brazil, 1991.

CHING, J.; CHEN, J.; YEH, J.; PHOON, K. Updating Uncertainties in Friction Angles of Clean Sands. **Journal Of Geotechnical and Geoenvironmental Engineering**, [s.l.], v. 138, n. 2, p.217-229, Feb 2012.

CINTRA, J. C. A.; AOKI, N.; ALBIERO, J. H. **Admissible stress in direct foundations** ("*Tensão admissível em fundações diretas*"). São Carlos: Rima, 2003. 73 p.

CIRESAN, D. C.; MEIER, U.; GAMBERDELLA, L. M.; SCHMIDIBHUBER, J. Deep, Big, Simple Neural Nets for Handwritten Digit Recognition. **Neural Computation**, [s.l.], v. 22, n. 12, p.3207-3220, dez. 2010.

CONGRESSO BRASILEIRO DE MECÂNICA DOS SOLOS E ENGENHARIA GEOTÉCNICA, 18., 2016, Belo Horizonte. ***Estimativa de Recalque em Estacas Utilizando Redes Neurais Artificiais*.** Belo Horizonte: Cobramseg 2016 — 19-22 Outubro, Belo Horizonte, Minas Gerais, Brasil © Abms, 2016, 2016. 8 p.

COUTINHO, R. Q.; SOUZA NETO, J. B.; COSTA, F. Q. Design Strength Parameters of a Slope on Unsaturated Gneissic Residual Soil. **Advances In Unsaturated Geotechnics**, [s.l.], p.1-15, July 24, 2000.

DANTAS NETO, S. A.; INDRARATNA, B.; OLIVEIRA, D. A. F.; ASSIS, A. P. Modelling the Shear Behaviour of Clean Rock Discontinuities Using Artificial Neural Networks. **Rock Mechanics And Rock Engineering**, [s.l.], v. 50, n. 7, p.1817-1831, 10 mar. 2017.

DANTAS NETO, S. A.; SILVEIRA, M. V.; AMANCIO, L. B.; DOS ANJOS, G. J. M. Pile Settlement Modeling with Multilayer Perceptrons. **Electronic Journal Of Geotechnical Engineering.** [s.i.], p. 4517-4528. jun. 2014.

DAS, S. K.; BASUDHAR, P. K. Prediction of residual friction angle of clays using artificial neural network. **Engineering Geology**, [s.l.], v. 100, n. 3-4, p.142-145, set. 2008.

DAS, S. K. Artificial Neural Networks in Geotechnical Engineering. **Metaheuristics in Water, Geotechnical and Transport Engineering**, [s.l.], p.231-270, 2013. Elsevier. http://dx.doi.org/10.1016/b978-0-12-398296-4.00010-6.

DÉCOURT, L. General report / Discussion Session 2: SPT, CPT, Pressuremeter Testing and Recent Developments in In-Situ Testing – Part 2: The Standard Penetration Test, State-of-the-Art Report. (1989). **Proc. XII Int. Conf. on Soil Mech. Found. Eng.**, Rio de Janeiro, v. 4, p. 2405-2416

DIAS, R. D. **Aplicação de pedologia e geotecnia no projeto de fundações de linhas de transmissão.** 1987. 349 f. Tese (Doctorate) - Civil Engineering Course, Universidade Federal do Rio de Janeiro, Rio de Janeiro, 1987.

GHABOUSSI, J.; SIDARTA, D. E. New nested adaptive neural networks (NANN) for constitutive modeling. **Computers And Geotechnics**, [s.l.], v. 22, n. 1, p.29-52, jan. 1998.

GOKTEPE, A. B.; ALTUN, S.; ALTINTAS, G.; TAN, O. Shear strength estimation of plastic clays with statistical and neural approaches. **Building And Environment**, [s.l.], v. 43, n. 5, p.849-860, maio 2008.

GOMES, C. L. R. **Retroanálise em Estabilidade de Taludes em Solo: Metodologia para Obtenção dos Parâmetros de Resistência ao Cisalhamento.** 2003. 167 f. Dissertation (Master's) - Civil Engineering Course, Campinas State University, Campinas, 2003

GON, F. S. **Caracterização geotécnica através de ensaios de laboratório de um solo de diabásio da região de Campinas/SP.** 2011. 178 f. Dissertation (Master's) - Master's Course in Civil Engineering, School of Civil Engineering, Architecture and Urban Planning, Campinas State University, Campinas, 2011.

HAYKIN, S. **Neuronal Networks and learning machines.** 3. ed. Hamilton, Ontario, Canada: Pearson Prentice Hall, 906 p. 2009.

HAYKIN, S. **Redes Neurais: Princípios e Prática.** 2. ed. Hamilton, Ontario, Canada: Bookman, 2001. 900 p. Translation by: Paulo Martins Engel.

HATANAKA, M.; UCHIDA, A. Empirical correlation between penetration resistance and internal friction angle of sandy soils. **Soils and Foundations**, Tokyo, v. 36, n. 4, p. 1-9, 1996.

JUWAIED, N. S. Applications of artificial intelligence in geotechnical engineering. **ARPN Journal Of Engineering and Applied Sciences.** [s.i.], p. 2764-2785. April 8, 2018.

KEMPER, W. D.; ROSENAU, R. C. Soil Cohesion as Affected by Time and Water Content 1. **Soil Science Society Of America Journal**, [s.l.], v. 48, n. 5, p.1001-1006, 1984.

KOVÁCS, Z. L. **Redes Neurais Artificiais:** Fundamentos e Aplicações. 3. ed. São Paulo: Editora Livraria da Física, 2002. 174 p.

LAFAYETTE, K. P. V. **Estudo geológico-geotécnico do processo erosivo em encostas no parque metropolitano Armando de Holanda Cavalcanti - Cabo de Santo Agostinha/PE.** 2006. 358 f. Dissertation (Master's) – Civil Engineering Course, Federal University of Pernambuco, Recife, 2006

LAMBE, T. W.; WHITMAN, R. V. **Soil Mechanics.** Cambridge: Massachusetts Institute of Technology, 1969. 548 p.

LEE, I. M.; LEE, J. H. Prediction of pile bearing capacity using artificial neural networks. **Computers and Geotechnics**, v. 18, n.3, p. 189-200. 1996.

LIMA, A. F. **Comportamento geomecânico e análise de estabilidade de uma encosta da formação barreiras na área urbana da cidade do Recife.** 2002. 204 f. Dissertation (Master's) - Civil Engineering Course, Federal University of Pernambuco, Recife, 2002

LU, N.; LIKOS, W. J. **Unsaturated soil mechanics.** New Jersey: John Wiley & Sons, Inc, 569 p. 2004.

MAGALHÃES, J. S. L. A. **Estudo de estabilidade da encosta alto do Padre Cícero no município de Camaragibe-PE.** 2013. 107 f. Dissertation (Master's) - Civil Engineering Course, Federal University of Pernambuco, Recife, 2013.

MARQUES, R. F. **Estudo da capacidade de carga de estacas escavadas com bulbos, executadas em solo não saturado da formação barreiras da cidade de Maceió - AL.** 2006. 158 f. Dissertation (Master) - Civil Engineering Course, Federal University of Pernambuco, Recife, 2006.

MCCULLOCH, W. S.; PITTS, W. A logical calculus of the ideas immanent in nervous activity. **The Bulletin Of Mathematical Biophysics.** Great Britain, p. 115-133. jan. 1943.

MEYERHOF, G. G. (1956). Penetration Test and bearing Capacity of Cohesionless Soil. **Journal of Geotechincal Engineering Div**., ASCE, Vol 82, SMI.

MORAES, L. S. **Estacas escavadas com base injetada.** 2010. 168 p. Thesis (Doctorate) - Doctorate Course in Geotechnics, University of São Paulo, São Carlos, 2010.

NAJJAR, Y. M.; BASHEER, I. A.; NAOUSS, W. A. On the identification of compaction characteristics by neuronets. **Computers And Geotechnics**, [s.l.], v. 18, n. 3, p.167-187, January 1996.

OLSEN, R. S. (Org.). **Normalization and Prediction of Geotechnical Properties Using the Cone Penetrometer Test (CPT).** Vicksburg: U.S. Army Corps of Engineers, 1994.

PECK, R. B.; HANSON, J. B.; THORNBURN, S. (1974). **Foundation Engeneering, 2nd Edition**, John Willey & Sons, New York.

PEIXOTO, A. S. P. **Estudo do ensaio SPT-T e sua aplicação na prática da engenharia de fundações.** 2001. 359 f. Thesis (Doctorate) – Course of Agricultural Engineering, Campinas State University, Campinas, 2001

PENUMADU, D.; ZHAO, R. Triaxial compression behavior of sand and gravel using artificial neural networks (ANN). **Computers And Geotechnics**, [s.l.], v. 24, n. 3, p.207-230, abr. 1999.

PÉREZ, N. B. M. **Análise de transferência de carga em estacas escavadas em solo da região de Campinas/SP.** 2014. 205 f. Dissertation (Master's) - Civil Engineering Course, School of

Civil Engineering, Architecture and Urban Planning, Campinas State University, Campinas, 2014.

RIBEIRO, V.; VILLAR, L.; MENDONÇA, A.; CALDAS, M. Análise de uma contenção em retangulões instrumentada. **Congresso Brasileiro de Mecânica dos Solos e Engenharia Geotécnica**, Porto de Galinhas, 16. (2012).

SAMUI, P. Three-Dimensional Site Characterization Model of Bangalore using Support Vector Machine. **ISRN Soil Science**, [s.l.], v. 2012, p.1-10, 2012.

SANTANA, L. G. Estimativa de Parâmetros de Resistência ao Cisalhamento de Solos a Partir de Sondagens SPT e Comparação com Resultados de Ensaios Triaxiais. In: **Congresso Brasileiro de Mecânica dos Solos e Engenharia Geotécnica**, 18., 2016, Belo Horizonte. **Anais.** Belo Horizonte: Cobramseg, p. 1 - 8. 2016.

SANTOS, M. A. A. **Influência das condições tridimensionais de tensão e fluxo na estabilidade de um talude em solo não saturado.** 2007. 204 f. Dissertation (Master) - Civil Engineering Course, University of Brasilia, Brasilia, 2007

SCHMIDHUBER, J. Deep learning in neural networks: An overview. **Neural Networks**, [s.l.], v. 61, p.85-117, Oct 2014.

SHAHIN, M. A.; JAKSA, M. B.; MAIER, H. R. Artificial neural network applications in geotechnical engineering. **Australian Geomechanics: journal and news of the australian geomechanics society.** St Ives, p. 49-62. Mar. 2001.

SHARMA, L. K.; SINGH, R.; UMRAO, R. K.; SHARMA, K. M.; SINGH, T. N. Evaluating the modulus of elasticity of soil using soft computing system. **Engineering with Computers**, [s.l.], v. 33, n. 3, p.497-507, Sep 24, 2016.

SHOOSHPASHA, I.; AMIRI, I.; MOLAABASI, H. An Investigation of Friction Angle Correlation with Geotechnical Properties for Granular Soils Using GMDH Type Neural Networks. **Scientia Iranica**, Tehran, v. 22, n. 1, p.157-164, jan. 2015.

SILVA, M. M. **Estudo geológico-geotécnico de uma encosta com problemas de instabilidade no município de Camaragibe-PE.** 2007. 436 f. Thesis (Doctorate) – Civil Engineering Course, Federal University of Pernambuco, Recife, 2007

SOUZA, J. M. **Abordagem qualitativa e quantitativa de encostas urbanas aplicada a dois taludes no município de Vitória.** 2012. 192 f. Dissertation (Master's) – Civil Engineering Course, Federal University of Ouro Preto, Ouro Preto, 2012

SOUZA, A. P. L. **Estudos geotécnicos e de estabilidade de taludes da encosta do alto do Padre Cícero no município de Camaragibe-PE.** 2014. 177 f. Dissertation (Master's) – Civil Engineering Course, Federal University of Pernambuco, Recife, 2014

SUZUKI, S. **Propriedades geomecânicas de alguns solos residuais e coluviais ao longo do oleoduto Curitiba-Paranaguá.** 2004. 329 f. Dissertation (Master's) - Civil Engineering Course, Federal University of Rio de Janeiro, Rio de Janeiro, 2004

TERZAGHI, K.; PECK, R. B. **Soil Mechanics in Engineering Practice.** 3. ed. New York: John Wiley & Sons, Inc, 1996. 664 p

TIZPA, P.; CHENARI, R. J.; FARD, M. K.; MACHADO, S. L. ANN prediction of some geotechnical properties of soil from their index parameters. **Arabian Journal of Geosciences**, [s.l.], v. 8, n. 5, p.2911-2920, Feb 23, 2014.

WEI, Y.; WU, X.; XIA, J.; MILLER, G. A.; CAI, C.; GUO, Z.; ARASH, H. The effect of water content on the shear strength characteristics of granitic soils in South China. **Soil and Tillage Research**, [s.l.], v. 187, p.50-59, April 2019.

APPENDIX A – TRAINING AND TESTING DATABASE

Depth (m)	N_{SPT}	σvo' (kPa)	c' (kPa)	Φ (°)	γ (kN/m³)	Soil type	Group	Test Type	Saturation	Source
3.00	14.00	50.03	30.00	34.00	16.68	clayey sand	sandy	Triaxial	Saturated	Santana (2016)
1.50	2.00	25.95	47.00	44.20	17.30	clayey sand	sandy	Direct shear	Saturated	Da Silva (2007)
4.30	5.00	74.38	4.40	38.90	17.30	clayey sand	sandy	Direct shear	Saturated	Da Silva (2007)
4.90	10.00	84.76	3.80	31.50	17.30	clayey sand	sandy	Direct shear	Saturated	Da Silva (2007)
1.50	3.00	24.90	3.70	31.20	16.60	clayey sand	sandy	Direct shear	Saturated	Da Silva (2007)
1.50	3.00	24.90	45.70	31.30	16.60	clayey sand	sandy	Direct shear	Unsaturated	Da Silva (2007)
5.70	19.00	94.62	6.30	40.40	16.60	clayey sand	sandy	Direct shear	Saturated	Da Silva (2007)
6.30	18.00	104.58	2.20	35.00	16.60	sandy clay	clayey	Direct shear	Saturated	Da Silva (2007)
1.50	7.00	26.25	3.80	29.40	17.50	clayey sand	sandy	Direct shear	Saturated	Da Silva (2007)
1.50	7.00	26.25	42.30	43.70	17.50	clayey sand	sandy	Direct shear	Unsaturated	Da Silva (2007)
2.50	6.00	41.50	9.70	26.30	16.60	sandy clay	clayey	Direct shear	Saturated	Da Silva (2007)
2.50	6.00	41.50	9.80	29.20	16.60	sandy clay	clayey	Direct shear	Unsaturated	Da Silva (2007)
6.00	11.00	99.60	3.00	27.60	16.60	sandy clay	clayey	Direct shear	Saturated	Da Silva (2007)
2.00	5.00	33.83	27.39	35.70	16.92	sandy clay	clayey	Direct shear	Unsaturated	Magalhães (2013)
2.00	5.00	33.85	8.72	34.20	16.93	sandy clay	clayey	Direct shear	Saturated	Magalhães (2013)
2.00	4.00	36.12	35.08	28.10	18.06	sandy clay	clayey	Direct shear	Unsaturated	Magalhães (2013)
2.00	4.00	36.09	6.97	29.50	18.04	sandy clay	clayey	Direct shear	Saturated	Magalhães (2013)
2.00	4.00	32.45	13.76	36.50	16.22	clayey sand	sandy	Direct shear	Unsaturated	Magalhães (2013)
2.00	4.00	32.68	3.30	35.10	16.34	clayey sand	sandy	Direct shear	Saturated	Magalhães (2013)
1.50	6.00	22.50	10.00	35.00	15.00	clayey sand	sandy	Direct shear	Unsaturated	Anna (2014)
1.50	6.00	27.75	1.00	32.00	18.50	clayey sand	sandy	Direct shear	Saturated	Anna (2014)
1.50	5.00	24.45	7.02	35.32	16.30	sandy clay	clayey	Direct shear	Unsaturated	Anna (2014)
1.50	5.00	29.25	2.85	31.62	19.50	sandy clay	clayey	Direct shear	Saturated	Anna (2014)
1.50	11.00	27.30	28.75	32.92	18.20	sandy clay	clayey	Direct shear	Unsaturated	Anna (2014)
1.50	11.00	30.45	6.19	30.73	20.30	sandy clay	clayey	Direct shear	Saturated	Anna (2014)

Depth (m)	N_{SPT}	σvo' (kPa)	c' (kPa)	Φ (°)	γ (kN/m³)	Soil type	Group	Test Type	Saturation	Source
0.75	4.00	12.75	71.40	41.60	17.00	clayey sand	sandy	Direct shear	Unsaturated	Coutinho (Design Strength Parameters)
0.75	4.00	12.75	10.80	31.90	17.00	clayey sand	sandy	Direct shear	Saturated	Coutinho (Design Strength Parameters)
8.70	20.00	147.90	7.00	29.50	17.00	sandy silt	silty	Direct shear	Unsaturated	Coutinho (Design Strength Parameters)
8.70	20.00	147.90	5.30	31.40	17.00	sandy silt	silty	Direct shear	Saturated	Coutinho (Design Strength Parameters)
1.04	2.00	18.14	28.00	31.00	17.44	clayey sand	sandy	Direct shear	Unsaturated	Lima (2002)
1.04	2.00	18.88	10.00	32.00	18.16	clayey sand	sandy	Direct shear	Saturated	Lima (2002)
1.10	13.00	25.21	84.00	34.00	22.92	silty sand	sandy	Direct shear	Unsaturated	Lima (2002)
1.10	13.00	23.80	1.00	16.00	21.63	silty sand	sandy	Direct shear	Saturated	Lima (2002)
1.00	3.00	17.41	10.00	31.60	17.41	clayey silt	silty	Direct shear	Saturated	Suzuki (2004)
3.50	14.00	62.22	8.00	33.00	17.78	clayey silt	silty	Direct shear	Saturated	Suzuki (2004)
3.50	5.00	61.77	11.00	31.50	17.65	sandy silt	silty	Direct shear	Saturated	Suzuki (2004)
2.40	2.00	29.52	20.00	29.00	12.30	clayey sand	sandy	Direct shear	Unsaturated	Santos (2007)
2.40	2.00	29.52	3.00	27.00	12.30	clayey sand	sandy	Direct shear	Saturated	Santos (2007)
5.00	6.00	71.00	20.00	27.00	14.20	clayey sand	sandy	Direct shear	Unsaturated	Santos (2007)
5.00	6.00	71.00	4.70	27.00	14.20	clayey sand	sandy	Direct shear	Saturated	Santos (2007)
7.70	11.00	117.04	27.00	36.00	15.20	clayey sand	sandy	Direct shear	Unsaturated	Santos (2007)
7.70	11.00	117.04	4.20	30.00	15.20	clayey sand	sandy	Direct shear	Saturated	Santos (2007)
11.70	5.00	184.86	35.00	31.00	15.80	clayey sand	sandy	Direct shear	Unsaturated	Santos (2007)
11.70	5.00	184.86	14.00	30.00	15.80	clayey sand	sandy	Direct shear	Saturated	Santos (2007)
1.10	5.00	16.23	9.76	31.20	14.75	sandy silt	silty	Direct shear	Unsaturated	Marques (2006)
1.10	5.00	16.23	0.00	31.90	14.75	sandy silt	silty	Direct shear	Saturated	Marques (2006)
3.10	4.00	47.59	15.75	27.20	15.35	sandy silt	silty	Direct shear	Unsaturated	Marques (2006)
3.10	4.00	47.59	0.00	30.00	15.35	sandy silt	silty	Direct shear	Saturated	Marques (2006)
5.10	8.00	92.51	17.18	31.60	18.14	sandy silt	silty	Direct shear	Unsaturated	Marques (2006)
5.10	8.00	92.51	0.00	31.80	18.14	sandy silt	silty	Direct shear	Saturated	Marques (2006)
7.20	16.00	132.19	7.25	32.70	18.36	silty sand	sandy	Direct shear	Unsaturated	Marques (2006)

Depth (m)	N_{SPT}	σvo' (kPa)	c' (kPa)	Φ (°)	γ (kN/m³)	Soil type	Group	Test Type	Saturation	Source
7.20	16.00	132.19	0.00	34.90	18.36	silty sand	sandy	Direct shear	Saturated	Marques (2006)
8.40	19.00	150.61	21.65	36.10	17.93	silty sand	sandy	Direct shear	Unsaturated	Marques (2006)
8.40	19.00	150.61	1.64	27.90	17.93	silty sand	sandy	Direct shear	Saturated	Marques (2006)
2.44	4.00	47.53	6.31	28.37	19.48	silty sand	sandy	Direct shear	Saturated	De Souza (2012)
2.44	4.00	47.53	59.05	43.23	19.48	silty sand	sandy	Direct shear	Unsaturated	De Souza (2012)
4.70	22.00	85.16	8.05	30.11	18.12	silty sand	sandy	Direct shear	Saturated	De Souza (2012)
4.70	22.00	85.16	93.49	41.99	18.12	silty sand	sandy	Direct shear	Unsaturated	De Souza (2012)
2.44	4.00	47.53	4.80	24.70	19.48	silty sand	sandy	Triaxial	Saturated	De Souza (2012)
4.70	22.00	85.16	12.36	23.75	18.12	silty sand	sandy	Triaxial	Saturated	De Souza (2012)
1.02	10.00	17.87	94.45	54.46	17.52	silty sand	sandy	Direct shear	Unsaturated	De Souza (2012)
1.02	10.00	17.87	13.50	26.96	17.52	silty sand	sandy	Direct shear	Saturated	De Souza (2012)
1.37	10.00	24.00	7.40	39.69	17.52	silty sand	sandy	Direct shear	Unsaturated	De Souza (2012)
1.37	10.00	24.00	2.72	37.15	17.52	silty sand	sandy	Direct shear	Saturated	De Souza (2012)
1.02	10.00	17.87	9.17	24.23	17.52	silty sand	sandy	Triaxial	Saturated	De Souza (2012)
1.37	10.00	24.00	0.00	27.02	17.52	silty sand	sandy	Triaxial	Saturated	De Souza (2012)
1.50	2.00	24.00	0.00	35.00	16.00	silty sand	sandy	Triaxial	Saturated	Gomes (2003)
1.50	2.00	24.00	11.00	22.30	16.00	silty sand	sandy	Triaxial	Unsaturated	Gomes (2003)
1.50	15.00	27.00	37.20	25.70	18.00	clayey sand	sandy	Triaxial	Saturated	Gomes (2003)
1.50	15.00	27.00	68.90	24.10	18.00	clayey sand	sandy	Triaxial	Unsaturated	Gomes (2003)
1.80	24.00	28.96	33.10	33.40	16.09	silty sand	sandy	Direct shear	Unsaturated	Lafayette (2006)
1.80	24.00	28.96	1.60	33.80	16.09	silty sand	sandy	Direct shear	Saturated	Lafayette (2006)
4.80	25.00	74.40	43.70	41.30	15.50	silty sand	sandy	Direct shear	Unsaturated	Lafayette (2006)
4.80	25.00	74.40	8.20	30.30	15.50	silty sand	sandy	Direct shear	Saturated	Lafayette (2006)
1.80	30.00	26.24	56.10	35.70	14.58	silty sand	sandy	Direct shear	Unsaturated	Lafayette (2006)
1.80	30.00	26.24	1.80	35.00	14.58	silty sand	sandy	Direct shear	Saturated	Lafayette (2006)
12.30	28.00	196.19	45.60	41.00	15.95	silty sand	sandy	Direct shear	Unsaturated	Lafayette (2006)
12.30	28.00	196.19	7.60	31.30	15.95	silty sand	sandy	Direct shear	Saturated	Lafayette (2006)
0.50	7.00	8.85	23.00	31.00	17.70	sandy clay	clayey	Direct shear	Unsaturated	Dias, R. D. (1987)

Depth (m)	N_{SPT}	σvo' (kPa)	c' (kPa)	Φ (°)	γ (kN/m³)	Soil type	Group	Test Type	Saturation	Source
0.50	7.00	8.80	14.00	26.00	17.60	sandy clay	clayey	Direct shear	Saturated	Dias, R. D. (1987)
1.50	7.00	24.60	32.00	26.00	16.40	sandy clay	clayey	Direct shear	Unsaturated	Dias, R. D. (1987)
1.50	7.00	24.45	16.00	24.00	16.30	sandy clay	clayey	Direct shear	Saturated	Dias, R. D. (1987)
0.50	11.00	8.85	54.60	30.50	17.70	sandy clay	clayey	Direct shear	Unsaturated	Dias, R. D. (1987)
0.50	11.00	8.40	32.00	27.90	16.80	sandy clay	clayey	Direct shear	Saturated	Dias, R. D. (1987)
1.50	10.00	24.30	39.00	38.60	16.20	sandy clay	clayey	Direct shear	Unsaturated	Dias, R. D. (1987)
1.50	10.00	24.15	31.00	33.50	16.10	sandy clay	clayey	Direct shear	Saturated	Dias, R. D. (1987)
0.50	40.00	8.55	41.50	35.60	17.10	sandy clay	clayey	Direct shear	Unsaturated	Dias, R. D. (1987)
0.50	40.00	8.15	25.00	28.70	16.30	sandy clay	clayey	Direct shear	Saturated	Dias, R. D. (1987)
7.00	10.00	160.30	0.00	37.00	22.90	sand	sandy	Direct shear	Saturated	Abdelsalam, Suleiman & Sritharan (2014)
13.70	28.00	345.24	0.00	39.00	25.20	sand	sandy	Direct shear	Saturated	Abdelsalam, Suleiman & Sritharan (2014)
2.10	26.00	42.42	7.20	37.00	20.20	sand with gravel	sandy	Direct shear	Saturated	Abdelsalam, Suleiman & Sritharan (2014)
7.60	40.00	182.40	32.20	29.00	24.00	sand with gravel	sandy	Direct shear	Saturated	Abdelsalam, Suleiman & Sritharan (2014)
13.70	24.00	324.69	0.20	41.00	23.70	sand with gravel	sandy	Direct shear	Saturated	Abdelsalam, Suleiman & Sritharan (2014)
1.00	25.00	20.20	0.00	28.00	20.20	clayey sand	sandy	Direct shear	Saturated	Abdelsalam, Suleiman & Sritharan (2014)
3.50	45.00	84.00	10.00	32.00	24.00	clayey sand	sandy	Direct shear	Saturated	Abdelsalam, Suleiman & Sritharan (2014)
11.50	90.00	272.55	40.00	35.00	23.70	clayey sand	sandy	Direct shear	Saturated	Abdelsalam, Suleiman & Sritharan (2014)
4.00	30.00	80.00	35.60	24.00	20.00	silty sand	sandy	Direct shear	Saturated	Ribeiro *et al.* (2012)
4.00	30.00	80.00	112.30	30.10	20.00	silty sand	sandy	Direct shear	Unsaturated	Ribeiro *et al.* (2012)
1.00	18.00	17.00	8.00	15.00	17.00	clayey silt	silty	Direct shear	Saturated	Camelo, Lopera & Perez (2017)
6.00	35.00	96.00	10.00	26.00	16.00	clayey silt	silty	Direct shear	Saturated	Camelo, Lopera & Perez (2017)
13.00	45.00	208.00	17.00	21.00	16.00	clayey silt	silty	Direct shear	Saturated	Camelo, Lopera & Perez (2017)
22.00	12.00	401.72	37.70	17.00	18.26	clayey silt	silty	Direct shear	Saturated	Camelo, Lopera & Perez (2017)
1.00	10.00	20.00	20.00	25.00	20.00	silt	silty	Direct shear	Saturated	Camelo, Lopera & Perez (2017)

Depth (m)	N_{SPT}	σvo' (kPa)	c' (kPa)	Φ (°)	γ (kN/m³)	Soil type	Group	Test Type	Saturation	Source
5.00	15.00	95.00	20.00	23.00	19.00	silt	silty	Direct shear	Saturated	Camelo, Lopera & Perez (2017)
10.00	20.00	200.00	24.00	27.00	20.00	silt	silty	Direct shear	Saturated	Camelo, Lopera & Perez (2017)
15.00	20.00	270.00	24.00	28.00	18.00	silt	silty	Direct shear	Saturated	Camelo, Lopera & Perez (2017)
1.00	5.00	19.00	11.00	28.00	19.00	silty sand	sandy	Direct shear	Saturated	Camelo, Lopera & Perez (2017)
6.00	8.00	114.00	8.00	30.00	19.00	silty sand	sandy	Direct shear	Saturated	Camelo, Lopera & Perez (2017)
10.00	20.00	180.00	20.00	25.00	18.00	silt	silty	Direct shear	Saturated	Camelo, Lopera & Perez (2017)
14.00	30.00	252.00	15.00	28.00	18.00	silt	silty	Direct shear	Saturated	Camelo, Lopera & Perez (2017)
20.00	25.00	420.00	20.00	28.00	21.00	silty sand	sandy	Direct shear	Saturated	Camelo, Lopera & Perez (2017)
1.50	2.00	21.95	0.00	33.40	14.63	silty sand	sandy	Direct shear	Saturated	Test data form construction of *Centro de Eventos do Ceará*
1.50	2.00	21.93	0.00	32.50	14.62	silty sand	sandy	Direct shear	Saturated	Test data form construction of *Centro de Eventos do Ceará*
1.50	5.00	22.01	0.00	31.30	14.67	silty sand	sandy	Direct shear	Saturated	Test data form construction of *Centro de Eventos do Ceará*
3.00	4.00	43.29	4.00	27.70	14.43	silty sand	sandy	Direct shear	Saturated	Test data form construction of *Centro de Eventos do Ceará*
15.00	26.00	306.01	0.00	36.50	20.40	silty sand	sandy	Direct shear	Saturated	Test data form construction of *Alberto Sá* Tunnel
4.50	2.00	98.18	3.00	16.20	21.82	clayey sand	sandy	Triaxial	Saturated	Test data form construction of *Germano Frank* Tunnel
9.00	42.00	17.85	46.00	5.31	19.80	clayey sand	sandy	Triaxial	Saturated	Test data form construction of *Germano Frank* Tunnel

APPENDIX B – CORRECTION FACTOR DATABASE

Depth (m)	N_{SPT}	σvo' (kPa)	c' (kPa)	Φ (°)	γ (kN/m³)	Soil type	Group	Test Type	Saturation	Source
1.30	5.00	20.00	6.00	30.50	15.60	clayey sand	sandy	Triaxial	Saturated	Menezes (1990) *apud* Carvalho (1991)
2.30	2.00	35.40	5.00	29.50	15.50	clayey sand	sandy	Triaxial	Saturated	Menezes (1990) *apud* Carvalho (1991)
3.30	3.00	50.80	6.00	30.00	15.80	clayey sand	sandy	Triaxial	Saturated	Menezes (1990) *apud* Carvalho (1991)
4.30	4.00	67.40	12.50	29.00	16.90	clayey sand	sandy	Triaxial	Saturated	Menezes (1990) *apud* Carvalho (1991)
5.30	5.00	84.70	1.00	31.00	17.20	clayey sand	sandy	Triaxial	Saturated	Menezes (1990) *apud* Carvalho (1991)
6.30	3.00	102.10	25.50	25.00	17.00	clayey sand	sandy	Triaxial	Saturated	Menezes (1990) *apud* Carvalho (1991)
7.30	7.00	120.70	4.50	28.00	18.30	clayey sand	sandy	Triaxial	Saturated	Menezes (1990) *apud* Carvalho (1991)
8.30	7.00	139.20	18.00	23.00	19.00	clayey sand	sandy	Triaxial	Saturated	Menezes (1990) *apud* Carvalho (1991)
9.30	9.00	157.00	9.00	26.00	18.40	clayey sand	sandy	Triaxial	Saturated	Menezes (1990) *apud* Carvalho (1991)
10.30	7.00	176.00	43.00	14.00	18.90	clayey sand	sandy	Triaxial	Saturated	Menezes (1990) *apud* Carvalho (1991)
1.50	2.10	15.00	0.00	32.00	15.00	clayey sand	sandy	Triaxial	Saturated	Agnelli (1997) *apud* Peixoto (2001)
2.50	0.60	30.00	14.00	31.00	15.40	clayey sand	sandy	Triaxial	Saturated	Agnelli (1997) *apud* Peixoto (2001)
3.50	1.50	46.00	22.00	20.00	15.70	clayey sand	sandy	Triaxial	Saturated	Agnelli (1997) *apud* Peixoto (2001)
4.50	1.50	62.00	24.00	28.00	16.30	clayey sand	sandy	Triaxial	Saturated	Agnelli (1997) *apud* Peixoto (2001)
5.50	1.50	78.00	14.00	29.00	16.50	clayey sand	sandy	Triaxial	Saturated	Agnelli (1997) *apud* Peixoto (2001)
7.50	4.10	94.00	20.00	29.00	16.50	clayey sand	sandy	Triaxial	Saturated	Agnelli (1997) *apud* Peixoto (2001)

Depth (m)	N_{SPT}	σvo' (kPa)	c' (kPa)	Φ (°)	γ (kN/m³)	Soil type	Group	Test Type	Saturation	Source
7.50	4.10	110.00	0.00	32.00	16.50	clayey sand	sandy	Triaxial	Saturated	Agnelli (1997) *apud* Peixoto (2001)
8.50	5.50	126.00	35.00	28.00	16.60	clayey sand	sandy	Triaxial	Saturated	Agnelli (1997) *apud* Peixoto (2001)
10.50	6.60	142.00	16.00	30.00	16.60	clayey sand	sandy	Triaxial	Saturated	Agnelli (1997) *apud* Peixoto (2001)
10.50	6.60	158.00	14.00	29.00	16.60	clayey sand	sandy	Triaxial	Saturated	Agnelli (1997) *apud* Peixoto (2001)
12.50	7.70	174.00	49.00	25.00	16.60	clayey sand	sandy	Triaxial	Saturated	Agnelli (1997) *apud* Peixoto (2001)
12.50	7.70	190.00	26.00	29.00	16.60	clayey sand	sandy	Triaxial	Saturated	Agnelli (1997) *apud* Peixoto (2001)
1.00	4.92	16.00	0.00	32.20	16.00	clayey sand	sandy	Triaxial	Saturated	Menezes (1997) & Segantini (2000) *apud* Peixoto (2001)
2.00	2.55	30.80	3.00	31.80	14.80	clayey sand	sandy	Triaxial	Saturated	Menezes (1997) & Segantini (2000) *apud* Peixoto (2001)
3.00	2.70	45.70	2.00	32.50	14.90	clayey sand	sandy	Triaxial	Saturated	Menezes (1997) & Segantini (2000) *apud* Peixoto (2001)
5.00	3.92	75.30	2.00	33.30	14.80	clayey sand	sandy	Triaxial	Saturated	Menezes (1997) & Segantini (2000) *apud* Peixoto (2001)
7.00	4.48	107.10	3.00	33.00	15.90	clayey sand	sandy	Triaxial	Saturated	Menezes (1997) & Segantini (2000) *apud* Peixoto (2001)
9.00	6.88	143.90	16.00	30.30	18.40	clayey sand	sandy	Triaxial	Saturated	Menezes (1997) & Segantini (2000) *apud* Peixoto (2001)
11.00	8.38	179.30	20.00	28.80	17.70	clayey sand	sandy	Triaxial	Saturated	Menezes (1997) & Segantini (2000) *apud* Peixoto (2001)
13.00	8.43	216.90	20.00	28.80	18.80	clayey sand	sandy	Triaxial	Saturated	Menezes (1997) & Segantini (2000) *apud* Peixoto (2001)
15.00	10.33	250.90	17.00	30.10	17.00	clayey sand	sandy	Triaxial	Saturated	Menezes (1997) & Segantini (2000) *apud* Peixoto (2001)
3.00	2.00	45.00	0.00	29.03	15.00	clayey sand	sandy	Triaxial	Saturated	Machado (1998) *apud* Moraes (2010)
5.00	3.00	75.00	10.50	31.20	15.00	clayey sand	sandy	Triaxial	Saturated	Machado (1998) *apud* Moraes (2010)
8.00	6.00	111.00	26.90	26.40	18.00	clayey sand	sandy	Triaxial	Saturated	Machado (1998) *apud* Moraes (2010)

Depth (m)	N_{SPT}	σvo' (kPa)	c' (kPa)	Φ (°)	γ (kN/m³)	Soil type	Group	Test Type	Saturation	Source
1.00	2.00	14.10	7.40	22.00	14.10	clayey sand	sandy	Triaxial	Saturated	Pérez (2014)
2.00	4.00	28.20	7.90	21.00	14.20	Silty clay	clayey	Triaxial	Saturated	Pérez (2014)
3.00	4.00	42.20	11.60	22.00	14.00	Silty clay	clayey	Triaxial	Saturated	Pérez (2014)
4.00	5.00	56.60	5.80	23.00	14.40	Silty clay	clayey	Triaxial	Saturated	Pérez (2014)
5.00	7.00	72.10	24.00	21.00	15.50	Silty clay	clayey	Triaxial	Saturated	Pérez (2014)
6.00	7.00	87.40	42.40	22.00	15.30	Silty clay	clayey	Triaxial	Saturated	Pérez (2014)
7.00	7.00	102.80	41.90	22.00	15.40	Silty clay	clayey	Triaxial	Saturated	Pérez (2014)
8.00	7.00	118.00	26.40	22.00	15.20	Silty clay	clayey	Triaxial	Saturated	Pérez (2014)
1.00	2.00	10.96	7.40	22.00	14.10	Clayey silt	silty	Triaxial	Saturated	Gon (2011)
2.00	4.00	22.18	7.90	21.00	14.20	Silty sand	sandy	Triaxial	Saturated	Gon (2011)
3.00	2.00	32.70	11.60	22.00	14.00	Silty sand	sandy	Triaxial	Saturated	Gon (2011)
4.00	4.00	46.00	5.80	23.00	14.40	Silty sand	sandy	Triaxial	Saturated	Gon (2011)
5.00	4.00	61.50	24.00	21.00	15.50	Silty sand	sandy	Triaxial	Saturated	Gon (2011)
6.00	7.00	72.30	42.40	22.00	15.30	Sandy clay	clayey	Triaxial	Saturated	Gon (2011)
7.00	7.00	84.00	41.90	22.00	15.40	Sandy clay	clayey	Triaxial	Saturated	Gon (2011)
8.00	7.00	92.00	26.40	22.00	15.20	Sandy clay	clayey	Triaxial	Saturated	Gon (2011)